Coordinated Voltage and Reactive Power Control for Renewable Dominant Smart Distribution Systems

by

Monsef Tahir

A thesis
presented to the University of Waterloo
in fulfillment of the
thesis requirement for the degree of
Doctor of Philosophy
in
Electrical and Computer Engineering

Waterloo, Ontario, Canada, 2019

Examining Committee Membership

The following served on the Examining Committee for this thesis. The decision of the Examining Committee is by majority vote.

External Examiner:	Dr. Medhat M. Morcos Professor Department of Electrical and Computer Engineering Kansas State University
Supervisor:	Dr. Ramadan A. El-Shatshat Lecturer, Director of the Electric Power Eng Program Department of Electrical and Computer Engineering University of Waterloo
Co-Supervisor:	Dr. Magdy Salama Professor Department of Electrical and Computer Engineering University of Waterloo
Internal Member:	Dr. Mehrdad Kazerani Professor Department of Electrical and Computer Engineering University of Waterloo
Internal Member:	Dr. Kshirasagar Naik Professor Department of Electrical and Computer Engineering University of Waterloo
Internal-external Member:	Dr. Eihab Abdel-Rahman Professor, Assoc Chair Grad Studies Department of System Design Engineering University of Waterloo

Author's Declaration

I hereby declare that I am the sole author of this thesis. This is a true copy of the thesis, including any required final revisions, as accepted by my examiners.

I understand that my thesis may be made electronically available to the public.

Abstract

Driven by their economic and environmental advantages, smart grids promote the deployment of active components, including renewable energy sources (RESs), energy storage systems (ESSs), and electric vehicles (EVs), for sustainability and environmental benefits. As a result of smart grid technologies and the amount of data collected by smart meters, better operation and control schemes can be developed to allow for cleaner energy with high efficiency, and without breaching network operating constraints.

Power distribution networks may face some operational and control challenges as the integration of intermittent energy sources (wind and PV power systems) increases. Some of these challenges include voltage rise and fluctuation, reverse power flow, and the malfunction of conventional Volt/Var control devices. Depending on their location, RESs may introduce two issues related to the Volt/Var control problem, the first of which is that the severity of loading variations will be greater than the case without RESs. The second occurs when the RES is connected between the load center and any regulating devices. The power in-feed from the intermittent RESs may not only mislead the regulator's control circuit, resulting in unfavorable voltage, but may also enforce the regulator taps to operate randomly following bus voltage variations.

This thesis investigates and presents a methodology for the Volt/Var control problem in Smart Distribution Grids (SDGs) under the high penetration and fluctuation of RESs. The research involves the application of predictive control actions to optimally set Volt/Var control devices before the predicted voltage violation takes place. The main objective of this controller is to manage and control the operation of Volt/Var devices in an optimal way that improves the voltage profile along the feeders, reduces real power losses and minimizes the number of Volt/Var device taps and/or switching movements under all loading conditions and for high penetration RESs.

This thesis first presents a very Short-Term Stacking Ensemble (STSE) forecasting model for solar PV and wind power outputs that is developed to predict the generated power for intervals of 15 minutes. The proposed model combines heterogeneous machine learning algorithms composed of three well-established models: Support Vector Regression (SVR); Radial Basis Function Neural Network (RBFNN); and Random Forest (RF) heuristically via SVR. The STSE model aims to minimize the prediction error associated with renewable resources when used in the real-time operation of power distribution networks.

Secondly, a day-ahead Predictive Volt/Var Control (PVVC) model is developed to find the optimal coordination between Volt/Var control devices under the high penetration and power variations of RESs. The objective of the PVVC model is defined as simultaneous minimization of voltage deviation at each bus, power losses, operating cycle of regulation equipment, and RES curtailment. The benefit of using smart inverter interface RESs with the capability of injective/absorbing reactive power is examined and applied as ancillary services for voltage support.

Thirdly, a Sequential Predictive Control (SPC) Strategy for smart grids is developed. The model uses the past and currently available data to forecast demand and RES outputs for intervals of 15 minutes, with real-time updating mechanisms. It then schedules the settings and operations of Volt/Var control devices by solving the Volt/Var control problem in a rolling horizon optimization framework. Because the optimization must be solved in a short interval with a global solution, a solution methodology for linearizing the nonlinear optimization problem is adapted. The original control problem, which is a Mixed-Integer Nonlinear Programming (MINLP) optimization problem, is transformed into a Mixed Integer Second Order Conic Programming (MISOCP) problem that guarantees a global solution through convexity and remarkably reduces the computational burden. Case studies carried out to compare the proposed model against state-of-the-art models provides evidence for the proposed model's effectiveness. Results indicate that the SPC is capable of accurately solving the control problem within small time slots.

The proposed models aim to efficiently operate SDGs at a high penetration level of RES for a day-ahead, as well as in real-time, depending on the preference of network operators. The primary purpose is to minimize operating costs while increasing the efficiency and lifespan of Volt/Var control devices.

Acknowledgments

First and foremost, I wish to express my gratitude to Allah, whose countless bounties enabled me to successfully accomplish this thesis.

I would also like to express my sincere gratitude to my advisors, Dr. Ramadan El-Shatshat and Prof. Magdy Salama, for their professional guidance, advice, continual support, and encouragement. I would also like to thank all the members of my Ph.D. committee for their constructive comments.

My deepest thanks and endless appreciation go to my parents for their continuous support, love, care, and encouragement, as well as to my dear wife Fatma, and my lovely children, Yazan and Yasmin.

Dedication

This thesis is dedicated to:

To my beloved father, Ali

To my beloved mother, Fatima

To my lovely wife, Fatima,

To my dearest son Yazan, and my sweet daughter, Yasmin

To my beloved brothers and sisters

For your support, love, and encouragement.

Table of Contents

List of Figures

List of Tables

List of Acronyms

ADS	Active Distribution System
ANFIS	Adaptive Neuro-Fuzzy Inference Systems
ANN	Artificial Neural Network
SCB	Switched Capacitor Bank
CCU	Central Control Unit
DG	Distributed Generator
DN	Distribution Network
DNO	Distribution Network Operators
ELM	Extreme Learning Machine
EMS	Energy Management System
ESS	Energy Storage System
FL	Fuzzy Logic
FNN	Forward Neural Network
GA	Genetic Algorithm
HKF	Hybrid Kalman Filters
IBRES	Inverters-Based-RES
LDC	Line Drop Compensation
MAE	Mean Absolute Error
MAPE	Mean Absolute Percentage Error
MILP	Mixed Integer Linear Programming
MINLP	Mixed-Integer Nonlinear Programming
MISOCP	Mixed-Integer Second-Order Cone Programming
ML	Machine Learning
MLP	Multilayer Perceptron
NWP	Numerical Weather Prediction
OLTC	On-Load Tap Changing
OPF	Optimal Power Flow
PDS	Passive Distribution Systems

PDS	Power Distribution System
PSO	Particle Swarm Optimization
PVVC	Predictive Volt/Var Control
RBFNN	Radial Basis Function Neural Network
RES	Renewable Energy Source
RF	Random Forest
RMSE	Root Mean Square Error
SPC	Sequential Predictive Control
SDG	Smart Distribution Grid
SM	Smart Meter
SOM	Self-Organizing Map
STSE	Short-Term Stacking Ensemble
SVR	Step Voltage Regulator
WNN	Wavelet Neural Networks

Chapter 1
Introduction

1.1 Preamble

Driven by government incentives to install more clean energy resources, photovoltaic (PV) systems and wind turbines, which can be installed at different voltage levels, are globally among the fastest-growing renewable energy sources (RESs). The deployment of these renewable sources will consequently have a positive impact on the reduction of greenhouse gas emissions in the current electric grid. It was reported that the installed capacity of wind energy had increased worldwide by a factor of almost 75 in the past two decades, jumping from 7.5 gigawatts (GW) in 1997 to some 564 GW by 2018 [1]. In Canada, the Canadian Wind Energy Association believes that wind energy can satisfy 20 % of Canada's electricity demand by 2025, reaching a capacity of 55 GW [2]. In contrast, in 2017, the capacity of PV Generation represented 2% of the world power output, reaching a capacity of almost 400 GW and generating 460 TWh. By 2023, solar PV is expected to grow to 580 GW, as calculated by the International Energy Agency (IEA) [3].

The introduction of RESs can benefit a distribution network in terms of voltage support, loss reduction, equipment capacity release, and GHG emission reduction. All these remarkable benefits can be achieved only if energy resources are sized and located optimally in the network, and if their output is constant or adjustable to the network needs. However, with RESs such as wind or solar systems, these benefits fail to be fully achieved due to the intermittent output that depends on weather conditions as well as their locations, as some of them are not utility-owned. As an example, the output power of PV systems ranges from zero at night to the rated value during the daytime, depending on weather conditions. The high penetration level of RESs in distribution systems is accompanied by challenges such as voltage profile variation due to the variations in power outputs. In addition, renewable sources may cause reverse power flow at times of high penetration with light loads, which interfere with local controllers of Volt/Var devices such as on-load tap changer (OLTC), step voltage regulator (SVR), and switched capacitor (SC) banks. The local control variables of OLTC and SVR operate based on line drop compensator that regulates bus voltage next to the regulator bus, given that power flows from the regulator bus to the next bus. However, reverse power flow or injecting power between the regulator and the regulation point can confuse the local regulator controller, which leads to inappropriate or excessive operations.

The development of smart grid technology has allowed for many previous issues to be addressed. The smart grid is able to have a two-way flow of electricity and information, which allows it to accept energy from distributed RESs and for the monitoring of real-time data. With this extra information, it becomes easier to optimally and efficiently operate the power system in the presence of these RESs. The purpose of this dissertation is to present a methodology by which the Volt/Var settings, given the existence of RESs, are optimal. The malfunction of voltage regulators as a result of the random operation of renewable distributed energy units will be minimized. This work is further extended to formulate an optimum coordination plan that harmonizes the operation of different voltage and var control equipment. The primary goal is to improve the voltage profile along the feeders and reduce real power losses with a minimum number of Volt/Var device taps and/or switching movements under all loading conditions and for high penetration RESs. The case study results demonstrate that the proposed methodology can achieve higher efficiency at minimum cost compared to traditional tools.

1.2 Motivation

Unfortunately, distributed RESs cannot fit seamlessly in a conventional power grid that is designed without a specific distributed generation in mind. The random variations in power produced by weather-based generation cause different levels of uncertainty that affect a variety of decisions. The integration of RESs in a significant capacity with utility distribution systems has many benefits but, at the same time, faces many challenges. Issues pertaining to the impact of RESs on the power distribution system operation and control become extremely important for safety and quality as well as for the proper functioning of the power system. Of particular concern is their impact on the distribution system voltage profile and the operation of Volt/Var control devices. Although the Volt/Var control problem in distribution systems has been previously studied, it was under completely different operating conditions, with and without RESs; different solution methodologies for day-ahead or short time intervals were proposed. However, most of the related work does not consider the impact of RES output variations when it comes to short time operations and its impact on the optimal Volt/Var control solution. Also, no significant coordination between different control components was used, and no large scale implementation of intelligent tools was adopted. Motivated by the associated problems of the high penetration of intermittent energy sources, and the limitations of the existing tools for solving the Volt/Var problem, this research addresses these issues and provides solutions for Volt/Var control in highly renewable dominant smart distribution systems. This work also presents a day-ahead and sequential predictive Volt/Var control methodology to optimally operate smart grids to account for the

variations in generation and demand. The proposed methodology makes use of artificial intelligence tools to forecast RES output power and demand.

1.3 Research Objectives

The ultimate goal of this research is to investigate and introduce a new methodology for the Volt/Var control problem in smart distribution networks under the high penetration of renewable energy sources and all loading conditions. Managing and controlling the operation of Volt/Var control devices under high penetration of RESs will achieve the following objectives:

- Voltage profile along the feeders will be improved
- Active power losses will be minimized
- The Volt/Var device operations will be decreased

The objectives of this research will focus on three main respects:

1. Developing a very short-term forecasting algorithm to predict the outputs of PV and wind power systems for 15 minutes ahead. It is then extended to incorporate recent smart meter measurements into the forecasting model to be used with the short-term operation.
2. Developing a coordinated predictive control strategy for a day-ahead with limit RESs power variations, and make use of inverter interfaced RESs as ancillary service in coordination with the Vol/Var control devices to improve system performance
3. Developing a short-term Sequential Predictive Control (SPC) strategy based on real-time updated PV/Wind forecaster for optimum and cost-effective operation. The control problem will be solved following the rolling horizon approach with intervals of 15 minutes to minimize the uncertainties associated with RESs.
4. Developing an efficient solution based on a MISOCP convex optimization to guarantee the global solution. The nonconvex Volt/Var control problem will be converted into a convex formulation by linearizing the objective function subject to linear and conic constraints.

1.4 Thesis Outline

In addition to this introductory chapter, the following describes the structure of the remaining chapters.

Chapter 2 presents an introduction and a literature survey regarding the short-term forecasting of PV, wind, and load. Furthermore, a survey of previous work is conducted in the area of Volt/Var control in power distribution systems.

Chapter 3 introduces a very-short term ensemble forecasting model for PV, Wind, and demand. Artificial Neural Network (ANN), Radial Basis Function (RF), and Support Vector Regression (SVR) are used to build the stacked ensemble model, which is composed of two prediction layers.

Chapter 4 presents a day-ahead predictive Volt/Var control scheme for a smart distribution grid dominated by PV and Wind power systems. The model forecasts the generated power and demand for a day-ahead and then solves an optimization problem to coordinate the operation of the Volt/Var control devices at unity and variable power factors of inverter-based RESs. The objective is to minimize the overall operating cost in terms of power losses, the operational cost of Volt/Var devices, and minimizing the impact of RES power variations on the voltage profile.

Chapter 5 introduces a new sequential predictive control scheme based on real-time forecasting mechanisms for operating smart distribution systems subjected to high penetration and fluctuations of PV and wind systems. The problem is solved based on the rolling horizon optimization technique for intervals of 15 minutes. The original Volt/Var control problem, which is a MINLP optimization problem, is transformed into a MISOCP optimization problem to guarantee a global solution and solve the problem in a very-short time domain.

Chapter 6 presents the thesis summary, contribution, and directions for future work.

Chapter 2
Literature Review and Background

2.1 Preamble

Current interest in applying energy efficiency programs has driven distribution system operators to integrate more Renewable Energy Sources (RESs) and at the same time, develop effective methods for forecasting RES outputs and efficiently operating distribution systems. The following sections present a review of what has been achieved in literature in terms of RES and load forecasting, Vol/Var control in ADS and smart grids, and what techniques have been used to formulate and solve the voltage and reactive power control problem.

2.2 Survey on PV and Wind Power Forecasting

Solar and wind power generators are expected to play a substantial role on a global level as one of the leading Renewable Energy Sources (RESs) for future use. Translated into numbers, by 2023, solar PV is expected to grow to 580 GW, as calculated by the International Energy Agency (IEA) [3]. On the other hand, at a very fast pace of development, wind capacity evolved from 7.5 gigawatts (GW) in 1997 to some 564 GW by 2018 [1]. On a global scale, the revenue involved with renewable power ($285.9 billion) was more than twice the investment allocated to the conventional energy sources ($130 billion)at the end of 2015 [4]. As an example, in Canada, the government has set a target to reduce 20% greenhouse gas emission by the year 2020, considering a baseline from the year 2006. Most of these targets are expected to be met through RESs [5]. The penetration of RESs offers many advantages along with particular challenges to the operational reliability of the power system. The intermittent and fluctuating nature of PV and wind energy systems pose a significant challenge on grid stability and power resource scheduling. Hence, accurate forecasting can relieve some of these challenges and help network operators to schedule their resources in advance.

RES forecasting techniques, in general, can be classified into three main categories: (1) Numerical Weather Prediction models (NWP); (2) statistical and probabilistic models methods; and (3) Machine Learning (ML) and hybrid methods [6][7].

Reviewing their recent development and applications, ML has shown a unique ability in the area of RES forecasting. It has become one of the most popular approaches for either short or long term PV and wind power forecasting.

2.2.1 Solar PV Forecasting

Solar PV power forecasting depends on several factors, such as solar irradiance, reflectivity, estimation of PV cell temperature, and inverter efficiency [8]. The maximum power output is defined by

$$P = \mu\, SI\, [1 - 0.05(t_0 - 25)] \qquad 2.1$$

where μ is the conversion efficiency (%) of the solar cell array; S is the array area (m^2); I is the solar radiation (w/m^2); and t_0 is the outside air temperature (°C).

Forecasting PV output for several minutes, hours, days, or even years ahead is an essential practice conducted by power utilities to relieve the technical challenges raised by the intermittency of the generated power [7]. Different prediction horizons will correspond to specific needs of decision-making activities in power systems [9].

- Very short-term forecasting (from minutes to hours)
- Short-term forecasting (up to 1- 2 days ahead)
- Medium-term forecasting (up to 7 days ahead)
- Long-term forecasting (from 1 month to years)

Very short-term PV forecasting is an essential practice for effective operation and control of power grids. Accurate It is a necessary procedure particularly when solving a day-ahead or real-time Volt/Var control problem. From literature, several review papers summarized the previous and current PV forecasting techniques, as presented in [10][7][11][12][13] and [14]. Auto-Regressive Moving Average (ARMA), is one of the time series forecasting models used to forecast PV outputs due to its ability to extract useful statistical properties. [8]. The main drawback of the ARMA model is that the statistical properties of the time series do not change over time. Another popular statistical model used for PV forecasting is the Auto-Regressive Integrated Moving Average (ARIMA) model. The ARIMA model has the advantage of capturing the periodical cycle better than the ARMA model, as discussed in [15][16]. Artificial Intelligence (AI) has also shown a unique ability in solar PV forecasting, and it is used in several applications for approximating highly nonlinear system behavior.[17], Presented a one-day ahead forecasting model for a PV system based on Support Vector Machine(SVM) and the characteristic of weather classification. A Multilayer Perceptron (MLP) for short-term forecasting of PV output is presented in [18]. The inputs to the MLP are solar radiation, solar elevation angle, and temperature. A study in [19] presented a methodology based on the dynamics of Artificial Neural

Network (ANN) for hourly PV forecasting. First, the model predicts the main atmospheric parameters, namely, solar irradiance and air temperature, then uses another ANN model to predict the PV output.

A hybrid model based on Particle Swarm Optimization (PSO) with Extreme Learning Machine (ELM) technique for PV forecasting is presented in [9]. The PSO is used to update the weights of the ELM so that the prediction accuracy is improved. A PV power forecasting method based on a combination of a Genetic Algorithm (GA), PSO and Adaptive Neuro-Fuzzy Inference Systems (ANFIS) presented in [20]. The proposed hybrid method employs binary GA in the first stage to identify the most relevant subset of the input variables, while a combination of the GA and PSO algorithm in the second stage is used to optimize the ANFIS model. A weather-based hybrid method, combining Self-Organizing Map (SOM), Learning Vector Quantization (LVQ), SVR, and the fuzzy inference method for a day ahead forecasting of PV power output is presented in [21]. The proposed method comprises classification, training, and forecasting stages. The SOM and LVQ are used to classify the historical data, which is used in the training of SVR. When all SVRs are trained, the fuzzy inference selects the best predictor among them.

Ensemble method, which is popular in statistics and machine learning, uses multiple predictors to obtain an aggregated decision, which is better than any of the base predictors when applied individually [17]. Using real PV measured data, and various weather forecasts, a solar-time based analog ensemble PV forecasting method is presented in [22]. This method utilizes solar time, earth declination angle, and weather data to characterize historical measurement power data using table look-ups and weighted blending models. An ensemble method based on aggregating the outputs of Auto-Regressive, Forward Neural Network (FNN) and Radial Basis Function models is presented in [23]. The FNN and RBF were trained with PSO to enhance the training performance of the model.

Several PV generation forecasting models, based on physical, statistical, artificial, hybrid, and ensemble forecasting models, are proposed in the literature. Hybrid and ensemble models seem to have more generalized and accurate forecasting compared to classical forecasting models. Recent forecasting approaches focused more on ensemble models for their ability to combine individual models to form one output by either competing or collaborating.

2.2.2 Wind Power Forecasting

Wind power is generated by propelling a turbine to rotate, which converts the mechanical power to electrical power. The conversion from wind speed to Wind power is shown as [24]

$$P = \frac{1}{2}\,\rho\, A\, C_p(\lambda, \beta) v^3 \qquad 2.2$$

where ρ is the air density, A is the area of the turbine blade when rotating, $C_p(\lambda, \beta)$ is the efficiency, which is affected by two parameters: tip speed ratio λ and blade pitch angle β, and v is the up-wind speed.

The high intermittency and uncertainty associated with wind power have brought some challenges to power system operators, such as increasing the operating costs by increasing the requirements on primary reserves. Hence, the need to apply a robust and accurate forecasting model has become a persistent requirement. Several forecasting techniques, which were successfully applied to forecast wind power for minutes, and one hour ahead, are reported in the literature. In [25][26][27][28][29], a comprehensive overview of current and new developments in wind power forecasting is presented. A classification of wind power forecasting according to time–scale, ranging from very-short-term (a few minutes) to long-term (weeks or years), is discussed in [29].

Generally, forecasting models are classified into three categories: statistical models, artificial intelligence-based models, and hybrid/ensemble models. Statistical models such as AR, ARMA, ARIMA, Bayesian approach, and gray predictions are used for short-time forecasting, but the prediction error increases when the variations from the entered data are high [29]. Artificial intelligence-based models such ANN, SVR, and fuzzy logic, as well as heuristic techniques, are widely applied in wind power forecasting because of their ability to efficiently handle the non-linear relationship between variables [30]. Probabilistic wind power forecasting using RBFNN is proposed in [31]. The developed RBFNNs are trained with an ordinary orthogonal least square algorithm, and their parameters are optimally tuned using PSO. In other attempts, the forecasting accuracy of RBFNN showed some improvement when the RBFNN parameters are automatically selected using a GA as presented in [32]. An investigation into the performance of an SVR algorithm against that of MLP proved the effectiveness of SVR for wind speed prediction [33]. For improving the prediction accuracy of SVR, optimization algorithms are usually used to tune its parameters, which are the regularization parameter

C, ε-insensitive loss function, and the bandwidth of the Kernel function. Parameter tuning of an SVR using GA to improve forecasting accuracy by minimizing prediction error is presented in [34].

Ensemble models for wind power forecasting, such as bagging and boosting ensemble algorithms are presented in [35]. In [12], a review of ensemble methods for wind and solar power forecasting is presented, in which the author classified the ensemble models into competitive and cooperative models. A Random Forest (RF) ensemble algorithm for combining SVRs from base learners is presented in [36]. Hence, the author used an intelligent weighting approach that takes into account weather situations and past forecasts of the models. Authors in [37] investigated some methods for predicting the probability density function of a generated wind power from wind farm locations. They constructed probability density forecasts from weather ensemble predictions, which is a type of weather forecast generated from atmospheric models.

The high penetration of wind power systems imposes some challenges to power systems operation and planning due to its intermittent nature. Therefore, accurate, short-term Wind power forecasting has become essential, particularly in the context of smart grid operation and control. Several forecasting techniques are proposed in the literature. Some of them are good at short-term predictions, while others perform better in long-term predictions. However, very short-term forecasting models in the scale of minutes still an active area of research. Developing a very short-term forecaster able to capture the high nonlinearity in wind variations will positively impact the operation of power grids.

2.2.3 Load Forecasting

Short-Term Load Forecasting (STLF) is an essential task for energy planning, generation reserve, dispatching schedules, system security, and solving the Volt/Var control problem in distribution networks [38]. A review paper of electricity load forecasting, which discusses previous and current trends in load forecasting is presented in [39]. From literature, statistical models, such as auto-ARMA [40][41], ARIMA [42], and Seasonal ARIMA (SARMIA) [43] are widely used for short-term load forecasting.

In [44], a review paper investigated the application of AI-based on short-term load forecasting techniques. Short term load forecasting via SVR with tuned parameters is proposed in [45]. The proposed model has achieved forecasting accuracy comparable to sophisticated ensemble methods such as bagging and Random Forest(RF). New algorithms to train RBF networks for 24-hours electric load

forecasting is presented in [46]. The algorithm compared with the state-of-the-art model, and it shows a reliable forecasting accuracy. A Neural network algorithm for short-term load forecasting based on real data collected for 18 months, is proposed in [47]. The approach decomposing the load curve into daily average power and intraday power variation, where each model with different variables and complexities forecasts each component separately. A long short-term memory (LSTM) recurrent neural network-based framework applied for short-term load forecasting is discussed in [48]. Multiple benchmarks are comprehensively tested and compared to the proposed LSTM load forecasting framework on a real-world dataset.

Hybrid models are also used to improve forecasting accuracy, as discussed in [49], where PSO algorithm optimized the ANN weight values for hourly load forecasting. In [50], Wavelet Neural Networks (WNN) with data pre-filtering is developed to forecast loads for 1-hour using a moving window approach. Wavelet neural networks trained by Hybrid Kalman Filters (WNNHKF) for one-hour load forecasting is presented in [51].

From the literature, it seems that the variation in load data is less dependent on weather conditions, and the patterns from one day to another are almost the same. A small difference is observed between individual and hybrid models in terms of forecasting accuracy if the parameters of the individuals are optimally selected. However, the existing models are not performing very well when it comes to very short-term forecasting.

2.3 Power Distribution System (PDS)

Power distribution systems can be classified into two categories: passive distribution systems (PDS) and active distribution systems (ADS). A brief introductory followed by the role of Volt/Var control devices in both systems will be presented. In addition, the impact of high penetration of RES on the operation of ADS followed by a review of Volt/Var control techniques from literature is discussed.

2.3.1 Passive distribution systems

PDS is a typical distribution system fed solely from a distribution substation that services one or more primary feeders. In such systems, there is only one source and direction for power flow from a substation to users [52]. On-Load Tap Changer (OLTC), Step Voltage Regulator (SVR), and Switched Capacitor (SB) are the main components for voltage regulation and reactive power compensation in PDS. Figure 2.1 shows a typical PDS. Generally, OLTC/SVR and SC regulate the system's voltage and reduce losses based on their local control circuits and settings.

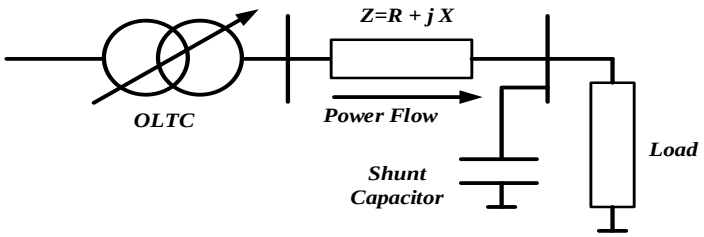

Figure 2.1 Simple passive distribution system

2.3.2 Active distribution system

ADS, as shown in Fig 2.2, is a new paradigm of the conventional distribution system that includes centralized and distributed generation from dispatchable and nondisposable energy sources. The presence of Distributed Generation (DG) and specifically RESs into the distribution system changes the topology of the system and the way it controlled.

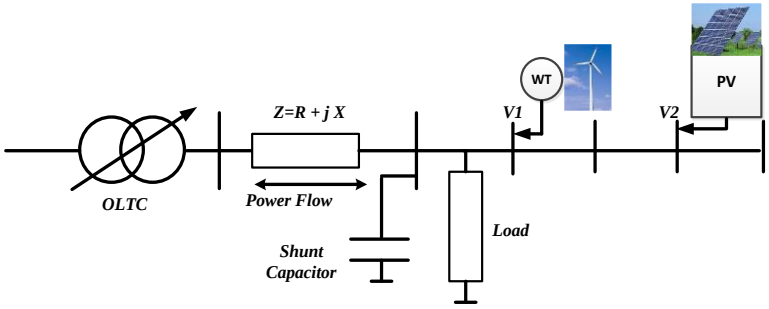

Figure 2.2 Simple active distribution system

The integration of RESs has several economic and operational benefits as discussed in [53][54][55][56]. However, the high penetration level of RESs may create some operational challenges such as reverse power flow, voltage fluctuation, undesirable or frequent operation of Volt/Var control devices. The coming is a brief introduction to the conventional Volt/Var control devices and the impact of the stochastic nature of RESs on system operation.

2.3.3 Voltage regulators

Voltage regulators such as OLTC and SVR play a primary role in regulating the voltage on feeders to maintain it within certain limits as shown in Equation 2.3, where V_i is the nominal voltage and

V^{min} and V^{max} are voltage limits. OLTC transformer regulates the secondary voltage at the substation, while SVR can be connected at the distribution substation or downstream the substation.

$$V^{min} \leq V_i \leq V^{max} \quad 2.3$$

OLTC/SVR are able to change the voltage in the range of ± 5% or ± - 10% [57]. Changing the taps of OLTC and SVR is determined by the Line Drop Compensator (LDC) that estimates the voltage drop along the line and regulate the voltage based on compensation circuit current I_{com}, load side voltage V_{reg} and equivalent parameters R' and X'. Figure 2.3 shows the control circuit and how it is connected to the line with line equivalent parameters R_{Line} and X_{Line}.

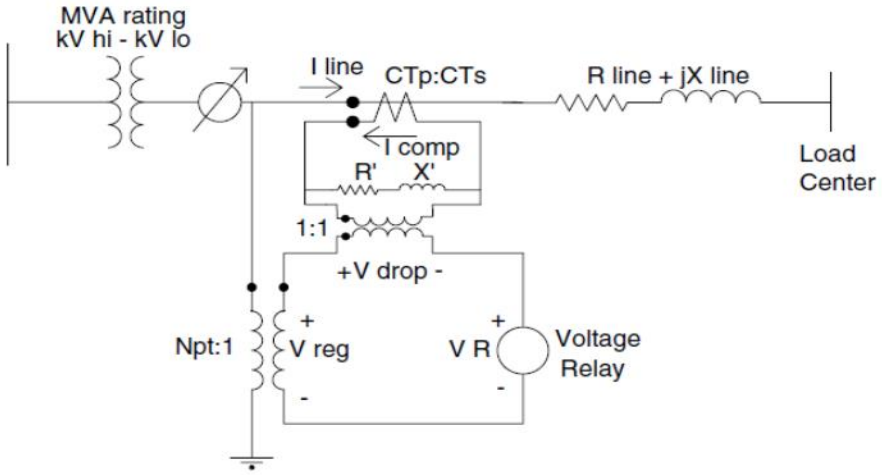

Figure 2.3 Line drop compensator circuit [30]

The voltage drop V_{drop} and the relay voltage V_R are calculated from Equations 2.4 and 2.5 as follows:

$$V_{drop} = I_{com}\,(R' + jX') \quad 2.4$$

$$V_R = V_{reg} - V_{drop} \quad 2.5$$

When the voltage at the load center or the regulation point estimated by the voltage drop exceeds the limit, the LDC issues a control signal to the motor to adjust the tap up or down to regulate the voltage.

2.3.4 Switched capacitor bank

Fixed and switched capacitors are widely used in distribution systems at secondary substation bus and feeders. The line reactive power can be reduced by installing an SC at the substation or the feeder. SCs

are modelled as a constant susceptance connected in either wye or delta. The operation of shunt capacitors is based on current, voltage, time, temperature, KVAR, or intelligent control modes[58].

2.4 Impact of RESs on Voltage and Volt/Var Control Devices

The high integration of RESs usually causes some technical challenges to network operators. Given their remarkable benefits [53][54][55][56], the fluctuation in the generated power from RESs is one of the main reasons for voltage fluctuation, which may lead to frequent operations for the Volt/Var control devices. This unfavorable operating condition occurs if there is no coordination between the Volt/Var control devices. Also, if the control devices use their local control circuits, assuming that no power injected between the remote control point and the regulator.

2.4.1 Impact of RESs on system voltage

The operational conditions of power distribution systems are described by voltage and phase shift at each busbar, as well as, active and reactive power in each line. In ADS, the penetration level of RESs may particularly affect the voltage on the RES bus and generally on the system. Figure 2.4 shows a simplified diagram of a radial distribution system. The DG at bus 3 injects active and reactive power into the system. The voltage drop on the feeder can be calculated from Equation 2.6 where R_L and X_L are the resistance and reactance of the line. P_L and P_{DG} are the active power of load and DG; whereas Q_L and Q_{DG} are the reactive power of the load and DG, respectively. It can be seen from Equation 2.6 that if the active power from DG increased, the voltage at the end of the feeder V3 would increase.

$$V_3 - V_2 \cong \frac{R_L(P_L - P_{DG}) + X_L(Q_L \pm Q_{DG})}{V_2} \qquad 2.6$$

The presence of the DG at bus 3 may raise the voltage over the allowable limit according to the size of the DG relative to the load size, which may increase the general voltage of the feeder when the term $(P_L - P_{DG})$ is negative[59].

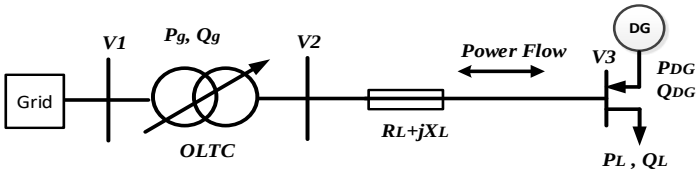

Figure 2.4 One-line diagram to illustrate the impact of DG on bus voltage

2.4.2 Impact of RESs on OLTC, SVR, and SC operations

Radial distribution system voltages are usually regulated using OLTC at the substation, SVR, and SC on feeders. OLTC and SVR operate based on LDC considering unidirectional power flow from the substation transformer to loads. The LDC estimates the line voltage drop and performs voltage correction based on line current, line R, and X parameters and load side voltage. Due to the presence of RESs, power flow could be unidirectional or bidirectional depending on the RES output and the load size. In the reverse power mode, where the power generated from the RES exceeds the load, the voltage regulator will be operating in reverse mode to regulate the substation voltage. If the set-point of the substation transformer is higher than the set-point of the regulator, the regulator will step down to lower the voltage [55]. The high penetration and fluctuation of RESs may increase the operation of OLTC/SVR if no efficient coordination scheme is applied [60]. The propagation of the voltage oscillation due to RESs output change may result in feeder voltages exceeding the voltage limits, which enforce the OLTC and SVR to regulate feeder voltage every time the voltage goes over or under the specified range [61]. Hence, frequent operations of tap changers of OLTC or SVR will result in a reduction of tap changers' life expectancy and higher maintenance costs[62].

The operation of SC is also sensitive to the installation of RESs based on its control mode. If the capacitor uses a voltage control mode, the RESs may affect the operation of the capacitor if overvoltage occurs. For SC using line current control mode, the RES changes the line current if it is connected downstream the capacitor. For the other control modes used by SC, such as time and temperature control modes, the RES impact the capacitor operation if it operates based on constant power factor,

which increases the feeder end voltage when the capacitor switched on and the RESs still operating [58].

2.5 Volt/Var Control in Active Distribution System

Recently, there is a significant interest in integrating distributed generation and specifically RESs into the distribution systems. However, the outputs of RESs are prone to intermittency and uncertainty, which leads to voltage rise, fluctuation, and improper conventional control operation. The conventional Volt/Var control devices such as OLTC, SVR, and SC are limited by their physical constraints, which can not respond to fast voltage variation triggered by a high fluctuation in the generated power from RESs. Therefore, a new Volt/Var control strategy should be considered for safe and reliable operation of power networks. From literature, several techniques of voltage and reactive power control are proposed. These techniques can be categorized based on communication requirements as centralized, distributed, and decentralized with a purely local option [63].

Volt/Var control problem is usually formulated as an optimization problem based on various objective functions subject to system constraints. An objective of minimizing total switching operations and determining the optimal coordination between the control devices is proposed in [64][65][66][67][68][69]. Here, the authors investigated and solved the Volt/Var control problem with the objective of minimizing the control effort. Minimizing the switching operations will minimize the associated operating costs and increases the expected life of the control devices. Such optimization problems are usually formulated as MINLP and solved using heuristic search techniques such as PSO and ANN. Control variables such as OLTC, SVR, SC, and RESs are coordinated by formulating an optimization problem for optimal operational scheduling so that voltage deviation and control effort are both minimized. The control process is solved from one centralized point considering a full communication infrastructure are exists. From the mentioned papers, the optimal scheduling is determined based on the hourly forecasting of load and RESs output for 24 hours. The DG's inverters are coordinated with the conventional Volt/Var control devices for optimal solution. Another type of research papers investigated and proposed solutions for Volt/Var control problem by formulating the problem such that the total system losses are minimized as proposed in [65][66][69] [70][71][72][73][74] [75][76] [77]. Authors here applied centralized control schemes to minimize losses by controlling the flow of reactive power. Control variables such as OLTC, SC, SVR, and inverters are coordinated by solving MINLP problem. Formulating the optimization problem to

minimize power losses in the network is commonly used to enhance system efficiency and reduce the operation cost. The hourly forecasting output power of renewable energy sources and demands is performed in [65][71][73][74], where power flow problem is solved for a day ahead to determine the optimum settings of control devices on hour basis. The optimization problems in [65][76] are formulated as MINLP and solved by heuristic techniques subjected to system constraints. Additionally, high penetration level of RESs is investigated in [71][75]. The problem solved by controllable loads and microgeneration shedding in coordination among control devices. Minimizing voltage deviation from a nominal value due to the variation in loading conditions or high penetration of renewable sourcess is another approach to solve the Volt/Var control problem. Authors of [78][72][67] proposed voltage control methodology to coordinate LTC, SVR, and inverters interfaced RESs to minimize voltage deviation. Usually, this objective function is applied when there is a high penetration level of intermittent power sources. This formulation mitigates the voltage variation caused by the fluctuation of RESs. A methodology for generation curtailment due to voltage constraints was addressed in [79]. The approach aims to satisfy system constraints by curtailing distributed renewable sources in the case of high voltage imposed by reverse power flow considering a voltage sensitivity factor. A methodology for incorporating charging station of PEV in controlling the distribution system voltage in two steps through a centralized controller and under the high penetration level of PVs was introduced in [80]. In general, centralized Volt/Var control problem in ADS are usually solved using one of the aforementioned three objective functions or a combination between them depending on the type and requirement of the problem. Other approaches choose different objective functions based on problem type such as maximizing the output power from DERS or curtailing them to satisfy system constraints.

The decentralized control is another type of control strategies used in ADS for Volt/Var control. Solving the optimization problem in decentralized control mode is similar to the one used in centralized control mode. However, in a decentralized control model usually there is more than one optimization problem to be solved. If the distribution system is zoned or sectionalized, then each zone or local control area requires an objective function to be optimized with or without coordination with other local areas. In literature, many research papers tackled the Volt/Var control problem using decentralized control. Numerous research work applied power loss minimization as an objective function, as in[81][82][83]. The authors investigated and proposed solutions to the problem when having a high penetration of RES installed on distribution level. A decentralized control approach was applied to coordinate control variables in order to improve voltage profile in the presence of high RESs output power. Moreover,

minimizing voltage deviation was the objective function used in [81][84][85][83][86][87][88]. In [81], a decentralized control approach is used to coordinate SVR, and SC for optimal voltage profile with the presence of a PV system using feed-forward neural network FFNN trained and optimal data generated by Genetic Algorithm. Authors of [84], proposed a decentralized reactive power control considering remote terminal units (RTUs) installed at each DG and shunt capacitors. Coordination among RTUs through communication channels was implemented to regulate voltage profile and minimize system losses. In [85], power factor control of DGs and multi-agent technology considering the response delay of shunt capacitor and OLTC are used to regulate bus voltage. While in [86], two stages control methodology for voltage control at busbar was proposed. In the first stage, the required reactive power from a connected DG unit to support a violated busbar voltage is estimated. In the second stage, if the violated busbar voltage cannot be regulated locally by the connected DG due to its capacity, a distributed algorithm exchange information with other controllers at neighbor busbar to compensate the reactive power in order to bring voltage to its desired limit. In addition, [87] proposed a control strategy for voltage rise due to the integration of distributed generation. The controller optimally limits the reactive power injected by DGs to a level prevents voltage violation and keeps the conventional voltage control approach runs by the distribution network operators. In [88], a decentralized voltage control scheme is proposed to handle the problem of high penetration of renewable generation. The suggested control approach aims to effectively control traditional voltage regulators OLTC, and SVR by using multi-agent control system that controls single areas locally rather than centralized control.

Several Volt/Var control methodologies and techniques are investigated and implemented in the literature. The new infrastructure of distribution systems depends on communications and smart meters to play an essential role in the successful control strategy. Passive systems controlled based on unidirectional power flow, while the active system is controlled based on bidirectional power flow due to the existence of RESs. In literature many papers tackled the problem of high penetration of RESs and their impact on voltage profile. Proper forecasting techniques of loads and renewable generations in order to predict the actual demand and output power respectively played an essential role in the appropriate control strategy. Researchers proposed solutions for appropriate control actions under large installation of RESs by minimizing the control efforts as a function of operational cost with or without coordination with RESs output. However, the high penetration and fluctuation of RESs make the Volt/Var control problem more complex. Therefore, better solution techniques that account for the

high uncertainty of these resources are needed. The very short-term operation and control of distribution system are better than the daily or hourly operations when PV and wind power systems are highly installed at the distribution level. The existing solution methodologies need to be accurate and fast in terms of computation cost with global solutions to cope with very fast variations of RESs and demand.

2.6 Discussion and Conclusion

Accurate forecasting of PV/wind power systems and demand is an important task for optimally operating ADS. From literature, the recent development in ML techniques will promote them to play an essential role in RESs output forecasting. With the increasing demand for RESs, accurate short-term forecasting will be the main focus of system operators to efficiently schedule power resource.

Different Volt/Var control methodologies and techniques are investigated and implemented in the literature. The new infrastructures of a distribution system depend on communication and smart meters to play an important role in the effectiveness of a successful control strategy. The method of controlling a passive distribution system differs from that of an active distribution system. For some distribution networks, it is feasible to apply centralized control if there is a full communication channel between all control equipment and the centralized controller. In contrast, the decentralized control approach can be applied locally or for specific zones, given that communication is only needed between local control devices. The existence of RESs, as well as variable demands, may cause changes in the operational situation. In traditional distribution networks, the OLTC, SVR, and SC regulate any violated voltages based on LDC without considering the stream of the power flow caused RESs. The issue of having a high penetration level of RESs into the distribution system causes voltage fluctuation at the connection point, which forces the voltage regulators to respond more frequently to marinating the voltage within limits.

Given the previous operating challenges, it seems there is a need for a control Volt/Var control model able to operate distribution systems under high penetration and fluctuation of RESs in a very short time intervals. A fast and efficient algorithm for solving the Volt/Var control problem with the incorporation of RES outputs forecasting has become a favorable solution.

Chapter 3
Very Short-Term Ensemble PV and Wind and Load Forecasting

3.1 Preamble

Due to the growing demand for clean and renewable energy, PV and wind power farms are being installed to a great extent in both transmission and distribution networks. However, the stochastic and intermittent nature of RES brings some real operational challenges to system operators, especially at large-scale penetration levels. Voltage fluctuation, reverse power flow, and frequent operations of Volt/Var control devices are some of the challenges that system operators may encounter. Therefore, system operators make use of PV, wind, and load forecasting to schedule their resources in advance to ensure efficient and cost-effective operation. Hence, an accurate very short-term forecasting model is required to account for generation/demand uncertainties, especially when it comes to smart grid operation and control.

Generally, PV/wind generation and demand can be forecasted based on two approaches. The first approach estimates the meteorological parameters such as solar irradiance, air temperature, wind speed/direction, and then predict the output power. The second approach uses historical and current records of power data to forecast future samples based on statistical or artificial methods [89]. In this chapter, a very Short-Term Stacking Ensemble (STSE) forecasting model is developed to predict the generated power from PV and wind systems for intervals of 15-minutes. The proposed approach combines a heterogeneous machine learning algorithm composed of three well-established models: Support Vector Regression (SVR), Radial Basis Function Neural Network (RBFNN), and Random Forest (RF) heuristically via SVR. The aim of the proposed STSE model is:

- Integrates heterogeneous algorithms to build a robust and generalized forecasting model
- Minimizes the prediction error by appropriately tunning the meat-learner parameter
- Accurately predicts PV/wind output power for short-term intervals
- Assists system operators in scheduling their energy resources and setting optimal control plans

The proposed STSE model is evaluated using evaluation metrics such as Root Mean Square Error (RMSE), Mean Absolute Error (MAE), and Mean Absolute Percentage Error (MAPE). Further analysis related to correlation and comparison with individual base models SVR, REFNN, RF, and classical models such as Multilayer Perceptron (MLP) is conducted. On the other side, historical residential load data, which has less variation compared with PV/wind data, is used to build an SVR forecasting model to predict power consumption for intervals of 15 minutes. Using SVR for load forecasting has been evaluated, and the results were comparable with the STSE model.

3.2 Stacking Ensemble Model

Ensemble learning improves the accuracy of machine learning by combining several models, which are initially developed to reduce the variability in classification/regression decisions and thereby increase generalization performance [90]. The stacking algorithm is an ensemble learning technique in which the predictions of individual learners in one layer are used to train a second layer learning algorithm (meta-learner)

In this thesis, the proposed STSE model combines three diversified time series forecasting techniques, which are SVR, RBFNN, RF, via SVR. The criterion for constructing an efficient ensemble predictor is based on; (i) reliability of the base predictors for forecasting time series data set, and (ii) the number of the predictors that can achieve high performance. The advantage of using an ensemble model is that it reduces the effect of the "concept drift" phenomenon [91], which causes problems because the predictions become less accurate as time passes.

3.2.1 Model structure

The proposed STSE model is illustrated in Figure 3.1. The process starts with preprocessing power data as discussed in Section 3.2.3 and then uses the processed time series data for training base learners located in the first layer (RF, RBFNN, and SVR). The outputs of the base learners are then used to train a second learner (SVR) located in the second layer to form the final prediction.

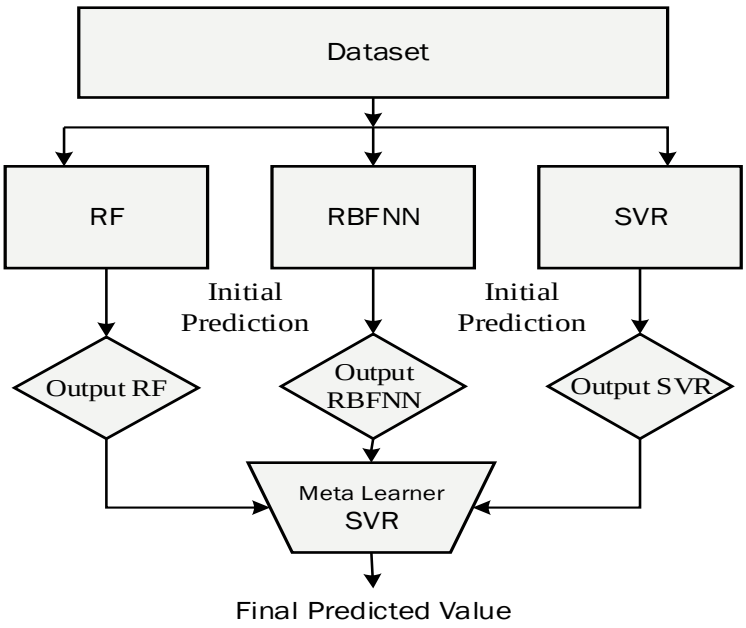

Figure 3.1 STSE Proposed forecasting model

The following is a brief description of each learning algorithm.

3.2.1.1 Support vector regression

SVR, which is based on Vapnik's concept of support vectors [92], is introduced firstly in [93]. The concept of SVR is based on the computation of linear regression function in a higher dimensional feature space. One of the main characteristics of SVR is that instead of minimizing the observed training error, it attempts to minimize the generalized error bound to achieve generalized performance. The generalization error bound is the combination of the training error and a regularization term that controls the complexity of the hypothesis space [94].

Giving a set of training samples:

$$\{(x_1, y_1), \dots \dots (x_n, y_n)\}\, with\, x_i \epsilon\, R^d \quad and \quad y_i \epsilon\, R$$

The linear regression model can be expressed as:

$$f(x) = w_1\, x_1 + w_2 x_2 + \cdots . w_n x_n + b = \langle w, x \rangle + b \qquad 3.1$$

where $w = [w_1\, w_{2,} \ldots, w_n]^T$ represents the vector of coefficients and b represents the bias. The regression problem can be addressed by solving the following constrained optimization problem [95].

$$\underbrace{Min}_{w,b,\xi,\xi^*_,} \ \frac{1}{2}\, w^T w + C\ \sum_{i=1}^{n}(\xi_i + \xi_i^*) \qquad 3.2$$

Subject to the following constraints

$$y_i - (w^T \emptyset(x_i) + b\,) \leq\ \varepsilon + \xi_i \qquad 3.3$$

$$(w^T \emptyset(x_i) + b\,) - y_i\ \leq \varepsilon + \xi_i^* \qquad 3.4$$

$$\xi_i, \xi_i^*\ \geq 0, \quad i = 1, \ldots, n \qquad 3.5$$

where x_i is mapped to a higher dimensional space by the Kernel function $\emptyset$. ξ_i^* and ξ are slack variables subject to the ε-insensitive tube. The parameters, which control the prediction accuracy, are the regularization parameter C , the width of the tube ε and the mapping function $\emptyset$. By applying the Lagrange multiplier method and fulfilling Karnsh-Kuhn-Tucker (KKT) conditions, the dual form is transformed into an optimization function as explained in appendix A [96].

3.2.1.2 Radial basis function neural networks

The RBFNN is a particular kind of neural network widely used in function approximation and time-series predictions. It is a three-layer feed-forward network consisting of an input layer, hidden layer, and an output layer. RBFNN generally uses a linear transfer function for the output units and a nonlinear transfer function for the hidden units. Its input layer consists of source nodes connected by weighted connections to the hidden layer, and the net input to a hidden unit is a distance measure between the input presented at the input layer and the point represented by the hidden layer [97].

3.2.1.3 Random Forest

Random forest is a non-parametric ensemble-based learning technique used for classification and regression suggested by L. Breiman [98]. RFs for regression are formed by growing trees depending on a random vector such that the tree predictor takes on numerical values as opposed to class labels. The output values are numerical, and we assume that the training set is independently taken from the distribution of the random vector. The random forest estimator is formed by taking the average over a number of trees similar to the classification scenario [98].

3.2.2 STSE algorithm

The design of the algorithm takes into consideration the diversity of the model and the proper selection of the base models. The pseudo-code of the proposed stacking ensemble algorithm is shown in algorithm 1.

Algorithm 1. Short-Term Staking Ensemble (STSE)

Input: Data set D = $\{(x_1, y_1), (x_2, y_2), \dots \dots \dots (x_m, y_m)\}$
First-level learning algorithm $L_1, \dots \dots L_n$;
Second-level learning algorithm$L$;

Process

% Train the 1st level individual learner h_t by applying the first level learning algorithm L_t to the original data set D

For $t = 1, 2, \dots, T$:
$h_t = L_t(D)$
End;

% Generate a new data set

$D' = \emptyset$;
For $i = 1,2, \dots ., m$
For $t = 1,2, \dots ., T$
$z_{it} = h_t(x_i)$ % *use* h_t *to predicit the training example* x_i
End;
$D' = D' \cup \{\left(\left(z_{i1}, z_{i2}, \dots \dots z_{ij}\right), y_i\right)\}$
End;
Train the 2nd level learner SVR using 2nd level algorithm L to the new data set D'

$h' = L(D')$

Output: $H(x) = h'\left(h_1(x), h_2(x), \dots \dots ., h_T(x)\right)$

3.2.3 Data Ppocessing and model evaluation

3.2.3.1 Data processing

The time-series data was measured chronologically from January 1, 2014, to Dec 31, 2014, with readings taken every 15 min. The measured data represents a very short-term interval recorded from PV, and wind power farms located on Waterloo, ON, Canada, whereas the load data was provided from a utility measured at the same date [99]. Winter season data from Jan 1, to March 30, 2014, is used to

train and test the model. The data is normalized between 0 and 1, according to Equation 3.6. The data is then divided into training and testing sets to train and evaluate the model.

$$x_i = \frac{P_i - P^{min}}{P^{max} - P^{min}} \quad 3.6$$

where $P = (P_1, P_2, \dots\dots, P_n)$ represents the original measured data before normalization and x_i is the i^{th} normalized data.

3.2.3.2 Model evaluation

To evaluate the prediction performance of the base models and the proposed stacked model, MAE, RMSE, and MAPE are the evaluation metrics defined as:

$$MAE = \frac{1}{N} \sum_{n=}^{N} |x_n - y_n| \quad 3.7$$

$$RMSE = \sqrt{\frac{1}{N} \sum_{n=1}^{N} (x_n - y_n)^2} \quad 3.8$$

$$MAPE = \frac{1}{N} \sum_{n=1}^{N} \left| \frac{x_n - y_n}{y_n} \right| \quad 3.9$$

where x_n and y_n are the forecasted and the desired values respectively, and N is the total number of samples.

3.2.4 Short and very-short term forecasting comparison

In this section, the hourly PV and wind power outputs are compared with the 15-min outputs on the same date and time. The purpose is to show that during the hourly forecast, some information between one hour and another will be missed in the hourly forecasting. The hourly forecast is acceptable when the penetration and output variations of renewables are relatively low. However, in operational scheduling or real-time operation of a distribution network under high penetration of renewables, short-time forecasting provides more information about the status of the system, and hence, proper control decisions can be effectively made. For demonstration, Figure 3.2 and Figure 3.3 show the difference between the hourly and 15 min outputs as specified from the circled and zoomed-in data for PV and wind power systems respectively.

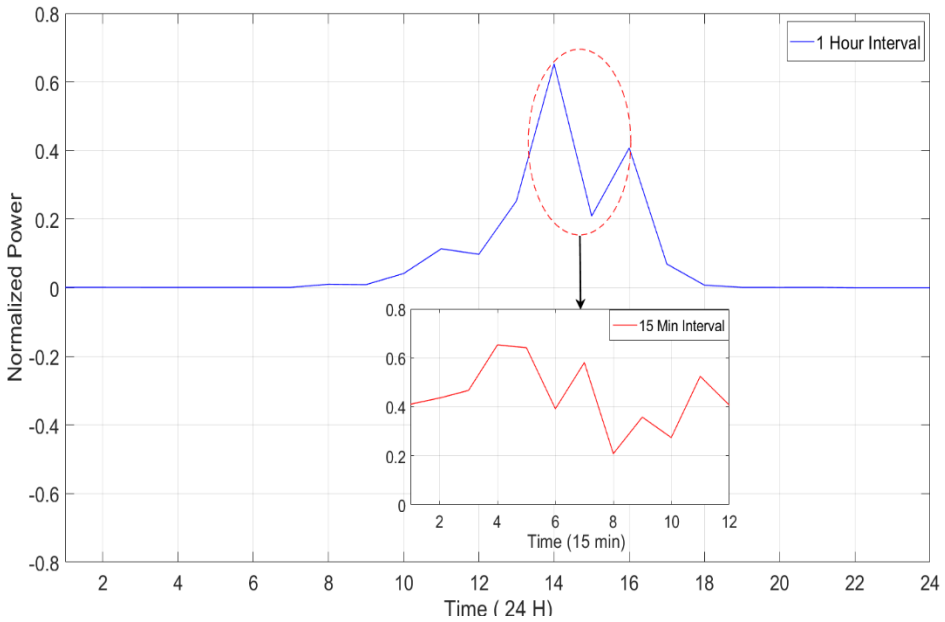

Figure 3.2. Hourly and 15min PV output

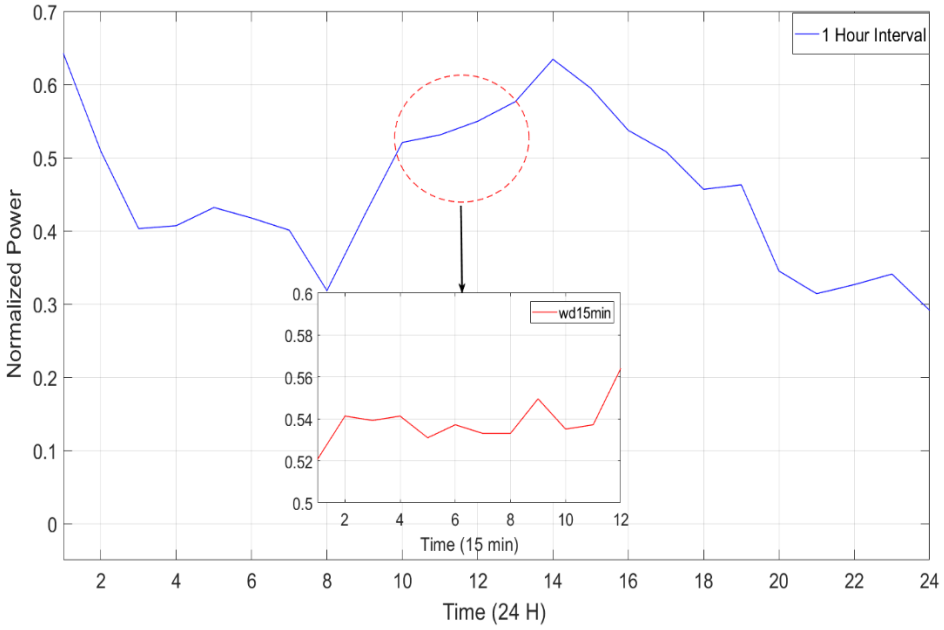

Figure 3.3. Hourly and 15min Wind output

It can be seen from both figures that the PV and wind power outputs on an hourly basis will miss some information about the actual variations that may occur at short time intervals. Therefore, the 15minutes forecasting interval is more reliable and efficient techniques to account for high variations that occur at short intervals, which affects the decisions of the network operator.

3.2.5 PV power forecasting

Figure 3.4 shows the normalized output data of a PV system measured at intervals of 15-minutes for one year from Jan 01, 2014 to Dec 31, 2014. Also, PV output for a selected three days from Feb 15, 2014, to Feb 17, 2014, is shown in the second plot of Figure 3.4. Generally, solar radiation plays a primary role in PV power generation. On sunny days, where solar radiation is almost the same, usually, there is a high correlation between power data from day to another. On the other side, on cloudy, rainy, or foggy days, solar radiation is affected by weather conditions, and hence, power varies to a great extent accordingly.

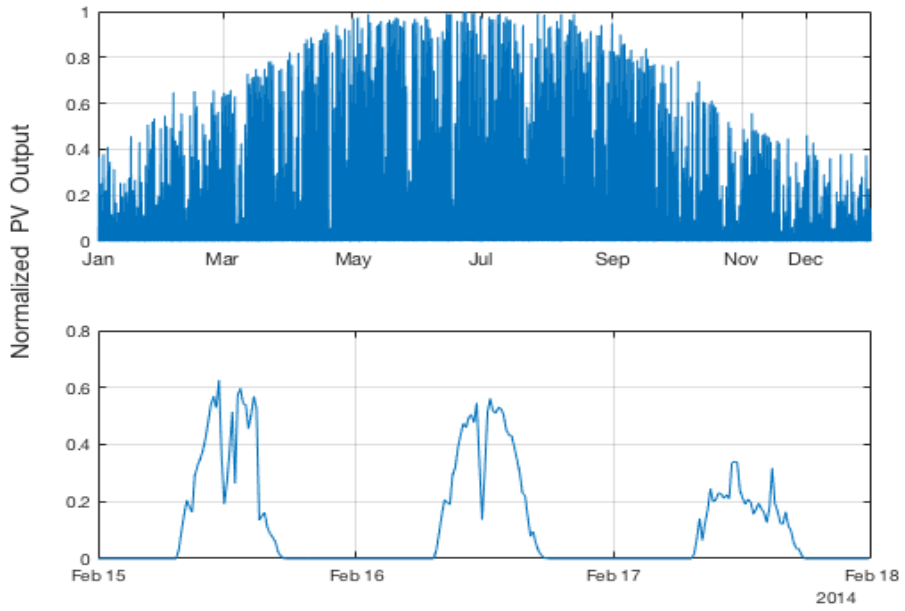

Figure 3.4 Normalized PV output

After processing and normalizing the recorded data, the STSE model is built for short-term PV output forecasting. To achieve a precise and generalized forecasting process, the parameters of the forecasted model need to be appropriately selected as they have a particular impact on the model performance.

From literature, some researchers tuned the parameters of the SVR and RBFNN by applying some optimization algorithms such as GA as discussed in [32][34] using the training data set. However, the tuning process using heuristic search techniques adds a more computational burden to the forecasting process. In this model, tuning the base learners' parameters and the meta-learner parameters SVR is performed using cross-validation from the libsvm library [100]. A cross-validation technique using preceding sections to forecast future segments in order is applied to follow the direction character of the time series forecasting. An experiment on the impact of the regularization parameter C is performed to check its effect on RMSE and MAE values. From Figure 3.5, it can be seen that changing the regularization parameter C from 0.01 to 100 has a small impact on the prediction accuracy

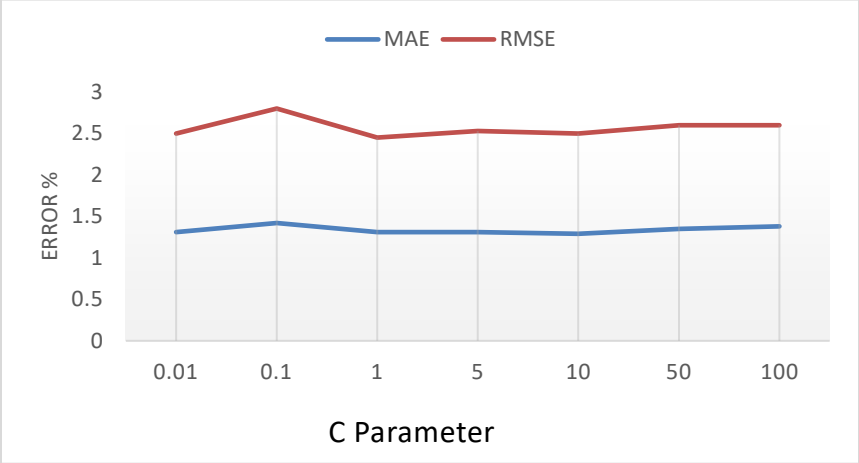

Figure 3.5. Impact of C Parameter on MAE and RMSE

The regularization parameter C is selected to be 1.0 as a trade-off between overfitting and generalization. The RBF Kernel, as shown in 3.10, is chosen to perform nonlinear prediction.

$$K(x, y) = \exp\left(-\frac{\|x_n - x_i\|^2}{2\sigma^2}\right) \qquad 3.10$$

where σ = 0.001 is a constant determining the width of the RBF kernel, and the term $\|x_n - x_i\|^2$, is the squared Euclidean distance between two feature vectors, and epsilon=0.001.

When the appropriate parameters of the meta-learner SVR are determined, the STSE model is applied to the data set to predict future PV outputs. Figure 3.6 shows the forecasting of the STSE model on a sample of the data set, March 30, 2014, with a prediction step of 15 min. As can be seen, there is an adequate match between the actual and predicted data.

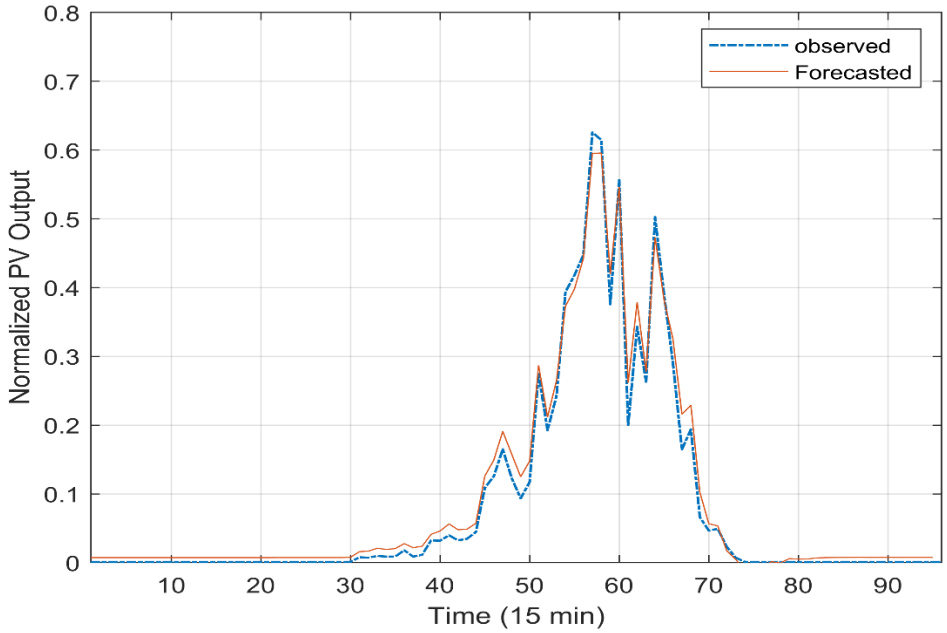

Figure 3.6 Prediction of the STSE model

A good correlation between the observed and the predicted data can be observed in Figure 3.7, which is 0.968. A value of correlation close to 1 indicates high accuracy of the forecasting model.

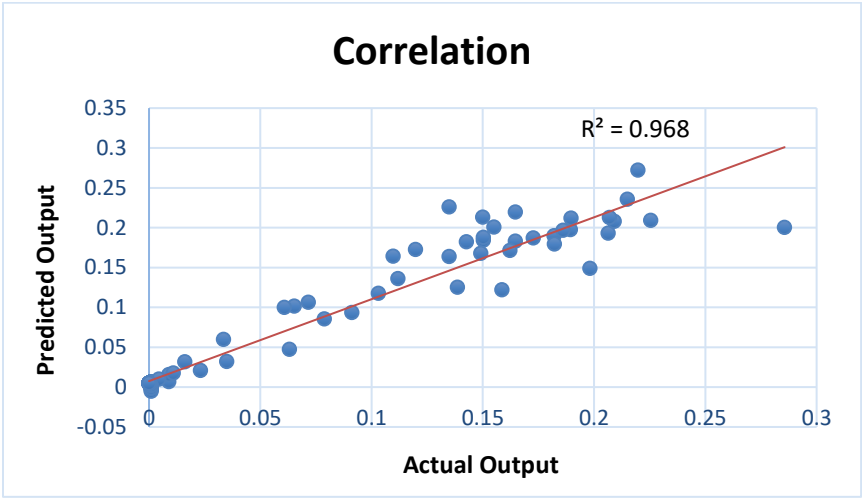

Figure 3.7. Correlation between actual and predicted data

To compare the prediction accuracy of the ensemble model, a comparison with the base models SVR, RBFNN, and RF on the same data set is conducted, where the base models trained and tested as stand-alone models. Figure 3.8 shows the performance of the base models SVR, RBFNN, and RF with a prediction step of 15 minutes. It can be seen from the figure that the ensemble model is the closest to the actual data line (dashed line) compared with the other models.

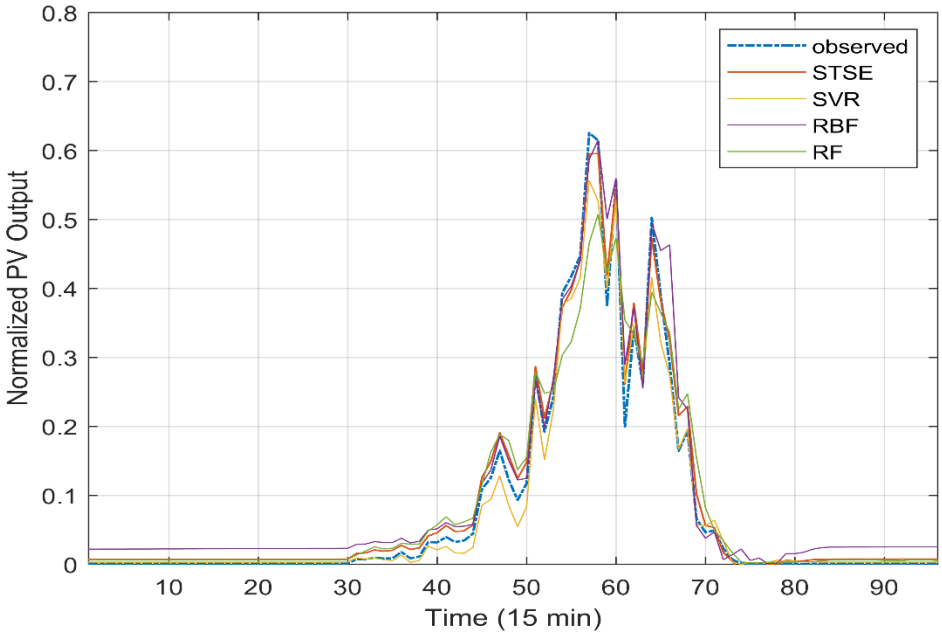

Figure 3.8. Prediction of All models

Although the individual models achieve a certain degree of accuracy, they are not exactly following the trend and the variability of the actual generated power compared with STSE.

Table 3-1 shows the performance metrics of each model after evaluation. The forecasting process has been conducted on each model individually at first, and then the proposed stacked model is used for comparison purposes. Noticeably, the proposed model outperformed the individual models in terms of prediction error minimization specifically for the RMSE. The strength of the model comes from its ability to learn from three heterogeneous models determined by different algorithms. Further comparison is conducted with other forecasting models such as MLP to compare the proposed model with state-of-the-art models.

Table 3-1**.** Comparison between the proposed and base models

Model	MAPE%	RMSE	MAE
SVR	0.82	0.0647	0.0351
RBFNN	3.53	0.0749	0.0403
RF	1.35	0.0601	0.0319
STSE	1.27	0.0445	0.0229
MLP	2.19	0.056	0.0324

The prediction accuracy of the proposed model for forecasting PV output for a very-short interval has been proven and compared with state-of-the-art models. The correlation and evaluation metrics show that the STSE model is efficient and reliable and can be used in power system control and operation.

3.2.6 Wind power forecasting

Wind power is generated by wind propelling a turbine to rotate, which converts the mechanical energy to electrical energy. Wind speed and direction determines the amount of electricity generated by a turbine. Changes in wind speed and direction lead to intermittent power generation, which brings severe challenges to the power system at the large-scale penetration level. Therefore, the proposed STSE model is applied to predict the generated power from past time-series wind power data.

Wind power data measured chronologically from January 1, 2014, to Dec 31, 2014, with readings taken every 15 minutes are used. The data are processed and normalized between 0 and 1 as discussed previously. Following the same procedure, the training process is conducted on a subsection from the data set from Jan 1 to March 30, 2014. Figure 3.9 shows the power data generated from a wind turbine for one year and for three selected days from Feb 15, to Feb 17, 2014. Unlike PV output, which is characterized by its periodicity due to irradiance time, wind power patterns are unlikely to repeat on a daily basis, and it has peaks and off-peaks depending on wind speed and direction.

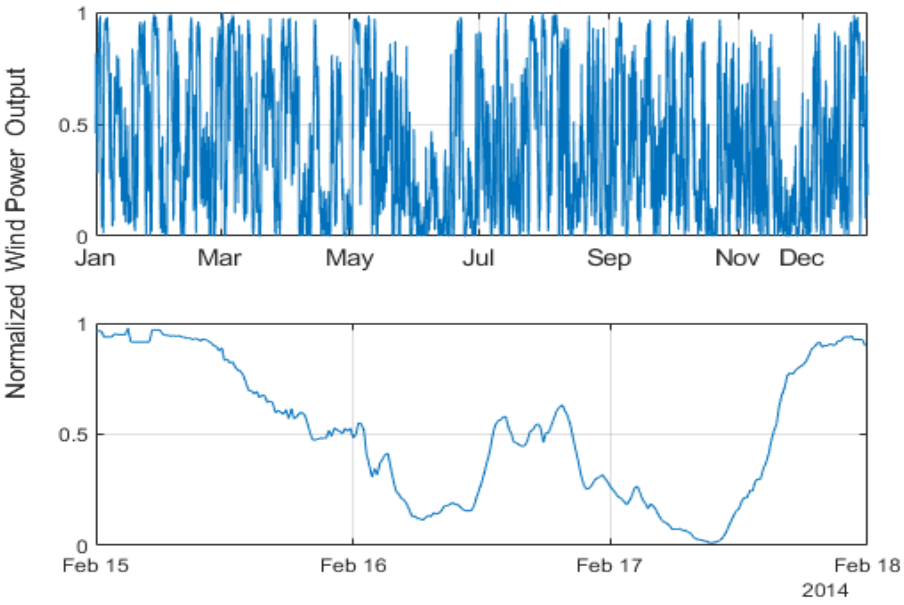

Figure 3.9. Normalized Wind Power Output

Tuning the base learners' parameters and the meta-learner parameters of SVR is conducted in the same way as discussed in section 3.2.3. The best estimate for the regularization parameter C is 5.0. Increasing the parameter C over 5 achieves the same accuracy, but the computational time will increase, as shown in Figure 3.10. The RBF parameter σ = 0.005 and epsilon=0.001.

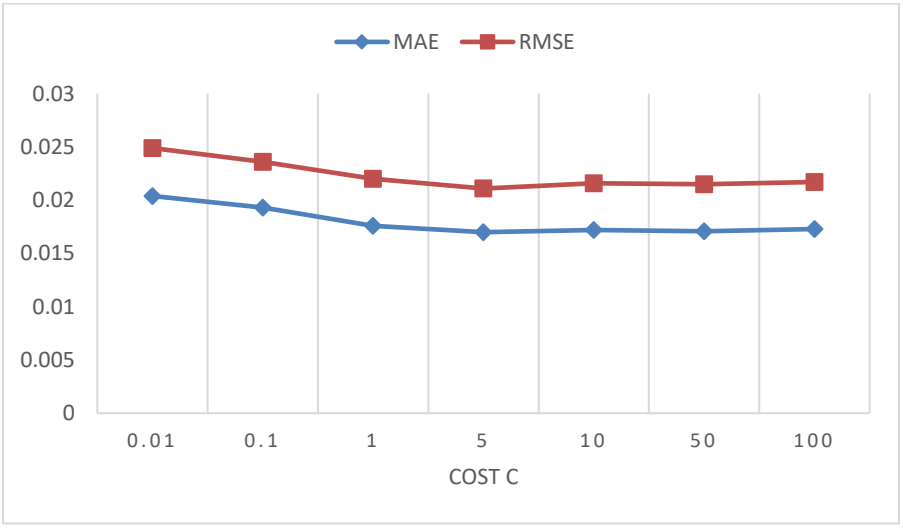

Figure 3.10. Impact C Parameter on MAE and RMSE

When the appropriate parameters of the meta-learner (SVR) are estimated, the ensemble model is applied to the test data to predict wind power output for intervals of 15-min. The prediction results from March 30, 2014, is shown in Figure 3.11. It is clear that the proposed model follows the patterns of the initially recorded wind power data. From interval 70 to the end, the staking ensemble model achieves the highest accuracy as the generated power becomes almost linear. The short-term prediction of 15-minute interval allowed for the capturing of the non-linearity in the generated power that occurs at short time scales, and the representation of the stochastic nature of the data.

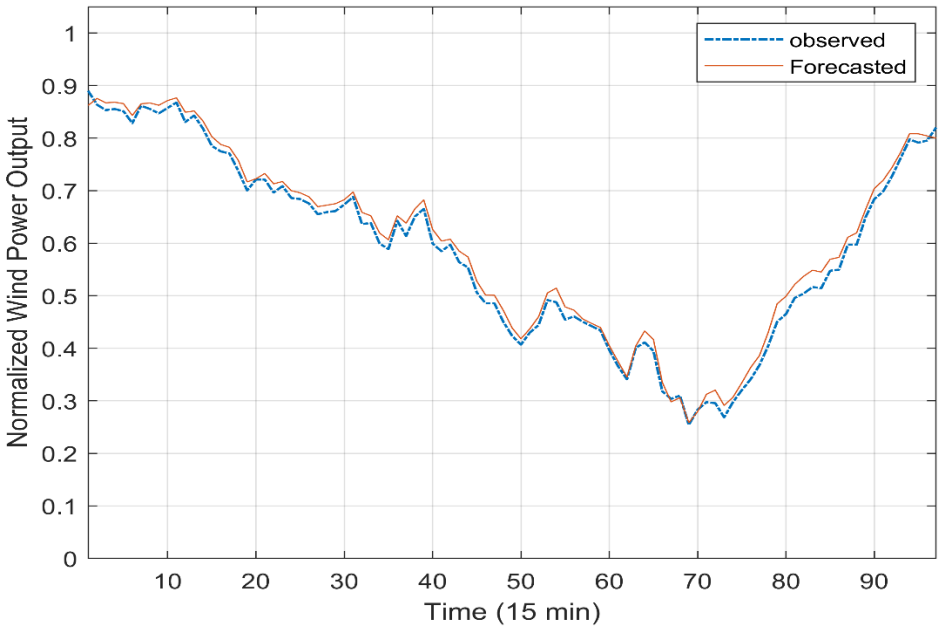

Figure 3.11. STSE model prediction

The correlation between the observed and predicted wind power data calculated can be observed in Figure 3.12, which is 0.9838. Correlation between the two values is an indication of how the predicted values are close to the original values. Training the three base models and combining their predictions via SVR after determining the appropriate parameters ensures the generalization of the model as well as minimization of the prediction error between the observed and actual value.

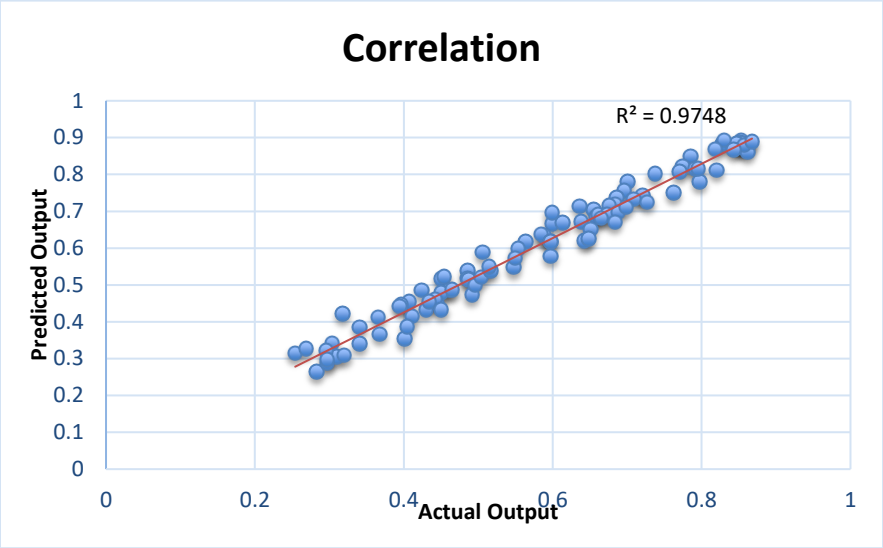

Figure 3.12. Correlation between actual and predicted data

The proposed time-series prediction model is compared with the stand-alone base learners, as discussed before for comparison purposes. Figure 3.13 shows the predictions of all models as individual models and the STSE model with the actual data.

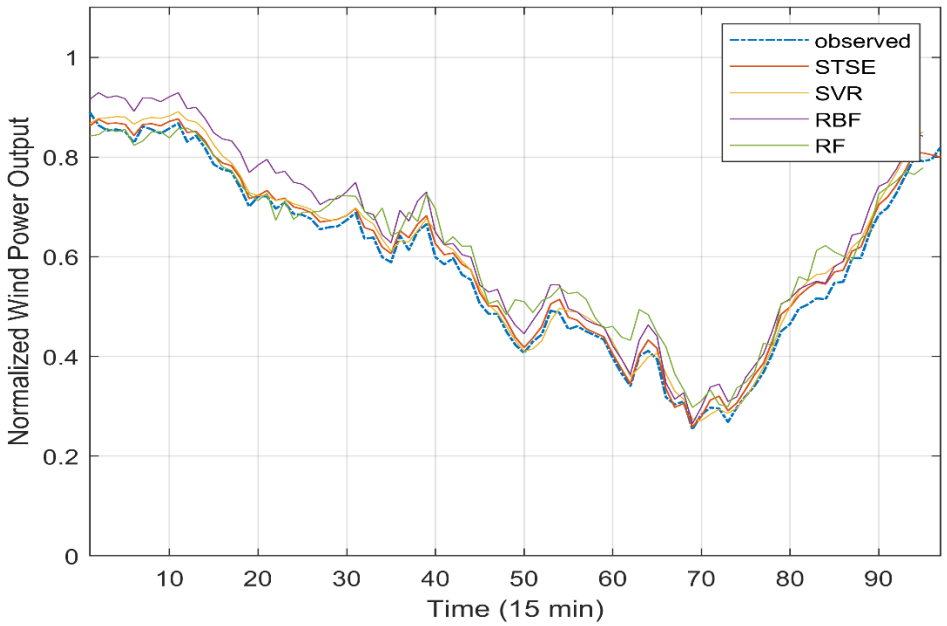

Figure 3.13. Prediction of All models

We can see that the proposed model outperforms all of the stand-alone models and achieves better prediction accuracy and the highest correlation to the original data set. RBF has the least correlation among all the models. Table 3-2 shows the performance metrics of each model after the evaluation of the test data set.

Table 3-2. Comparative forecasting results proposed and base models

Model	MAPE%	RMSE	MAE
SVR	13.57	0.1094	0.0932
RBFNN	5.921	0.0597	0.0487
RF	5.91	0.0597	0.0305
STSE	1.314	0.0248	0.0186
MLP	2.17	0.036	0.028

From the results, the proposed model has less prediction error compared with SVR, RBFNN, and RF. The RMSE of the stacked ensemble model is 0.0248, which is the lowest among the others. Other evaluation metrics like MAPE and MAE also indicates the successfulness of the STSE model in predicting the short time interval efficiently compared with classical models. MLP is also used for comparison, but less than the STSE model.

3.3 Load Forecasting

Electric load forecasting is another important task, which plays an essential role in the distribution system operation. System operators predict electricity consumption for a day ahead to balance generation and demand. Alternatively, operating smart grids dominated by RESs requires prediction on orders of minutes. Unlike PV and wind power systems, which depend on weather conditions, electricity load changes are mainly based on customer usage. Different types of customers have different kinds of load profiles such as residential, commercial, industrial, or a mixture of these. In this study, as we only consider residential customers, short-term load forecasting for intervals of 15-min ahead is conducted. For modeling simplicity and accuracy, we have tried the three base models SVR, RBFNN, and RF as individual models and compared the results with the proposed STSE model. We found that SVR performance is very efficient and close to the STSE model. Therefore, as we introduce a

forecasting model for a medium voltage distribution system, we forecast the aggregated load using SVR and compare the forecasting performance with RBFNN and RF models.

Figure 3.14 shows the normalized residential load profile from Jan 1, 2014, to Dec 31, 2014 [99]. We can see from the second plot that the load pattern does not change much from day-to-day. However, changes occur in peak values from season-to-season as seen from the first plot.

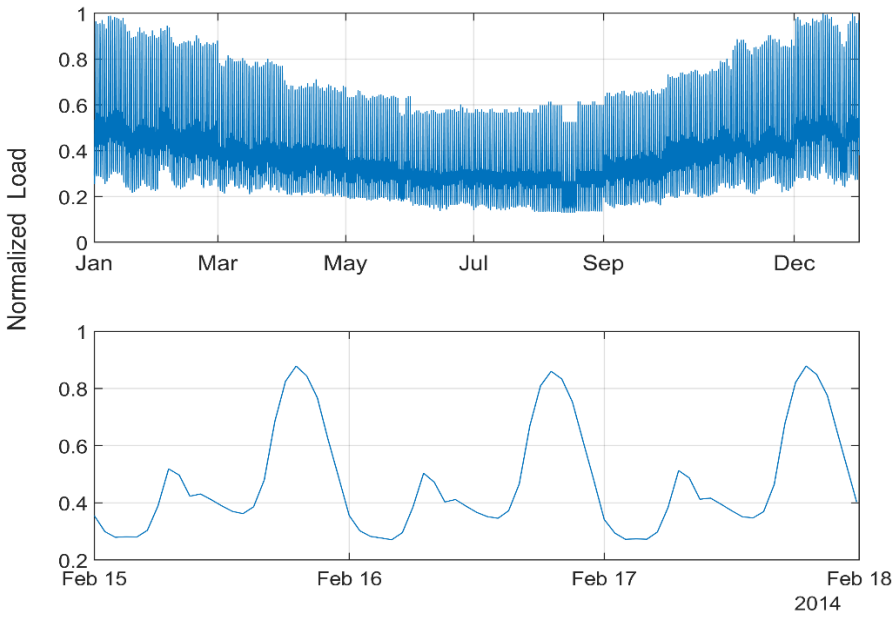

Figure 3.14 Normalized residential load profile

Figure 3.15 shows the performance of the SVR forecasting model on the visualized data from Figure 3.14. We can see that the SVR model follows the trend of the load profile. Three Kernel functions are used to determine the best mapping function used in the SVR model: RBF, Polynomial, and Linear.

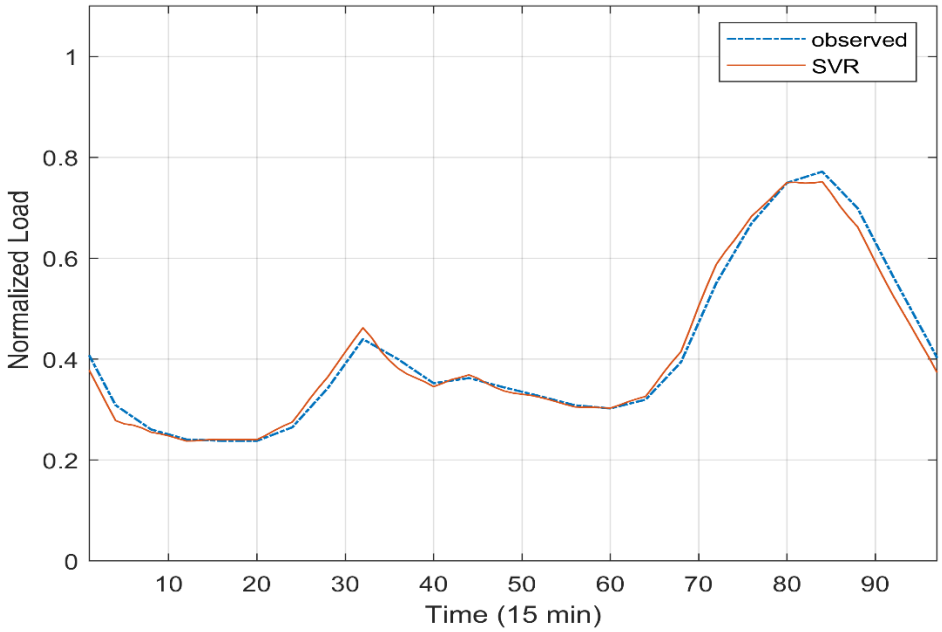

Figure 3.15. Forecasted load profile

The correlation between the actual data and the forecasted data is shown in Figure 3.16. Correlation equals 0.9982, which indicates that the actual and the predicted movements are associated.

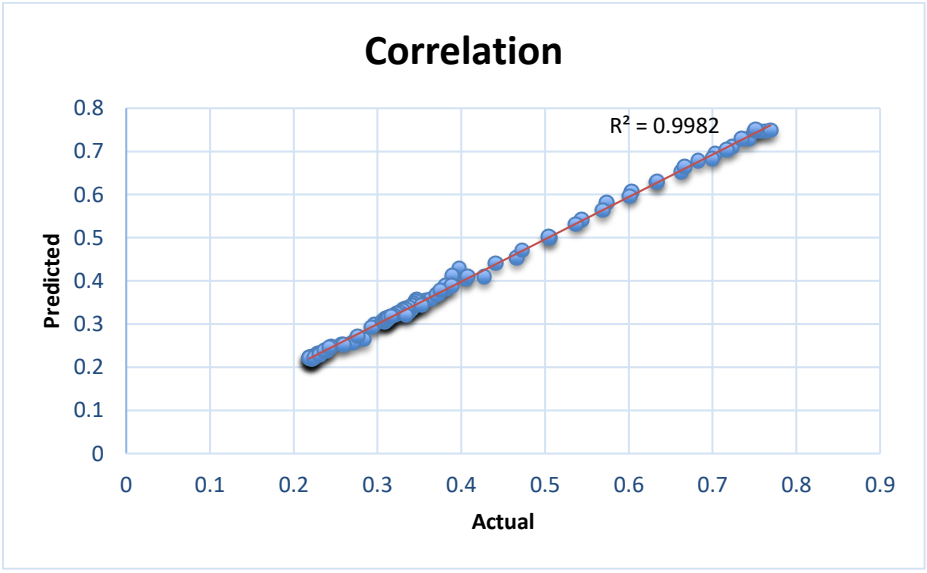

Figure 3.16. Correlation between actual and predicted data

A comparison with previous base models RBF and RF with the SVR model shows that SVR outperforms the other models and provides the best-fit model as shown in Figure 3.17.

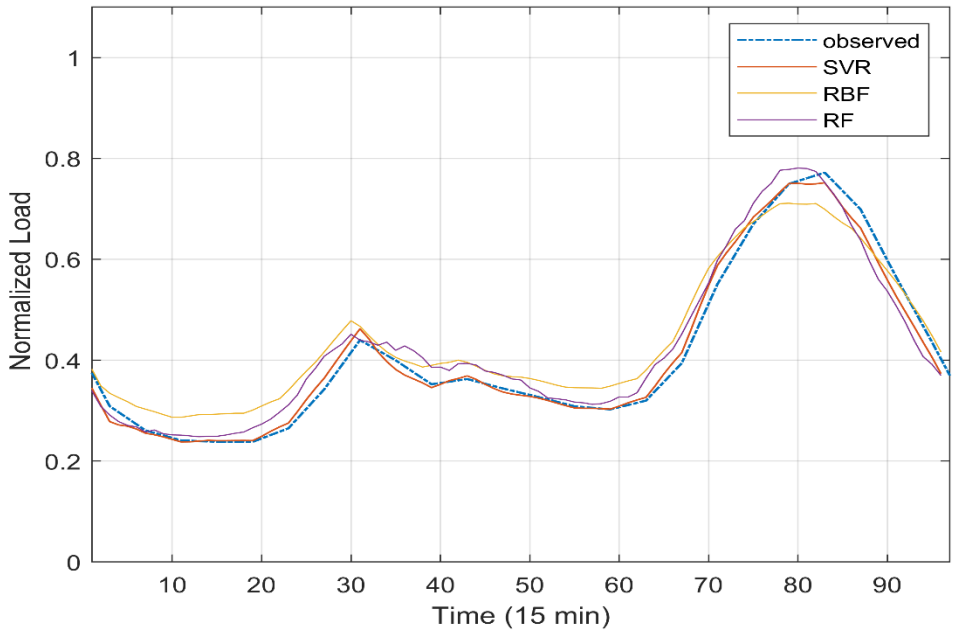

Figure 3.17. Prediction of SVR, RBF, and RF models

The parameters of the SVR model to achieve high accuracy are C=0.5, Kernel='RBF", epsilon=0.001, exponent=2. The evaluation metrics for the three learners are depicted in Table 3-3.

Table 3-3**.** Comparative forecasting results For SVR, RBF, and RF.

Model	MAPE%	RMSE	MAE
SVR	3.319	0.0074	0.004
RBF	6.24	0.027	0.022
RF	3.81	0.0187	0.015

3.4 Conclusion

Accurate forecasting of PV/wind power plays a significant role in improving the efficiency and reliability of power distribution systems. In this chapter, an STSE forecasting model has been established and applied to time series PV/wind power data for short-term power forecasting. The prediction models SVR, RBFNN, and RF are used to make the initial prediction. Then, the SVR model, which is trained by the outputs of the base models, is used to predict the final production. The evaluation of the stacked ensemble model based on RMSE, MAPE, RMS, and RAE, showed that the proposed model outperforms the individual base models and other models, such as MLP. Our results show that combining the base predictors via parameter tuned SVR improves the model prediction accuracy and generalization. Moreover, short-term forecasting of demand is conducted by the SVR model only. We conclude that SVR performs better than the other forecasting base models and is comparable with the STSE model when the variations in the data are relatively small.

Chapter 4
Optimal Predictive Volt/Var Control For Smart Distribution Grids

4.1 Preamble

One of many advantages of Smart Distribution Grids (SDGs) is to allow for high penetration of renewable energy sources (RESs) such as solar PV and wind power systems. Several technical and economic advantages result from integrating RESs into power system networks, including an increase in grid reliability and a reduction in the increasing demand [101]. However, many operational problems are highlighted in the literature related to the high integration of solar PV and wind power systems, particularly on the medium and low distribution systems. Some of these issues are summarized in the following points [101][102]:

- Voltage fluctuation and voltage regulation problem
- Changes in feeder loading, including overloading of the system components
- Malfunctioning of the voltage regulation equipment
- Variation of power factor
- Reverse power flow
- Planning of distribution systems

A review of the literature reveals that many research papers have proposed several techniques to control and operate SDGs dominated by RESs. Many of these techniques are discussed and summarized in [103]. Considering the conducted studies, managing a distribution system dominated by PV and wind farms, characterized by a high degree of uncertainty alongside their impact on the cost-effective operation of the network, still has room for improvement.

In this chapter, two versions of a model for an optimal day-ahead generic Predictive Volt/Var Control (PVVC) are proposed. The PVVC models are formulated as an optimization problem and solved sequentially for one day-ahead. The models aim to overcome the operational challenges, such as overvoltage, power losses, and frequent operations of Volt/Var devices, that are brought by the high integration of RESs. The first model operates the RESs at unity power factor, where the objective is defined as simultaneous minimization of voltage deviation at each bus, power losses, operating cycle of regulation equipment, and RES curtailment. Unlike the drop-based active power curtailment

technique used in [104], this model minimizes the active power curtailment in collaboration with Volt/Var control devices to maintain the system's voltages within limits and minimizes the total operating cost of the network. A day-ahead of Solar PV and wind power forecasting in addition to network topology and bus/line parameters are the inputs to the optimization model.

The second control model of this chapter, which operates the RESs at variable power factor, uses inverters interfaced with RES as an ancillary service for Volt/Var control. A dispatch schedule of PV and wind power inverters in coordination with OLTC, and SVR for minimizing power losses, operations of Volt/Var control devices, as well as improving the voltage profile, is developed.

4.2 PVVC With RESs at Unity Power Factor

In a power system, the Volt/Var control is an optimization problem used to maximize or minimize a certain objective subject to a network's physical and operating constraints. In this chapter, the PVVC problem is modeled as an optimization problem, which is used to solve the Volt/Var control problem in SDGs. The PVVC problem is a form of OFP modeled to maintain the system voltage profile within the security ranges and minimize system losses by controlling the reactive power flow through the Volt/Var control devices.

4.2.1 **Objective Function**

The proposed PVVC problem is formulated as an MINLP optimization problem and solved in GAMS [105] to minimize power losses, voltage deviation, OLTC, SVR, SC operations, and RES active power curtailment. A multi-objective optimization problem is developed and then transformed into a single objective function using the weighted sum method. The method, which provides a single solution point that reflects preferences presumably incorporated in the selection of a single set of weights [106], is more practical in comparison with other multi-objective programming methods [63]. Different solution methodologies for solving multi-objective functions, such as the adaptive weighted sum method [107] and improved ϵ-constrained approach [108], can also be used in solving the optimization problem. The objective function of the PVVC problem is described in Equation 4.1. The third, fourth, and fifth objectives are formulated in a way similar to the formulation in [60]. The first and second objectives are included for losses and voltage deviation minimization.

$$\text{Min } F = w_{loss}\frac{F_{loss}}{F_{los}^{0}} + w_{DV}\frac{F_{VD}}{F_{VD}^{0}} + w_{LTC}\frac{F_{LTC}}{F_{ltc}^{0}} + w_{svr}\frac{F_{SVR}}{F_{svr}^{0}} + w_{sc}\frac{F_{SC}}{F_{sc}^{0}} - w_{cur}\frac{F_{cur}}{F_{cur}^{0}} \quad 4.1$$

where $F_{loss}, F_{VD}, F_{LTC}, F_{SVR}, F_{CB}, F_{cur}$ are the single objectives of power losses, voltage deviation, OLTC operation, SVR operation, SC operation, and RES curtailment, respectively. F^{o} represents the maximum absolute value for each objective obtained from historical operation data to scale the objective and make it unitless in order to satisfy the weighted sum method [109].

A. F_{loss} = Active power losses

The first objective represents the total active power losses in all lines calculated from Equation 4.2.

$$F_{loss,t} = \sum_{t=1}^{24} \frac{1}{2} \sum_{(i,j)\epsilon N_b} g_{ij}(V_{i,t}^{2} + V_{i,t}^{2} - 2V_{i,t}V_{j,t}\,cos(\Theta_{ij,t})) \quad 4.2$$

V_i, V_j are the voltages at buses i and j, whereas, g_{ij} represents the line admittance, and N_b is the number of buses.

B. F_{VD} = Voltage deviation (VD)

The second objective is associated with the voltage deviation on each bus. The aim is to minimize the bus voltage to a reference point, where $V^{ref} = 1.0\ pu$.

$$F_{vd} = \sum_{t=1}^{t=24} \sum_{i=1}^{N_b} \left|V_{i,t} - V^{ref}\right| \quad 4.3$$

C. F_{LTC}= Switching operation of the OLTC transformer

The third objective is associated with the tap changes of the OLTC between consecutive intervals, as shown in Equation 4.4.

$$F_{LTC} = \sum_{t=1}^{24} \left|tap_{i,t}^{ltc} - tap_{i,t-1}^{ltc}\right| \quad 4.4$$

where $tap_{i,t}^{ltc}\ and\ tap_{i,t-1}^{ltc}$ represent tap positions of the OLTC at time $t, and\ t-1$, respectively.

D. F_{SVR}= Switching operation of the SVR

The fourth objective is associated with the SVR. Similar to the OLTC, the aim is to minimize the tap changes between consecutive time intervals:

$$F_{SVR} = \sum_{i\in N_{svr}} \sum_{t=1}^{24} \left|tap_{i,t}^{svr} - tap_{i,t-1}^{svr}\right| \quad 4.5$$

where $tap_{i,t}^{svr}$ and $tap_{i,t-1}^{svr}$ represent tap positions of the SVR at time $t, and\ t-1$, respectively, and N_{svr} represents the total number of step voltage regulators.

E. F_{SC}= Switching operation of the SC

The fifth objective is associated with the SC between consecutive time intervals:

$$F_{SC} = \sum_{i \in N_{SC}} \sum_{t=1}^{24} \left| Z_{i,t} - Z_{i,t-1} \right| \quad 4.6$$

where $\boldsymbol{Z_{i,t}}$ is a discrete number representing the SC units in service at node i and time t. N_{SC} represents the total number of capacitors in the system.

F. F_{Curt} = DGs Curtailment

The sixth objective is associated with the curtailment of active power from solar PV and wind power systems from the maximum power outputs:

$$F_{curt} = \sum_{i \in N_{dg}} \sum_{t=1}^{24} \left| P_{inv_{i,t}}^{max} - P_{i,t}^{cur} \right| \quad 4.7$$

where $P_{inv_{i,t}}^{max}$ and $P_{i,t}^{cur}$ are the maximum power and the curtailed power from the RES units. N_{dg} is the total number of RESs.

4.2.2 Equality and inequality constraints

The main conventional Volt/Var control variables are OLTC, SVR, and SC. Each one of the control variables has physical and operational limitations.

1. Power flow constraints

- Real power injection constraints:

$$P_{g,i,t} + P_{inv,i,t} - P_{d,i,t} = V_{i,t} \sum_{j=1}^{N_b} V_{j,t} (G_{ij} cos\theta_{ij,t} + B_{ij} sin\theta_{ij,t}) \quad 4.8$$

- Reactive power injection constraints:

$$Q_{g,i,t} + Q_{SC,i,t} - Q_{d,i,t} = V_{i,t} \sum_{j=1}^{N_b} V_{i,t} (G_{ij} sin\theta_{ij,t} - B_{ij} Q_{d,i,t_{ij}} cos\theta_{ij,t}) \quad 4.9$$

where $P_{g,i,t}$, $Q_{g,i,t}$ are the real and reactive power from the grid, whereas, $P_{d,i,t}$, and $Q_{d,i,t}$ are the real and reactive power for demand. $P_{inv,i,t}$ and $Q_{SC,i,t}$ the are active and reactive power from RES inverters and SCs.

2. Voltage constraints

Voltage must be within the specified ANSI C84.1 standard limit (i.e., 0.95-1.05 pu) [110]:

$$V^{min} \leq V_{i,t} \leq V^{max} \quad 4.10$$

3. Tap ratio of the LTC and SVR

As previously discussed, all Volt/Var control devices will be controlled from a centralized point instead of their local controllers. The physical constraints of both devices are the maximum and the minimum number of taps and the maximum daily number of operations. The objective is to minimize frequent operations, which decreases the device's lifespan and increases maintenance costs.

- OLTC constraints:

$$Tap_{ltc}^{min} \leq tap_t^{ltc} \leq Tap_{ltc}^{max} \quad , \forall_i \in N_{ltc} \quad 4.11$$

$$\sum_{t=1}^{24} \left| tap_t^{ltc} - tap_{t-1}^{ltc} \right| \leq \beta^{ltc} \quad 4.12$$

- SVR constraints:

$$Tap_{svr}^{min} \leq tap_{i,t}^{svr} \leq Tap_{svr}^{max} \quad , \quad \forall_i \in N_{svr} \quad 4.13$$

$$\sum_{t=1}^{24} \left| tap_{i,t}^{svr} - tap_{i,t-1}^{svr} \right| \leq \beta^{svr} \quad 4.14$$

where $\beta^{ltc}, and\ \beta^{svr}$ are the total number of LTC and SVR switchings per day.

4. SC Control

Switched capacitor banks are mainly used to improve the power factor by compensating the reactive power from inductive loads. An SC bank consisting of three units, which can be remotely controlled in discrete steps, is considered. The daily limit on the unit's switchings and the maximum reactive power when all capacitors are active are shown in the following equations [60]:

$$Q_{SC,i,t} = q_i^{SC} Z_{i,t} \quad , \forall_i \in N_{SC} \quad 4.15$$

$$\sum_{t=1}^{24} \left| Z_{i,t} - Z_{i,t-1} \right| \leq \beta^{SC} \quad 4.16$$

$$0 \leq Z_{i,t} \leq Z^{max} \quad 4.17$$

where q_i^{SC} is the reactive power capacity of each unit of the SC at node i, and $Z_{i,t}$ is a discrete number that represents the SC units in service at node i and time t. β^{SC} represents the maximum daily number of switchings for each unit. Z^{max} is the maximum number of banks of each SC.

5. RES active power curtailment constraint

The active power is limited by the apparent power limit of the inverter.

$$0 \leq \left| P_{inv_{d,t}}^{max} - P_{d,t}^{cur} \right| \leq S_{inv}^{max} \quad 4.18$$

where S_{inv}^{max} is the apparent power of the inverter.

6. Line capacity constraints

$$\left| I_{ij,t}^{t} \right| \leq \left| I_{ij,t}^{max} \right| \quad 4.19$$

where $I_{ij,t}^{max}$ is the maximum line capacity.

The summation of all weights must be equal to 1 in order to satisfy the weighted sum method when solving the optimization problem. The weight coefficients are determined based on a decision matrix, as explained in [109].

$$w_{loss} + w_{DV} + w_{LTC} + w_{svr} + w_{scb} + w_{cur} = 1 \quad 4.20$$

4.3 Assumptions

To solve the control problem and schedule the operation of SDG components, the following requirements are assumed to be available:

- Full communication infrastructure for information exchange.
- Smart meters at each bus for data measurements.
- The OLTC, SVR, and SC are switched according to a signal from a supervisory controller.

- An energy management system for solving the optimization problem and sending control signals to system components.

A Supervisory Control and Data Acquisition (SCADA) system, which plays the role of monitoring and controlling components, should be available. A SCADA system that sends field data back to the supervisor controller via a communications link, where the master permits the operator to perform remote control tasks [111].

4.4 Case Studies

In this section, case studies on the modified IEEE 33-Bus test systems are performed to evaluate the proposed control strategy. Numerical experiments are implemented using GAMS on a desktop computer with Intel Core (i3, 3.3GHz) and 8GB memory. COINBONMIN solver is used for solving the formulated MINLP control problem.

- *IEEE 33-Bus Test System*

The proposed model is evaluated on an IEEE 33-bus 11-kV radial distribution test system [34], as shown in Figure 4.1. The total active and reactive loads are 3,635 kW and 2,265 kVAR, respectively. The line parameters and load data are presented in Appendix B. The OLTC regulates the voltage on the secondary side of the substation transformer up to ± 10% with ±16 steps, where each step equals 5/8% pu. The SVR is placed on the main feeder between buses 6 and 7 to regulate the voltage by ± 10%. Two SC banks located at buses 18 and 33 each of which produces reactive power in steps of 150 kVAR and up to 450 kVAR. The permissible range of voltage deviation is limited by ± 5% of the nominal voltage at the slack bus.

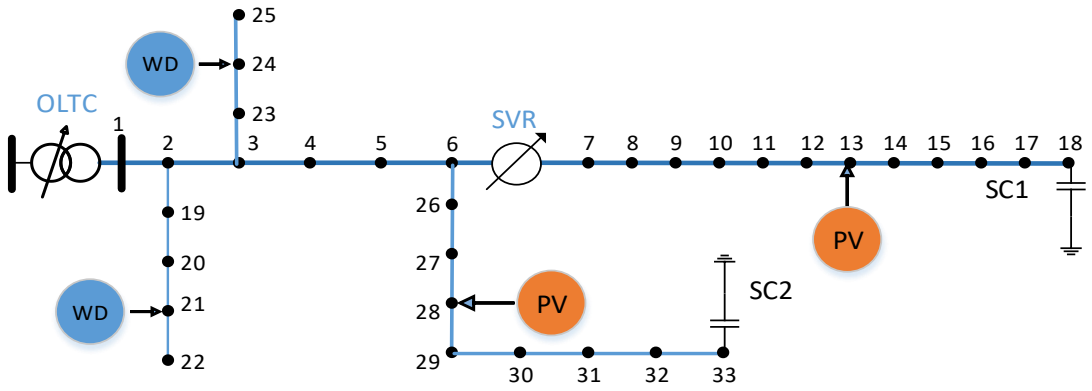

Figure 4.1. IEEE 33-Bus test system

Two scenarios, 30% and 60% of RES penetration are applied. The forecasted PV and wind power outputs are shown in Figure 4.2. The hourly load profile, as shown in Figure 4.3, is considered as the same profile for consecutive days. It can be seen from the normalized PV profile that the generated power changes during the day due to the change in weather conditions. Similarly, as the wind speed and direction change, the generated power from wind turbines changes accordingly. Hence, the fluctuation in the generated power under the high integration of renewables may bring serious operational and automation challenges to the network operators.

It should be noted that the location and size of the reactive compensation devices have an impact on the performance of the PVVC; however, the optimal placement of the components is beyond the scope of this study. The penetration level of the PV and wind power systems is calculated based on the formula from Equation 4.21, where the term RES_{rated} represents the summation of all renewable sources at their rated values, and S_{load} is the total demand. The rated capacity of PV and wind power systems is 0.0292 pu, 0.0279 pu, and 0.013 pu, 0.0098 pu, respectively. The weights in Equation 4.20 are: 0.2,0.06,0.14,0.13,0.07,0.4 respectively.

$$RES_{pen} = \frac{RES_{rated}}{S_{load}} x100\% \qquad 4.21$$

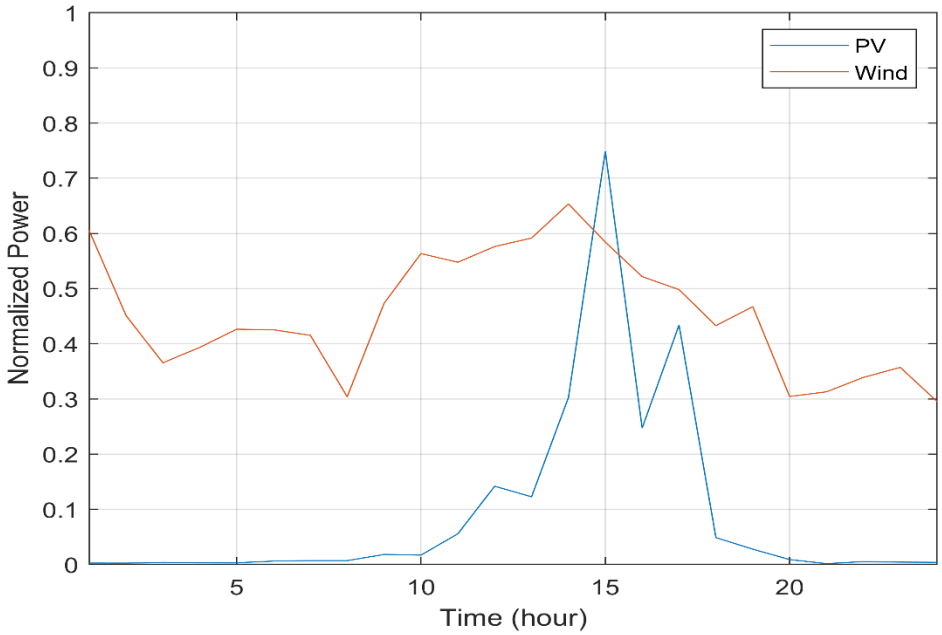

Figure 4.2. Forecasted PV and wind profiles

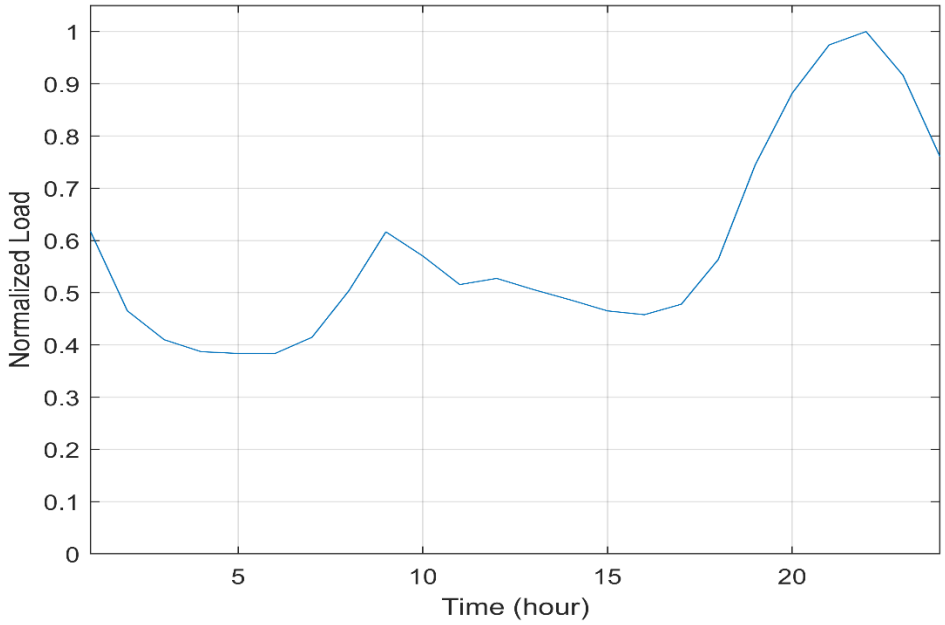

Figure 4.3. Normalized residential load profile

4.5 Simulation results

In this section, the two scenarios are applied to determine the impact of RESs output fluctuations on the operation of SDG. The two penetration levels are studied to determine the optimal coordination between the Volt/Var control devices and to examine RES curtailment options if needed for the secure and efficient operation of SDG.

4.5.1 Base case

To determine the impact of high penetration of RESs on voltage profile, power flow is performed without RES curtailment options. It can be seen from Figure 4.4 that voltage violation occurs on the buses connected to the PV and wind power systems. The voltage profile of RES buses 13, 21, 24, 28, as well as end-of-feeder buses 18 and 33, are considered as they experience higher voltage fluctuation and voltage drop than the others.

Buses 21 and 24, which are connected to the wind turbines, experience a voltage level that exceeds the limit of 1.05 p.u. In contrast, buses 13 and 28, which are connected to the PV systems, experience over-voltage as a result of light demand and high PV generation around 3:00 PM. Buses 18 and 33,

which are located at the end of the feeder, are considered for plotting as they may experience under-voltage at the end of the day when the demand is high, and the solar PV output is at a minimum.

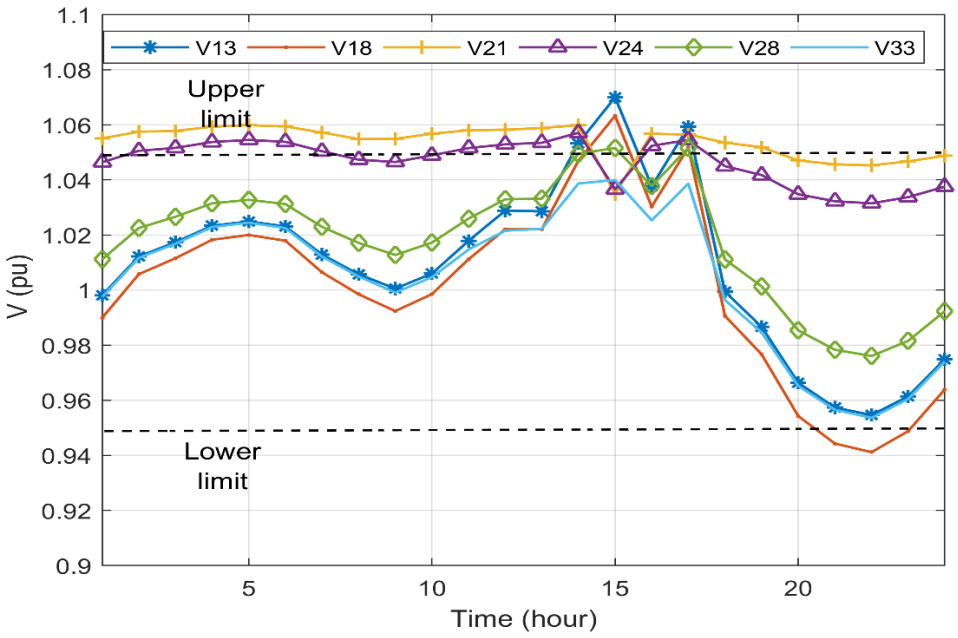

Figure 4.4. System voltage under no-curtailment options

4.5.2 Low RES penetration

This case examines the performance of the proposed model at a 30% penetration level of RESs. The objective function, as described in Equation 4.1, has been solved to minimize active power losses, voltage deviation, RES active power curtailment, and operations of the OLTC, SVR, and CB.

Figure 4.5 shows the voltage profile of the selected buses for the 24 hour simulation period. At 30% penetration level, the impact of RESs on the voltage profile is relatively small. The variations in the generated power from the PV and wind power systems at low penetration levels do not cause severe voltage violations or fluctuations problems. Under these operating conditions, the proposed PVVC model solved the problem efficiently and without the need to curtail any of the RESs.

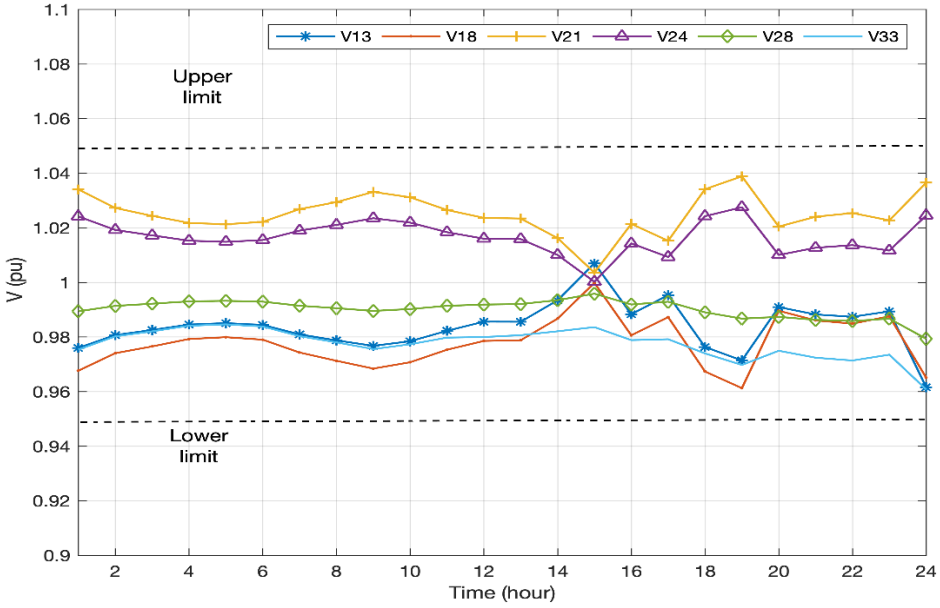

Figure 4.5. Voltage profile 30% penetration.

It can be seen from Figure 4.6 that the operation of both OLTC and SVR is minimized to the minimum limit. The OLTC switched once, counting for 1 tap from 1 to 0 position at 9:00 PM. On the other side, the SVR switched once, counting for 1 tap from position -2 to -1 at 11:00 AM. The operation of both devices in coordination with the SCs is scheduled according to the solution of the PVVC model, considering the minimization of losses, voltage deviation, and RES curtailment.

Table 4-1 shows the daily scheduled operation of the SC banks after solving the problem. The SC on bus 18 switched on one bank (150kVAR) from 8:00 – 11:00 PM. This is to offset the consumed reactive power because the demand during these intervals is high. The second SC at bus 33 switched off for the entire day as the voltage kept within the permissible limits.

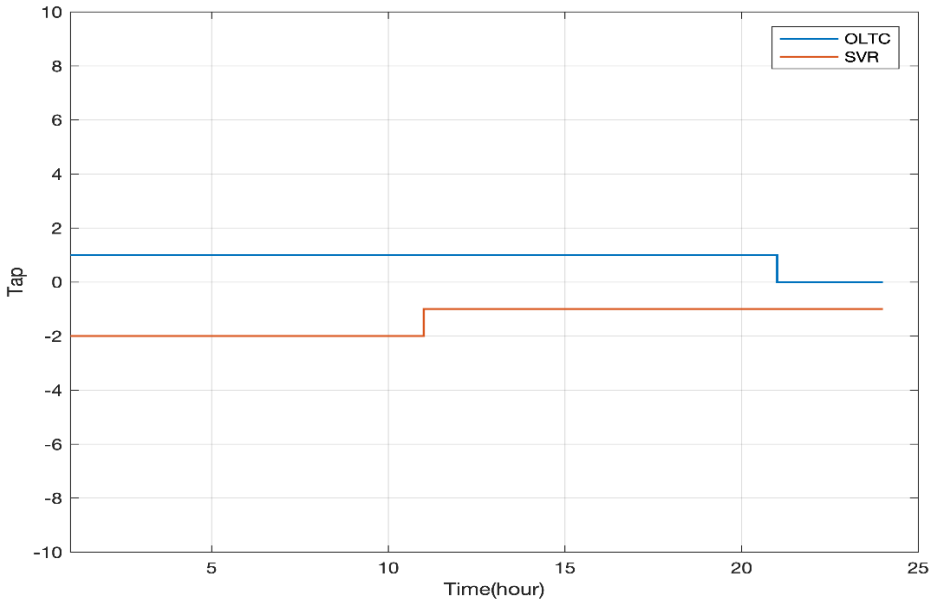

Figure 4.6. OLTC and SVR Tap operation at 30% penetration.

Table 4-1. Switched capacitor bank status

Time	Cap-18 (Q*K)	Cap-33 (Q*K)	Time	Cap-18 (Q*K)	Cap-33 (Q*K)
	K	K		K	K
1:00	0	0	13:00	0	0
2:00	0	0	14:00	0	0
3:00	0	0	15:00	0	0
4:00	0	0	16:00	0	0
5:00	0	0	17:00	0	0
6:00	0	0	18:00	0	0
7:00	0	0	19:00	0	0
8:00	0	0	20:00	1	0
9:00	0	0	21:00	1	0
10:00	0	0	22:00	1	0
11:00	0	0	23:00	1	0
12:00	0	0	24:00	0	0

4.5.3 High RES penetration

In the second case, the penetration level has been increased to 60%. At high integration of RESs with high power variations, the control problem becomes more challenging. Frequent operations of voltage regulators, reverse power flow, overvoltage, and voltage fluctuation are some of the challenges that need to be solved.

In this section, two scenarios are studied to verify the capability of the proposed algorithm in solving the control problem under the high penetration of solar PV and Wind power systems.

4.5.3.1 Scenario 1

The optimization problem is solved based on the minimization of power losses, voltage deviation, and RES curtailment only. In this scenario, when the penetration level is high, power curtailment at peak generation is an option if the voltage exceeds the permissible range and cannot be mitigated by the voltage regulators. In Figure 4.7, which shows the voltage profile of the selected buses, it can be observed that the voltages at bus 13 and bus 18 have a little spike due to the peak generation of the PV unit at 5:00 PM, where the demand is low, and the PV generated power is high.

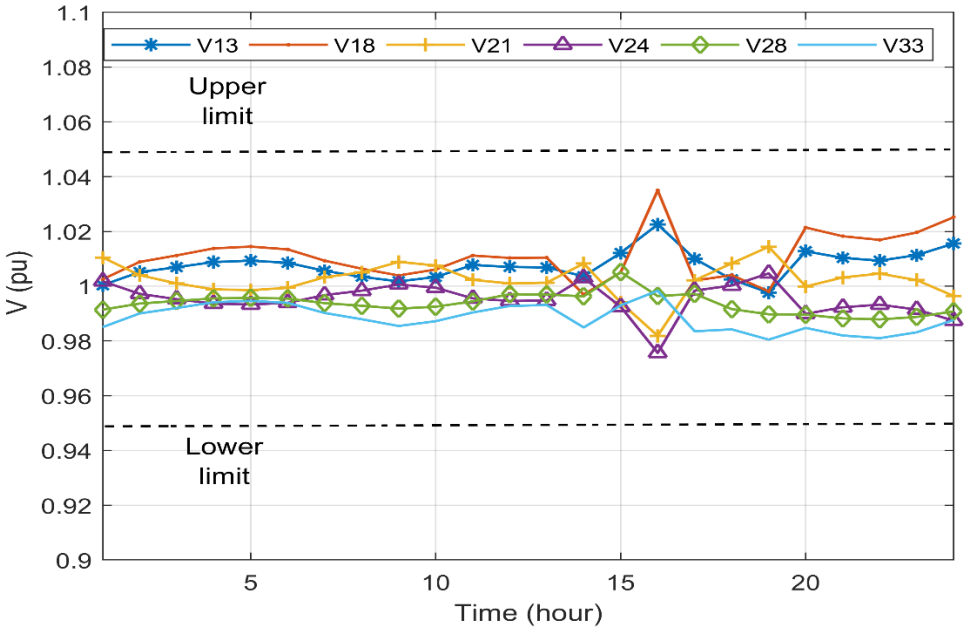

Figure 4.7. Scenario 1.Voltage profile at 60% penetration.

Minimizing the voltage deviation, as one of the sub-objective functions, has maintained the voltages on all buses close to the reference value. Additionally, as one of the sub-objectives is to minimize the active power curtailment from RESs if necessary, only the PV unit at bus 13 curtails some of its output during peak generation times. The amount of the curtailed power was 0.017 pu for the entire simulation period. This is a small curtailment as it happens for only one generation unit at the peak generation time to maintain the voltage at bus 13 within limits.

Figure 4.8 shows the daily operation of the OLTC and SVR under the 60% penetration level. Without considering the minimization of the Volt/Var control devices in the optimization process, and with highly integrated and fluctuated RESs, the OLTC and SVR will experience frequent operations as a response to voltage variation. Figure 4.8 also demonstrates that the OLTC switched seven times, counting for 18 taps, while the SVR switched six times, counting for 13 taps. The number of taps might be more or less depending on demand and RES generation. Therefore, it is essential to simultaneously coordinate the operation of the Volt/Var control device with RESs curtailment in order to minimize the total operating cost and ensure the optimal operation of the SDG.

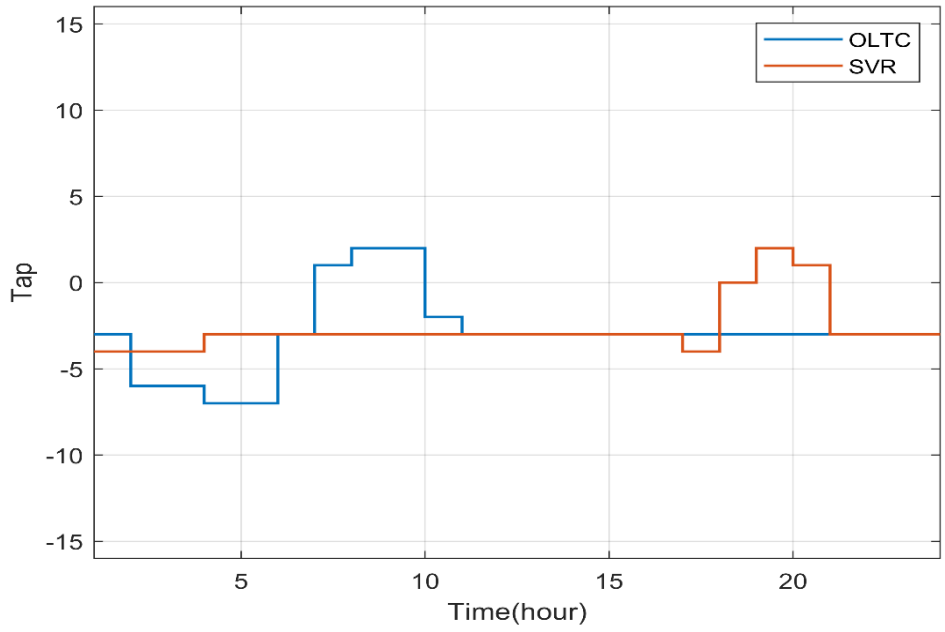

Figure 4.8**.** OLTC and SVR tap operation at 60% penetration (Scenario 1).

Table 4-2 shows the daily operation of both SC banks at buses 18 and 33, respectively.

Table 4-2. Switched capacitor bank status (Scenario 1).

Time	Cap-18 (Q*K)	Cap-33 (Q*K)	Time	Cap-18 (Q*K)	Cap-33 (Q*K)
	K	K		K	K
1:00	1	0	13:00	1	0
2:00	1	0	14:00	0	0
3:00	1	0	15:00	0	0
4:00	1	0	16:00	2	0
5:00	1	0	17:00	0	0
6:00	1	0	18:00	1	0
7:00	1	0	19:00	1	0
8:00	1	0	20:00	0	2
9:00	0	1	21:00	0	2
10:00	0	1	22:00	1	1
11:00	1	0	23:00	0	2
12:00	1	0	24:00	0	2

It can be observed that multiple switchings occur per day for both capacitors in the presence of high fluctuation of RES generation. The integer K in Table 4-2 determines how many banks are switched on/off during the simulation period. Similar to the OLTC and SVR, the number of switchings plays the main role in the device's end of life, which can be decreased if many switchings occur every day. The capacitor at bus 18 provided maximum reactive power of 300 KVAR at 4:00 PM, while switched between 0 and 1 for the rest of the day to post the voltage and keep it close to 1.0 p.u. The capacitor at bus 33 switched on two banks (K=2) from intervals 8:00-9:00 PM and 11:00-12:00 PM, which is the time of high demand and zero generation from PV units.

Figure 4.9 shows the 24-hour voltage profile of all buses under Scenario 1. One can notice that the voltage profile is minimized to the reference voltage except in the area where the PV generation is at its peak.

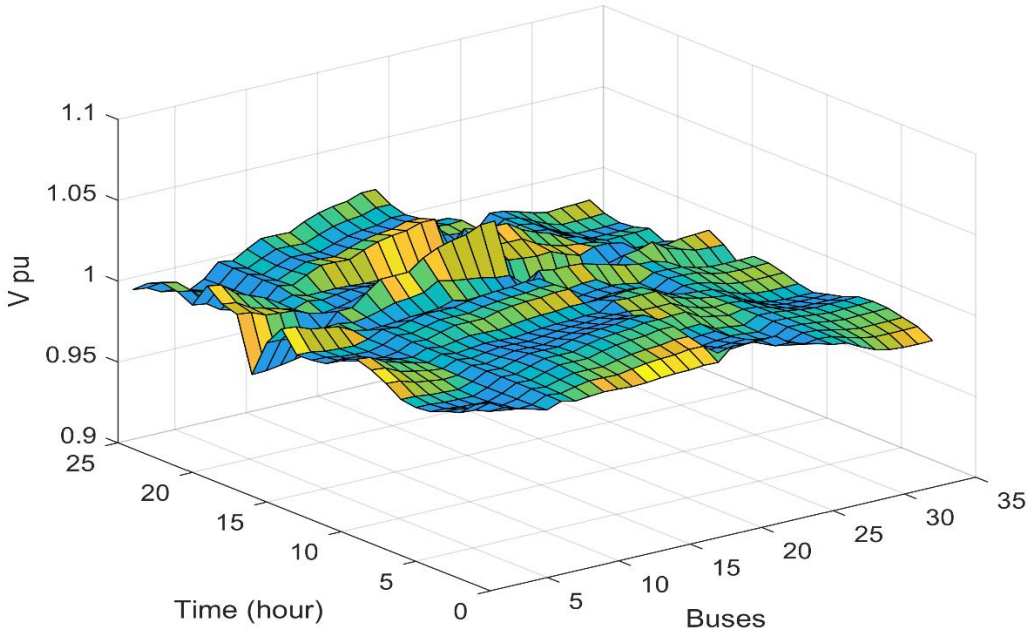

Figure 4.9. System's voltage profile for 24-hours (Scenario 1).

4.5.3.2 Scenario 2

In this scenario, the proposed PVVC model, as described in Equation 4.1, is applied to the test system at 60% penetration of RESs. The main objective is to minimize the total operating cost by including the switching cost of the Volt/Var control devices into the optimization problem.

Figure 4.10 shows the voltage profile of the selected buses for the 24 hour simulation period. It can be observed that the voltage profile is optimized to the reference value of 1.0 pu. A small voltage spikes

at buses 13 and 18 between intervals 2:00 PM and 5:00 PM due to the injected power from the PV unit at bus 13, where the generated power rapidly changes.

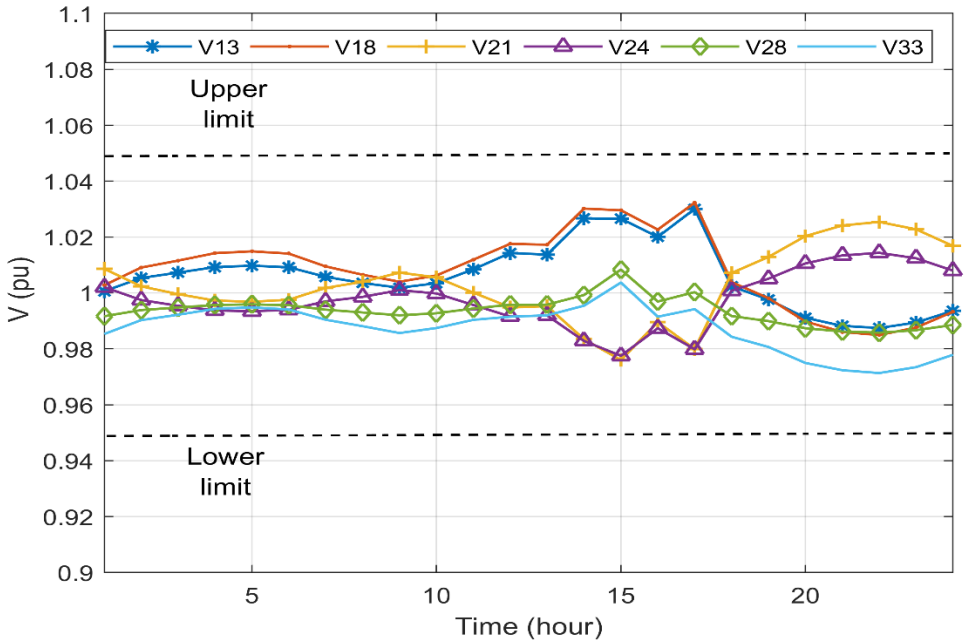

Figure 4.10.Voltage profile of the selected buses (Scenario 2).

RES power curtailment occurred for the PV unit at bus 13 only at 3:00 PM with the amount of 0.0163 pu. The amount of curtailed power is minimal compared with the actual output of the unit. Similar to the curtailment option in Scenario 1, in the middle of the day, when the PV unit produces the highest output, a portion of its output is curtailed to avoid the overvoltage that occurs at bus 13.

A remarkable reduction is observed in the operations of the OLTC and SVR, as shown in Figure 4.11. The OLTC switched only once at 3:00 AM, counting for 1 tap, while the SVR switched twice at 11:00 AM and 11:00 PM, counting for only 3 taps.

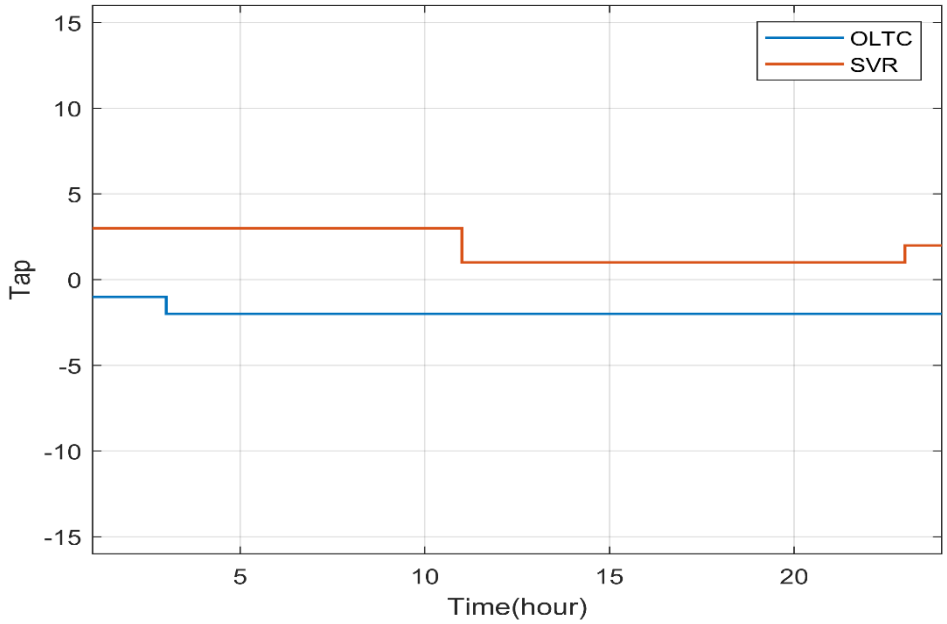

Figure 4.11.OLTC and SVR operation at 60% penetration (Scenario 2).

The SC bank operations have also reduced to the minimum possible option. The capacitor at bus 18 injected 150 KVAR during the 24 hours, while the capacitor at bus 33 stayed off for the entire simulation period, as shown in Table 4-3.

Table 4-3. Switched capacitor bank status

Time	Cap-18 (Q*K)	Cap-33 (Q*K)	Time	Cap-18 (Q*K)	Cap-33 (Q*K)
	K	K		K	K
1:00	1	0	13:00	1	0
2:00	1	0	14:00	1	0
3:00	1	0	15:00	1	0
4:00	1	0	16:00	1	0
5:00	1	0	17:00	1	0
6:00	1	0	18:00	1	0

7:00	1	0	19:00	1	0
8:00	1	0	20:00	1	0
9:00	1	0	21:00	1	0
10:00	1	0	22:00	1	0
11:00	1	0	23:00	1	0
12:00	1	0	24:00	1	0

The overall voltage profile of the system is optimized, as depicted in Figure 4.11. It can be seen that the voltage on each bus during the 24 hours operational schedule has kept close to the references value 1.0 pu. From the surface plot area, the impact of the high generation of the PV units, specifically at bus 13, which has the highest capacity among all the others, causes a small rise in voltage even after regulation. This small rise in voltage appears clearly as spikes between the time slots 2:00 PM and 6:00 PM, as shown in Figure 4.12.

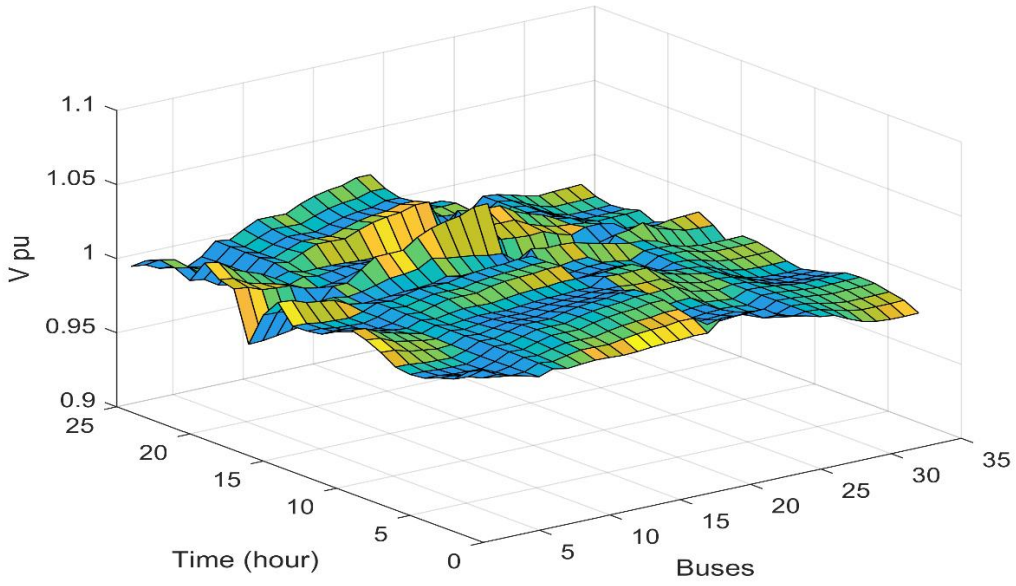

Figure 4.12.System voltage profile for 24-hours (Scenario 2).

4.6 Cost analysis

The main target of the developed PVVC model is to operate an SDG dominated by RESs with minimum cost while satisfying the operational and engineering constraints. The best scenario for both penetration levels was the solution of the complete objective function where the system's losses, voltage deviation, RES curtailment, and control equipment operation were all minimized. Similar to the cost associated with the switchings of the Volt/Var control devices and power losses discussed in [83]. It has calculated based on the price, expected lifetime, and the number of switchings to keep the transformer in service based on the expected lifetime. The cost reduction between the two studied scenarios are shown in Table 4-4 and Table 4-5. In this cost analysis, the power purchased from the main grid is not included.

Table 4-4. Operational cost at 30% RES penetration

Scenario	OLTC Oper/day	SVR Oper/day	Cap-18 Oper/day	Cap-33 Oper/day	Ploss (MW)/day	PV-Curt (MW)/day	Cost ($)
	1	1	2	0	2.23	0	194.5

Table 4-5. Operational cost at 60% RES penetration

Scenario	OLTC Oper/day	SVR Oper/day	Cap-18 Oper/day	Cap-33 Oper/day	Ploss (MW)/day	PV-Curt (MW)/day	Cost ($)
Scenario 1	18	13	11	6	2.22	0.468	442.04$
Scenario 2	1	3	1	0	2.241	0.352	234.94$

The total operational cost has been reduced from $442.04 to $234.94 at a 60% penetration level, which proves the effectiveness of the PVVC model. The model not only minimizes the operational costs but also minimizes the voltage deviations caused by RES variations.

4.7 PVVC With RESs at Variable Power Factor

Given the advances of power electronics, RESs can also provide fast and flexible reactive power support for voltage regulation [112]. A review of the literature reveals that several studies considered the dispatch schedule of an inverter-based RES in coordination with Volt/Var conventional control devices for optimal SDG operation. Furthermore, several studies investigated the advancement of having inverters operating in a 2-quadrant plane, which enables inductive and capacitive reactive power support for voltage regulation in the large-scale deployment of RESs. This section proposes a second PVVC control model for dispatching reactive power from inverters in coordination with OLTC and an SVR in an SDG dominated by PV and Wind power systems. The objective of the proposed strategy is to optimally operate the grid by minimizing active power losses, voltage deviation, reactive power from IBRESs, and reducing the frequent operations of OLTC and the SVR.

4.7.1 Reactive power from RES inverters

Current standards or guidelines, such as IEEE1547 [113], were established on the assumption that the integration of distributed generation is relatively low. However, the high penetration of RESs with a high degree of uncurtaining may push the grid voltage beyond the limits considered by ANSI C84.1 and disturb the regular operation of Volt/Var control devices [114]. Different types of organizations introduce a new concept in which users have to provide some ancillary services to the grid by adjusting the reactive power exchanged [115][116]. Hence, new codes allow the inverters to actively participate in the voltage regulation presented [117][118]. Figure 4.13 shows an inverter in a 2-quadrant P-Q plane mode. The inverter can be either capacitive (right side) or inductive (left side), as also shown in Figure 4.13.

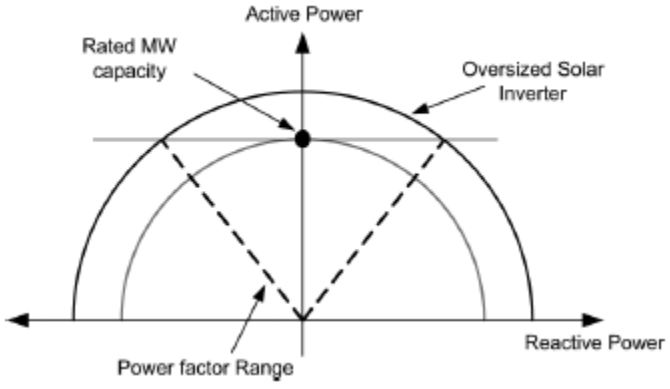

Figure 4.13. 2-quadrant P-Q control method[119] .

It has been discussed in the literature that oversizing the inverter by 10% will increase the capability of the reactive power when maximum real power is generated by the PV system [118][115]. Increasing the inverter size by 10% will maximize the apparent power of the inverter, $S_{inv} = 1.1P_{inv}^{max}$, hence the maximum available reactive power, $Q_{inv}^{max,t}$, is quantified by the remaining capacity of the inverter's rating, S_{inv}, as shown in the following formula [120]:

$$-\sqrt{(\boldsymbol{S_{inv}})^2 - (\boldsymbol{P_{inv}^t})^2} \leq \left|\boldsymbol{Q_{inv}^{max,t}}\right| \leq \sqrt{(\boldsymbol{S_{inv}})^2 - (\boldsymbol{P_{inv}^t})^2} \qquad 4.22$$

where P_{inv}^t is the instantaneous power at each interval t. In this study, the inverters of both PV and wind power systems will be assumed to have the same structure and operating conditions.

Given the capability of the inverters to actively participate in the Volt/Var control problem, their dispatch schedule for a day-ahead is essential in order to determine the required reactive power to regulate the system's voltage, minimize losses, as well as to reduce the operation of the Volt/Var control equipment.

4.7.2 Objective function

The PVVC problem is solved for a day-ahead, including the reactive power support from the inverters. The objective function is normalized and solved as a single weighted objective function, as formulated in Equation 4.23. The first five terms of the objective function are similar to the objective used in Equation 4.1. The sixth term represents the minimization of the reactive power from the inverters, as shown in Equation 4.24.

$$F = w_{loss}\frac{F_{loss}}{F_{los}^0} + w_{DV}\frac{F_{VD}}{F_{VD}^0} + w_{LTC}\frac{F_{LTC}}{F_{ltc}^0} + w_{svr}\frac{F_{SVR}}{F_{svr}^0} - w_{cur}\frac{F_{cur}}{F_{cur}^o} + w_{inv}\frac{F_{Qinv}}{F_{Qinv}^o} \qquad 4.23$$

$$F_{Qinv} = \sum_{i\in N_{inv}} \sum_{t=1}^{24} |Q_{inv,i,t}| \qquad 4.24$$

where $\boldsymbol{Q_{inv,i,t}}$ represents the reactive power from the inverter. Reactive power compensation using smart inverters is competitive compared to conventional reactive power devices. However, reactive power compensation using smart inverters increases the current flow, which increases losses and the

temperature of the devices. Therefore, the inverters' lifespan will be degraded with increasing reactive power utilization, incurring costs to the system's owner [121]. Therefore, minimizing the reactive power supplied by inverters could increase the lifespan of the devices. The weights in Equation 4.23 are: 0.22,0.05,0.15,0.14 ,0.41,0.03 respectively

The operation and device constraints are similar to the constraints described in Section 4.2.2. The only changes are shown in Equations 4.26 and 4.27 by adding the reactive power term $Q_{inv,i,t}$ in the reactive power injection constraint and its operational limit.

- Real power injection constraints:

$$P_{g,t} + P_{inv,i,t} - P_{d,i,t} = V_{i,t} \sum_{j=1}^{N_b} V_{j,t}(G_{ij} cos\theta_{ij,t} + B_{ij} sin\theta_{ij,t}) \quad 4.25$$

- Reactive power injection constraints:

$$Q_{g,i,t} + Q_{inv,i,t} - Q_{d,i,t} = V_{i,t} \sum_{j=1}^{N_b} V_{i,t}(G_{ij} sin\theta_{ij,t} - B_{ij} cos\theta_{ij,t}) \quad 4.26$$

Reactive power from IBRES constraints:

$$-\sqrt{(S_{inv})^2 - (P_{inv,i,t})^2} \leq \left|Q_{inv,i,t}\right| \leq \sqrt{(S_{inv})^2 - (P_{inv,i,t})^2} \quad 4.27$$

The formulated PVVC problem seeks the optimal dispatch schedule of the inverters in coordination with the OLTC and SVR. The power losses and voltage deviation minimization are also included to ensure the optimal operation of the network for a day-ahead under the high fluctuation of the generated power from RESs.

4.8 Case Study

The proposed model is evaluated using the same 33-Bus 11-kV test system, as shown in Figure 4.1. The location of the PV and wind power systems are the same. There are no SC banks because the target is to have reactive power only from the inverters.

The distribution test system feeds only residential customers with normalized daily load profiles, as illustrated in Figure 4.3, assuming this pattern is similar for consecutive days. The maximum penetration level of RESs considered in this study is 60%, calculated from the rated output power of PV and Wind farms as a percentage of the peak demand. The forecasted PV and wind power systems are the same as shown in Figure 4.2.

The dispatch schedule of the reactive power from PV and wind power systems are determined according to the system's requirements of reactive power from each inverter to keep the voltage at each bus close to 1.0 pu with minimum losses and minimum device operations. Figure 4.14 shows the voltage profile during the 24-hours on the selected buses after using smart inverters to inject/absorb reactive power in coordination with OLTC/SVR devices. Comparing the voltage profiles from Figure 4.4 and Figure 4.7, with and without RES curtailment options, it can be observed that the voltage profile in Figure 4.14 has a smoother pattern with less fluctuation and is closer to the desired reference voltage. It can be observed that the highest voltage point is 1.02 pu, which occurs on bus 13 at 3:00 PM, where the PV injects the maximum power. In contrast, 0.97 is the lowest voltage, which occurs at the end of the feeder at bus 18 during the high demand at the end of the day, where the PV generation is zero and the wind power supply is relatively small. The fluctuation in the voltage profile without deploying smart inverters, as shown in Figure 4.7, has almost vanished, and during the 24-hour simulation period, the voltage profile in Figure 4.14 becomes more flattened. The ability of the inverters to inject/absorb reactive power to offset the reactive power from the load, and to reduce the voltage increase as a result of high RES injection, has achieved better voltage control when coordinated with Volt/Var control equipment.

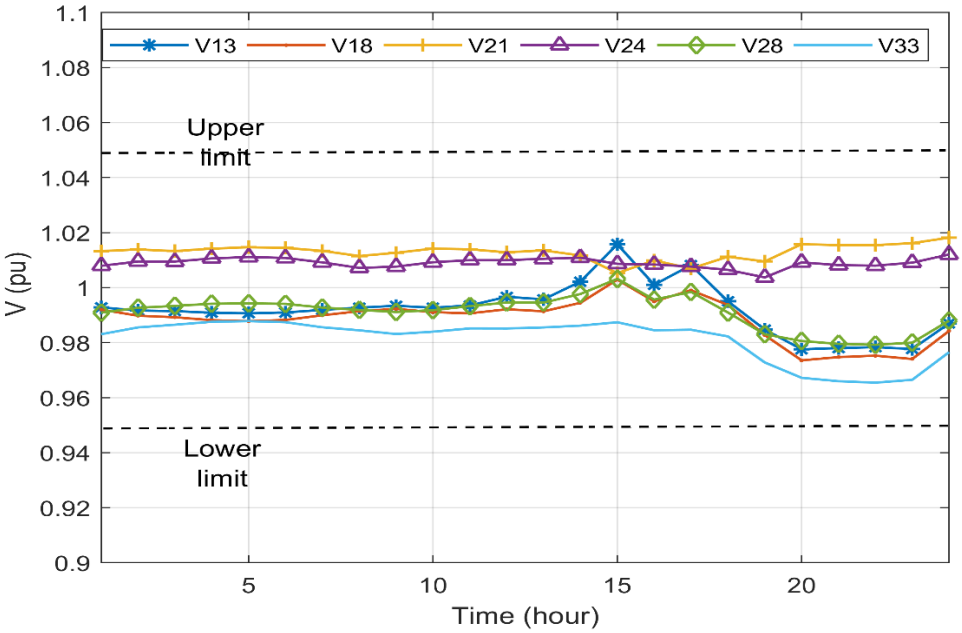

Figure 4.14. System voltage on the selected buses.

Figure 4.15 shows the dispatch of the PV inverters for 24-hours. The inverter at bus 13, which has a larger capacity, supplied/consumed most of the reactive power determined by the centralized controller to keep losses and voltage deviation at a minimum. Both inverters inject and consume reactive power following similar patterns due to the influence of the load shape and RES output profile, as well as the remaining available capacity in each inverter. Between intervals 6:00 AM- 11:00 AM and intervals 6:00 PM -11:00 PM, most of the reactive power is supplied to compensate for the reactive power consumed by the loads, so the voltage drop is kept at a minimum value. From intervals 2:00 PM – 5:00 PM, the injected active power from PV systems is high, which raises the voltage. Hence, the inverters start consuming reactive power in coordination with OLTC/SVR equipment to mitigate the voltage rise. Figure 4.16 shows the reactive power injected by wind inverters on buses 21 and 28. Given that the capacity of PV systems is larger than Wind systems, the reactive power share from Wind inverters is comparably small. Between 2:00 PM–5:00 PM, the inverters consume reactive power to contribute to voltage rise mitigation. Reactive power is subsequently supplied during load peak times, similar to PV inverters, to keep the voltage drop at a minimum.

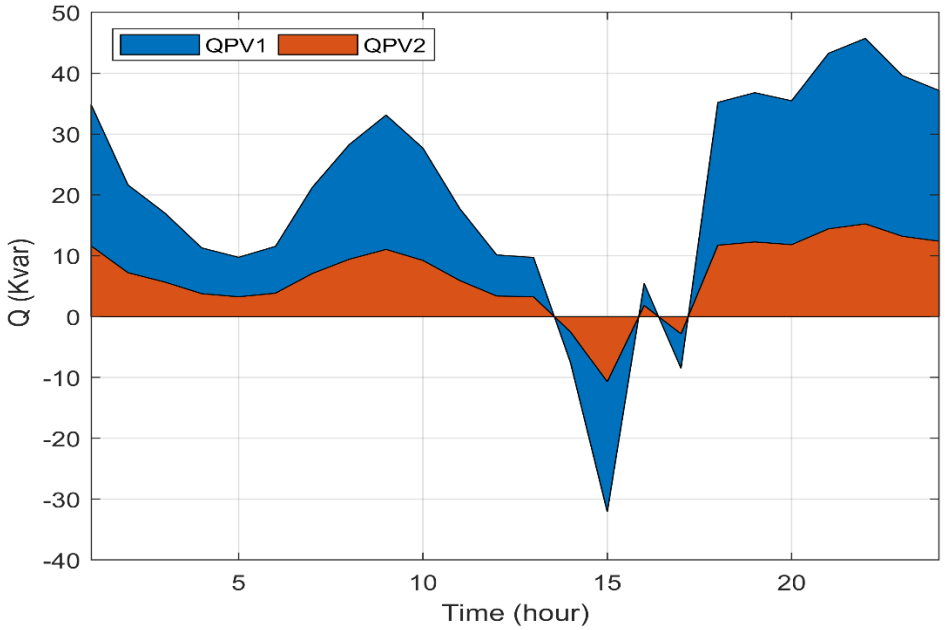

Figure 4.15. Inverter reactive power from PV.

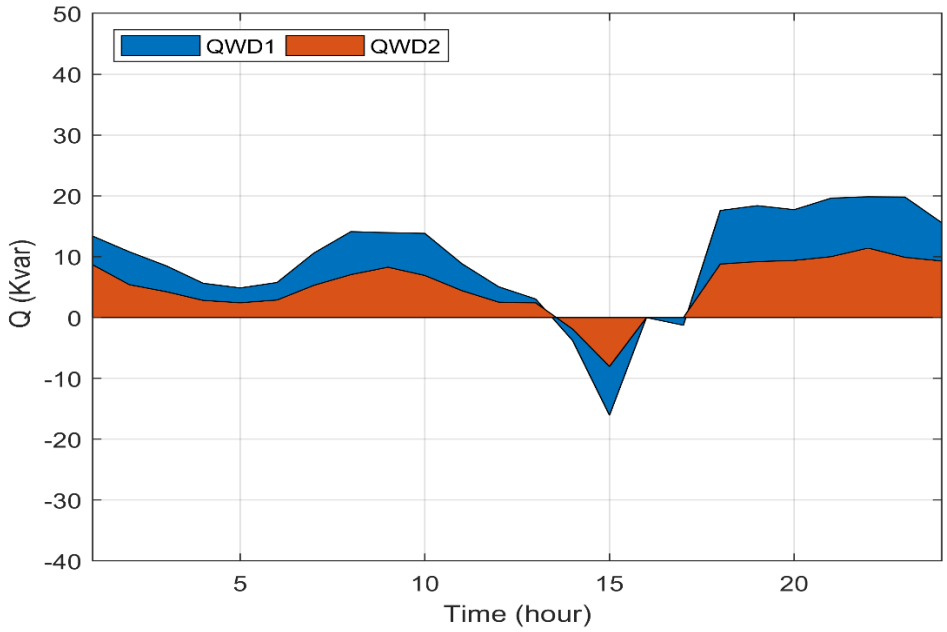

Figure 4.16. Inverter reactive power from wind farms

That small reactive power injection/consumption is dispatched between all four inverters to run the system at high efficiency and lower operating costs.

Figure 4.17 shows the switching operations of the OLTC and SVR. The daily operations of the OLTC and SVR are decreased to two switchings for the OLTC and two switchings for the SVR compared with the previous case, as shown in Figure 4.8. At 8:00 PM, the OLTC changed its tap from 3 to 5 and stayed at this level for the rest of the day. In contrast, the SVR stepped down one tap from 0 to -1 at 6:00 PM. The SVR subsequently stepped up one-step to 0 taps at 8:00 PM. The active contribution of the inverters assisted in minimizing the voltage variations and kept them close to the reference value, which positively reduced the operations of the OLTC and SVR. The centralized controller executed the coordination between the OLTC, SVR, and the inverters after solving the optimization problem, which at the end of the day reduces the operating costs associated with Volt/Var device operations and the total active losses of the distribution system.

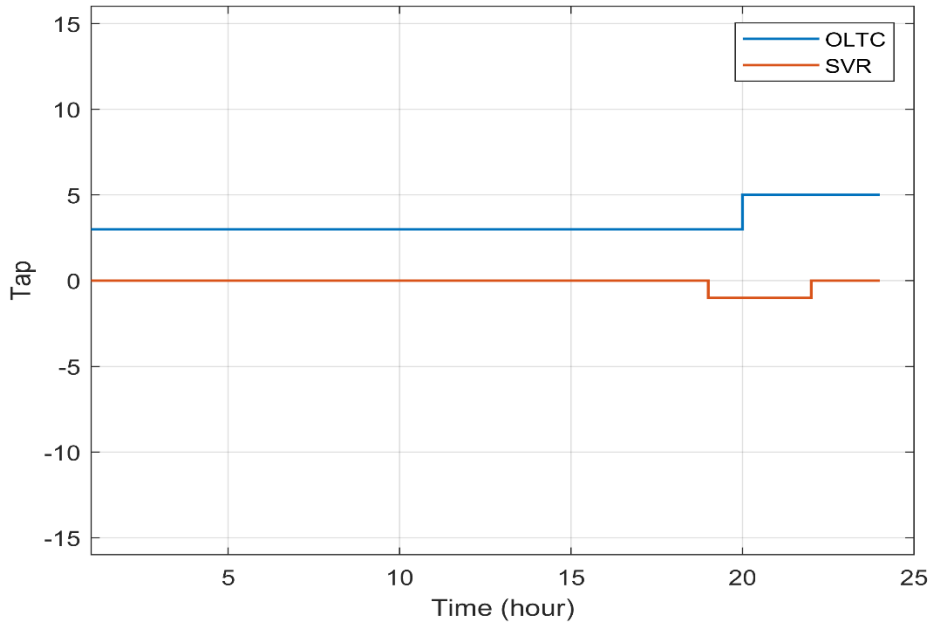

Figure 4.17. Switching operations of OLTC and SVR

Figure 4.18 shows the active power losses over the 24-hour simulation period, as well as a comparison between the active power losses when using reactive power from the inverters and when the inverters operate at a unity power factor with the curtailment option. It can be observed that when

using the reactive power from the inverters as ancillary services, the losses are further minimized. The contribution of the inverters in providing reactive power at load peak times reduces the reactive current coming from the substation, hence the term I^2R is reduced. Between 2:00 PM and 4:00 PM, a spike in power losses, namely "the blue line", is observed, due to the high active power injection from the PV systems. On the other side, the spike causes "the red line" to disappear, due to the curtailment action that occurs at that time. The active power losses reduce from 2.5MW to 1.75MW when using the inverters as a reactive power supply rather than supplying active power only.

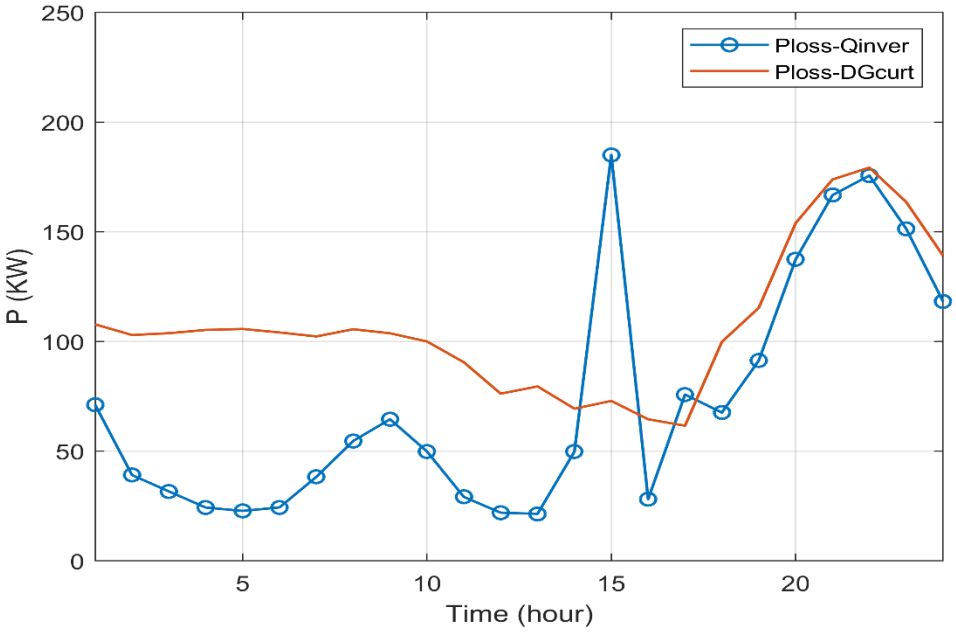

Figure 4.18. System active power losses

A summary of the operation cost in terms of Volt/Var devices operation and total active power losses during the simulation period is depicted in Table 4-6.

Table 4-6. Summary of the operational cost

	OLTC Oper/day	SVR Oper/day	Ploss (MW)/day	Cost ($)
Operational cost	2	2	1.75	166$

Figure 4.19 shows all voltages in the test system during the 24 hours (48 intervals). It can be observed that there are two main areas with a small voltage rise on buses 13 and 31, respectively. The area of voltage rise is due to the highly injected power from the PV systems. Moreover, the impact of wind farms on buses 21 and 24 appears on the graph as a small voltage rise for most of the day. Most importantly, all the voltages in the distribution network are within the permissible limit and close to the reference value.

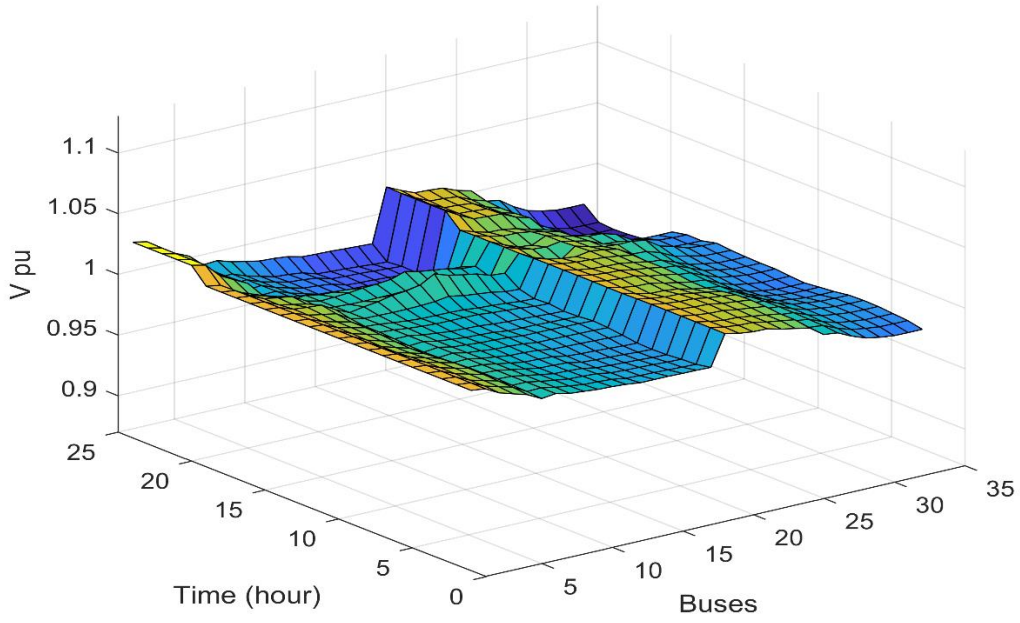

Figure 4.19. The surface plot for all voltages for 24 hours

4.9 Conclusion

High variations in PV and wind power outputs may occur in minutes or hours depending on weather conditions. The high variations under high penetration may bring serious operating challenges such as voltage fluctuation and frequent operation of Volt/Var devices such as SVR, OLTC, and SCs. Therefore, in this chapter, two generic predictive Volt/Var control models are developed. The first model coordinates the operation of the Volt/Var control equipment with curtailing part of the renewables at peak generation times to keep the system voltage profile within security limits. The developed model has shown an excellent ability to reduce the operations of the Volt/Var control devices while keeping the curtailment of RES sources at a minimum when the voltage violates the limits. The second model operates inverter-based RESs at variable power factor and uses them as ancillary services for reactive power support. Under this strategy, RES curtailment options at certain penetration levels are avoided, where the voltage rise can be mitigated by controlling the reactive power of the inverter at the connected bus. Oversizing the inverter by 10% from the rated capacity gives some extra capacity to inject or absorb reactive power even when the generation unit produces maximum power. The proposed control models improved the overall voltage profile and maximized the utility profit by minimizing losses. The models also minimized the frequent operations of the OLTC, SVR, and SCs, which reduces the maintenance cost and increases the operational lifespan of the equipment. The day-ahead operating schedule is acceptable to a certain degree of penetration and RESs output fluctuation. The operation depends heavily on the forecast of renewables and load. If the variations in the generated power are severe, a more precise forecasting tool and real-time operation of the smart grid is a favorable option. This will be discussed in the following chapter.

Chapter 5
A Sequential Predictive Control Strategy for Renewable Dominant Smart Distribution System

5.1 Preamble

In the previous chapter, the development of day-ahead Volt/Var control models for operating a Smart Distribution Grid (SDG) under high deployment of RESs was presented. Scheduled hourly operation is acceptable under some degree of uncertainty. However, solar PVs and wind power farms are known by their stochastic nature, consequently, it is challenging to predict power generation over a long period from the perspective of predictive or real-time operation. At a high integration level of solar PVs and wind power systems on a distribution level, several operational issues could occur, as discussed in the literature. Although Volt/Var control devices such as OLTC, SVRs, and SCs are effective in managing slow voltage variations, they might not be efficient with fast and high voltage fluctuations on a time scale of minutes. Hence, a fast and efficient Volt/Var control strategy that considers short-term changes in RESs generated power and demands is required.

In this chapter, a Sequential Predictive Control (SPC) Strategy for voltage and reactive power control is developed. The control strategy uses past and currently available data to forecast demand, and RES outputs for 15-minutes, then optimally schedule the next interval settings and operations of the Volt/Var control devices by solving an optimization problem in a rolling horizon approach. The STSE model proposed in Chapter 3 is used for forecasting PV/wind outputs and demand by sequentially updating itself each 15-minutes, based on the newly measured data. When the next forecasted generation and demand are available, the proposed control strategy is applied to ensure the optimal operation of SDGs. As the solution has to be accurately executed in a short time, a solution methodology to linearize the nonlinear control problem is adapted. The original MINLP control problem, which is very difficult and time-consuming to solve, is transformed into a Mixed Integer Second Order Cone Programming (MISOCP) problem, which is a convex problem subject to linear and conic constraints. The proposed control model is able to accurately predict the short-term RES output and demand then act accordingly to overcome any abnormal or undesirable operating conditions.

5.2 Forecasting With Forgetting and Updating Mechanism

At the large scale penetration of PV and wind power systems, real-time or sequential short-term operation of an SDG is required to account for the stochastic and intermittent nature RESs. Therefore, an online forecasting process based on the STSE model with a forgetting and updating mechanism is developed. The process works by omitting the oldest data points and sequentially retraining the model with new measured data while moving over the horizon, as shown in Figure 5.1. The figure explains the training process, which is updated at each new measured point. The initial training starts with the training vector from T-2: T0 to predict T1. When the next point T1 is available, the model forgets the outdated point T-2 and retrained by the new vector from T-1: T1 to predict T2. The advantage of the forgetting and updating technique is to keep the training data short and reduce the impact of concept drift [122].

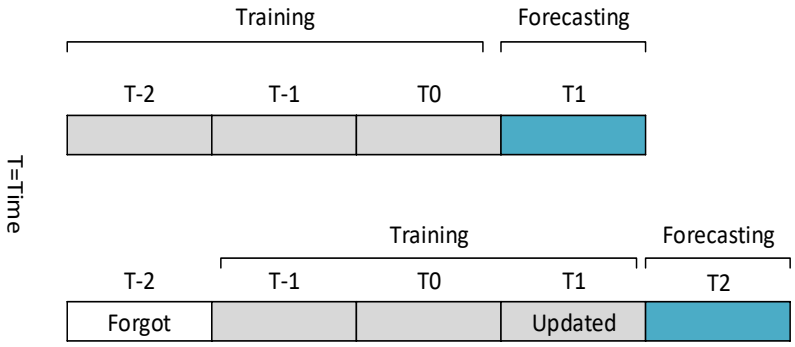

Figure 5.1. Forgetting and updating forecasting mechanism

5.3 Modeling the Sequential Predictive Control Strategy

The SPC is described by a mathematical model and formulated as an optimization problem using the branch flow model presented in [123]. The bus injection model focuses on nodal variables such as voltage, current, and power injections and does not deal directly with power flows on individual branches. Instead of nodal variables, the branch flow model focuses on currents and power on the branches [124].

5.3.1 Requirements for the sequential applications

To implement the proposed methodology, the following requirements need to be satisfied first [125]

1. A central control unit (CCU) and support for SCADA system.
2. An advanced metering infrastructure for real-time data measurements.
3. Remotely controllable equipment with commutable controllers.
4. An efficient and modern communication infrastructure.

5.3.2 Objective function

The SPC model is represented by an objective function, as shown in Equation 5.1, which is a linear weighted combination of minimum active power losses, switching operations of the OLTC/SVR, and voltage deviation. Each individual objective function is normalized to satisfy the weighted sum method, as discussed in Chapter 4. The weight coefficient of each term is shown in Table 5-2.

$$min\ F = w_{loss}F_{loss} + w_{DV}F_{VD} + w_{LTC}\ F_{LTC} + w_{svr}\ F_{SVR} \quad 5.1$$

The active power losses of the network are the power losses in all branches defined by the square of the line current $I_{ij,t}^2$ multiplied by the line resistance r_{ij} , where N_{br} is the set of branches.

$$F_{loss,t} = \sum_{ij \in N_{br}} r_{ij}\ I_{ij,t}^2 \quad 5.2$$

The second objective is the voltage deviation [126][127]. N_B is the set of buses.

$$F_{VD,t} = \sum_{i=1}^{N_B} \left| V_{i,t}^2 - 1 \right| \quad 5.3$$

The third objective is associated with the tap changes of the LTC transformer between consecutive intervals.

$$F_{LTC,t} = \sum_{ij \in N_{ltc}} \left| tap_{ij,t}^{ltc} - tap_{ij,t-1}^{ltc} \right| \quad 5.4$$

where N_{ltc} is the set of OLTC transformers and $tap_{ij,t}^{ltc}$ / $tap_{ij,t-1}^{ltc}$ are the tap positions at interval t and t-1, respectively.

Similarly, the fourth objective is associated with the tap changes of the SVR between consecutive intervals:

$$F_{SVR} = \sum_{ij \in N_{svr}} \left| tap_{ij,t}^{svr} - tap_{ij,t-1}^{svr} \right| \quad 5.5$$

where N_{svr} is the set of OLTC transformers and $tap_{ij,t}^{svr}$ / $tap_{ij,t-1}^{svr}$ are the tap positions at interval t and t-1, respectively.

5.3.3 Constraints

1. System operation constraints

Figure 5.2 shows a partial distribution feeder with a transformer. Transformer ij can be divided into branch mj, which contains a tap changer. The impedance of branch im is the same as branch ij. The branch flow model shown in Figure 5.2 is used to model the distribution network [110]. The mathematical representation of the model is described in the following:

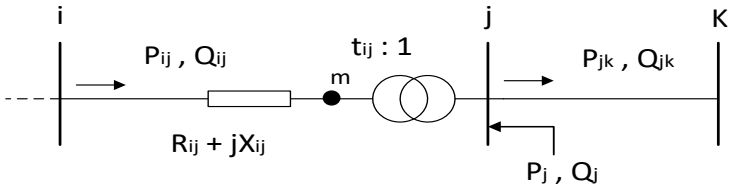

Figure 5.2. One-line diagram of the feeder with a transformer.

$$\sum_{ij \in N_{br}} (P_{ij,t} - r_{ij} I_{ij,t}^2) + P_{j,t} = \sum_{ij \in N_{br}} P_{jk,t} \quad 5.6$$

$$\sum_{ij \in N_{br}} (Q_{ij,t} - x_{ij} I_{ij,t}^2) + Q_{j,t} = \sum_{ij \in N_{br}} Q_{jk,t} \quad 5.7$$

$$V_{i,t}^2 - V_{j,t}^2 = 2\left(r_{ij} P_{ij,t} + x_{ij} Q_{ij.t}\right) - \left(r_{ij}^2 + x_{ij}^2\right) I_{ij,t}^2 \quad 5.8$$

$$I_{ij,t}^2 V_{i,t}^2 = (P_{ij,t}^2 + Q_{ij,t}^2) \quad 5.9$$

$$P_{j,t} = P_{j,t}^{inv} - P_{j,t}^{dem} \quad 5.10$$

$$Q_{j,t} = Q_{j,t}^{inv} - Q_{j,t}^{dem} \quad 5.11$$

Equations 5.6 and 5.7 represent the branch flow equations. $P_{ij,t}$ and $P_{jk,t}$ represent the active power flow in branches ij and jk, respectively, while $Q_{ij,t}\ and\ Q_{jk,t}$ represent the reactive power flow in branch ij and jk. Ohm's law for branch ij is expressed in Equation 5.8. Equation 5.9 determines the current magnitude in each line. Equations 5.10 and 5.11 represent the injected active and reactive power at node j. $P_{j,t}^{inv}\ and\ Q_{j,t}^{inv}$ represent the active and reactive power injected by the RES inverters at time t, while $P_{j,t}^{dem}\ and\ Q_{j,t}^{dem}$ are the demand active and reactive power of node j at time t.

2. Voltage and current security constraints

$$\left(V^{min}\right)^2 \leq V_{i,t}^2 \leq (V^{max})^2 \qquad 5.12$$

$$I_{ij,t}^2 \leq (I^{max})^2 \qquad 5.13$$

Where V^{max} and V^{min} are the maximum/minimum allowable voltage limits on each bus. I^{max} represents the maximum line current capacity.

3. RES operation constraints

$$P_{i,t}{}^{inv} = P_{i,t+1}^{fore} + \Delta P_{i,t}^{err} \qquad 5.14$$

$$-\sqrt{\left(S_i^{inv}\right)^2 - (P_{i,t}^{inv})^2} \leq \left|Q_{i,t}^{inv}\right| \leq \sqrt{\left(S_i^{inv}\right)^2 - (P_{i,t}^{inv})^2} \qquad 5.15$$

As discussed in Chapter 4, the reactive power provided by the RES inverter is limited by the active power at time t and the rated capacity of the inverter S_i^{inv}, where $P_{i,t}{}^{inv}$ is the injected active power from the RES inverter at time t calculated from the forecasted power $P_{i,t+1}{}^{fore}$ and the forecasting error $\Delta P_{i,t}^{err}$**.** The forecasting error is determined at the current time t, assuming that the trend and error between two consecutive intervals do not significantly deviate.

4. OLTC/SVR operation constraints

The OLTC and the SVR have the same constraints and relationship between the primary and the secondary voltage [127].

$$V_{j,t} = m_{ji,t}\, V_{i,t} \qquad 5.16$$

$$m_{ij,t} = m_{ij}^{min} + M_{ij,t}\,\Delta m_{ij} \quad 5.17$$

$$-M_{ij}^{-} \le M_{ij,t} \le M_{ij}^{-},\ \forall\, ij\ \in N_{ltc}, N_{svr} \quad 5.18$$

where m_{ji}^{min} is the initial turns ratio, while Δm_{ij} denotes the turns ratio for each step. The $M_{ij,t}$ integer variable represents the actual tap. M_{ij}^{-}, represents the maximum tap level for the OLTC/SVR.

The objective function and constraints that appear in the model's Equations 5.2 to 5.18 have continuous and discrete variables. They represent a non-convex and MINLP problem, which is difficult and time-consuming to solve. Equations 5.9 and 5.16 represent the nonlinear relationship between the variables. The integer variable that appears in Equation 5.17 converts the problem from an NLP problem into an MINLP problem. Hence, in order to solve the sequential predictive control problem, there is a need for an accurate and fast solution algorithm.

5.4 Mixed-Integer Second-Order Cone Programming (MISOCP)

Mixed-integer second-order cone programming problems (MISOCPs) can be expressed as [128]:

$$\min_{x \in X} \quad c^T x$$

subject to $\|A_i\, x + b_i\| \le a_{0i}^T x + b_{0i}\,, \qquad i = 1, \ldots, m$

where x is the $n - vector$ of decision variables. $X = \{(y, z): y \in Z^p\ , z \in R^k\ , p + k = n\}$, and the data are $c \in R^n\ , A_i \in R^{m_i\, x\, n}\ , b_i \in R^{m_i}\ , a_{0i} \in R^n\ \ for\ i = 1, \ldots, m.$

The notation $\|.\|$ denotes the Euclidean norm, and the constraints are said to define the second-order cone, also referred to as the Lorentz cone.

MISOCP is a specialized branch of convex MINLP. The concept of MISOCP is to minimize a linear objective function subject to a set of linear and second-order cone constraints. MISOC is an active research area, with several applications in many real-life fields such as finance and engineering. A thorough survey of the literature on the application of MISOCP algorithm is presented in [129]. In solving power distribution problems that require a fast and accurate solution, there are several methodologies to linearize a non-convex power flow problem as stated in [130][131][132][133]. The NLP and MINLP problems were converted to LP and MILP problems in the aforementioned linearization techniques. In [134], the radial load flow is modeled as a conic programming problem, which is a convex optimization problem that can be efficiently solved by existing algorithms. MINLP problems, which consist of integer variables such as transformer tap and capacitor sets, are converted

into a MINSOCP optimization problem by introducing binary linearization for the integer variables and cone relaxation [127]. In [135] a comparison between MILP and MISOCP for the optimal operation of DNs with energy storage devices showed that MISOCP is a more effective solution. Among all the linearization and convexification techniques, SOCP exhibits excellent performance in terms of a rapid and global solution.

To convert the original MINLP problem, convex relaxation is used to transform it into a MISOCP problem. The square representations of voltage and currents that appear in Equations 5.2, 5.3, 5.6-5.9 5.12, and 5.13 are replaced by new variables. Variable substitution is used to realize the linearization by letting $U_{i,t} = V_{i,t}^2 \ and \ l_{ij,t} = I_{ij,t}^2$.

The power loss objective function is linear when representing the current by its new variable $l_{ij,t}$ as shown in Equation 5.19. The remaining Equations 5.20-5.24 are the new representation of Equations 5.6-5.8 and 5.12-5.13.

$$F_{loss,t} = \sum_{ij \in N_{br}} r_{ij}\, l_{ij,t} \quad 5.19$$

$$\sum_{ij \in N_{br}} (P_{ij,t} - r_{ij}\, l_{ij,t}) + P_{j,t} = \sum_{ij \in N_{br}} P_{jk,t} \quad 5.20$$

$$\sum_{ij \in N_{br}} (Q_{ij,t} - x_{ij}\, l_{ij,t}) + Q_{j,t} = \sum_{ij \in N_{br}} Q_{jk,t} \quad 5.21$$

$$U_{i,t} - U_{j,t} = 2\left(r_{ij}\, P_{ij,t} + x_{ij} Q_{ij.t}\right) - \left(r_{ij}^2 + x_{ij}^2\right) l_{ij,t} \quad 5.22$$

$$\left(V^{min}\right)^2 \leq U_{i,t} \leq (V^{max})^2 \quad 5.23$$

$$l_{ij,t} \leq (I^{max})^2 \quad 5.24$$

Constraint 5.9 can be expressed as a convex constraint through SOCP relaxation [124] as follows:

$$\left\| \begin{matrix} 2P_{ij,t} \\ 2Q_{ij,t} \\ l_{ij,t} - U_{i,t} \end{matrix} \right\|_2 \leq l_{ij,t} + U_{ij,t} \quad 5.25$$

RES operational constraint from Equation 5.15 is a nonlinear quadratic constraint that can be converted into a rotated quadratic cone constraint [126]:

$$(P_{i,t}^{inv})^2 \ + (Q_{i,t}^{inv})^2 \ \leq 2\left(\frac{S_i^{inv}}{\sqrt{2}}\right)\left(\frac{S_i^{inv}}{\sqrt{2}}\right) \quad 5.26$$

$$(P_{i,t}^{inv})^2 + (Q_{i,t}^{inv})^2 \geq -2\left(\frac{S_i^{inv}}{\sqrt{2}}\right)\left(\frac{S_i^{inv}}{\sqrt{2}}\right) \quad 5.27$$

After the introduction of the new voltage and current variables, Equation 5.16 is rewritten as:

$$U_{j,t} = m_{ji,t}^2 \, U_{i,t} \quad 5.28$$

The integer variable $M_{ij,t}$ can be represented by a set of binary variables [136] as follows:

$$M_{ij,t} = \sum_{m=0}^{2M_{ij}^-} [(m - M_{ij}^-) b_{ij,t,m} \quad 5.29$$

$$\sum_{m=0}^{2M_{ij}^-} b_{ij,t,m} = 1 \quad 5.30$$

where $b_{ij,t,m}$ is a binary variable that belongs to the set [0,1]

By substituting 5.17 and 5.29 into 5.28

$$U_{j,t} = \sum_{m=0}^{2M_{ij}^-} [(m_{ij}^{min} + (m - M_{ij}^-)\Delta m_{ij})^2 \, U_{i,t} \, b_{ij,t,m}] \quad 5.31$$

A new variable $U_{ij,t}^c$ is introduced to represent the nonlinear product of $U_{i,t} b_{ij,t,m}$. In addition, new constraints are added to make the equation linear [137] as follows:

$$U_{j,t} = \sum_{m=0}^{2M_{ij}^-} [(m_{ij}^{min} + (m - M_{ij}^-)\Delta m_{ij})^2 \, U_{ij,t,m}^c \,] \quad 5.32$$

$$U_{ij,t,m}^c = U_{i,t} b_{ij,t,m} \quad 5.33$$

Equation 5.32 is linear, but 5.33 presents the product of a continuous variable and a binary variable that can be substituted by two equivalent linear constraints as shown below:

$$(V_i^{min})^2 \, b_{ij,t,m} \leq U_{ij,t,m}^c \leq (V_i^{max})^2 \, b_{ij,t,m} \quad 5.34$$

$$(V_i^{min})^2 \, (1 - b_{ij,t,m}) \leq U_{i,t} - U_{ij,t,m}^c \leq (V_i^{max})^2 \, (1 - b_{ij,t,m}) \quad 5.35$$

For the absolute term representing the consecutive tap changes of OLTC and SVR in the objective functions from Equations 6.4 and 6.5, new auxiliary variables $M_{ij,t}^+$, ${R_{ij,t}}^+$ are introduced. The linear equivalent to the objectives is shown:

$$tap_{ij,t}^{ltc} - tap_{ij,t-1}^{ltc} \leq M_{ij,t}^{+} \quad 5.36$$

$$tap_{ij,t-1}^{ltc} - tap_{ij,t}^{ltc} \leq M_{ij,t}^{+} \quad 5.37$$

$$M_{ij,t}^{+} \geq 0 \quad 5.38$$

And for the SVR:

$$tap_{ij,t}^{svr} - tap_{ij,t-1}^{svr} \leq R_{ij,t}^{+} \quad 5.39$$

$$tap_{ij,t-1}^{svr} - tap_{ij,t}^{svr} \leq R_{ij,t}^{+} \quad 5.40$$

$$R_{ij,t}^{+} \geq 0 \quad 5.41$$

so that the final objective of the OLTC and SVR is the minimization of

$$F_{LTC,t} = \sum_{ij \in N_{ltc}} (M_{ij,t}^{+}) \quad 5.42$$

$$F_{SVR,t} = \sum_{ij \in N_{svr}} (R_{ij,t}^{+}) \quad 5.43$$

For the voltage deviation, a linearization methodology similar to the formulation in [137] is used. By introducing a new positive auxiliary variable $Vaux_{i,t}$, the absolute value of Equation 5.3, is linearized as:

$$Vaux_{i,t} \geq V_{i,t} - 1 \quad 5.44$$

$$Vaux_{i,t} \geq 1 - V_{i,t} \quad 5.45$$

$$Vaux_{i,t} \geq 0 \quad 5.46$$

And the minimization of the voltage deviation is the minimization of the auxiliary variable as follows:

$$F_{VD,t} = \sum_{i \in N_B} Vaux_{i,t} \quad 5.47$$

Using the convex relaxation and linearization, the original MINLP problem is formulated as a MISOCP problem. The final objective function is:

Min (5.19), (5.42), (5.43), (5.47)

S.t (5.20)-(5.27), (5.30), (5.32),(5.34),(5.35), (5.36)-(5.41), (5.44)-(5.46)

5.5 Actual Implementation

The implementation of the proposed algorithm is shown in the flowchart of Figure 5.3 using the following steps:

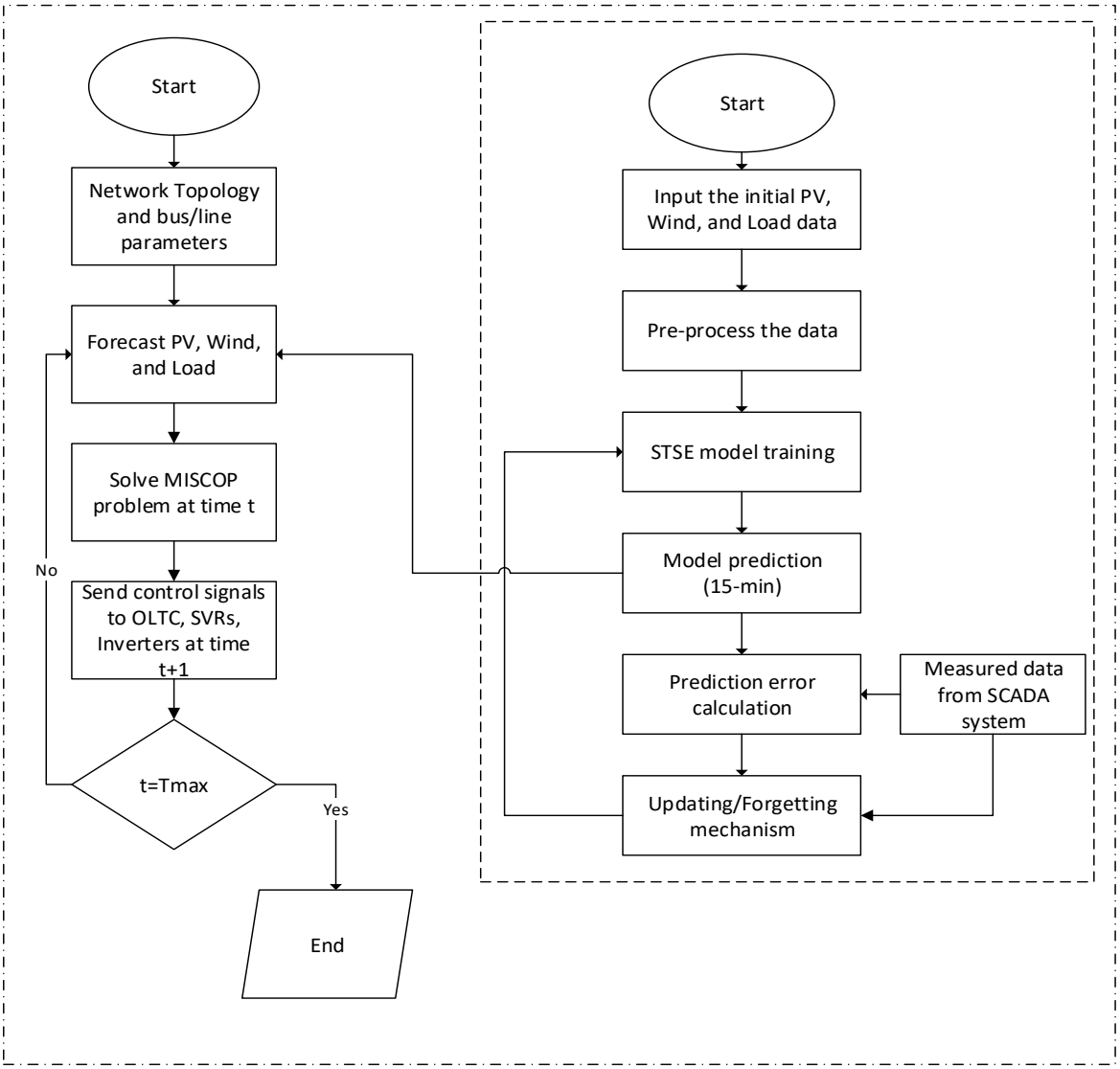

Figure 5.3. Flowchart of the proposed model

1. Initialization: In this phase, network information, such as configuration, line parameters, loads, and rated power of RESs, is provided to the central controller as inputs.

2. Monitoring: At this stage, smart meters at loads and generation units record and send the measured data to the central control unit (CCU) at time t.

3. Forecasting: At each time instant, short-term forecasting of PV, Wind, and load for 15minutes using the STSE model with the forgetting and updating mechanism as depicted in Figure 5.1, is implemented. The forecast is applied at time t to predict generation/demand at $t + 1$

4. System optimization: The system operators impose the network operating constraints regarding voltage limits, branch current, RES reactive power limits, and OLTC/SVR operating limits. When the operating constraints are identified, the CCU solves the optimization problem at the current time t to prepare for the optimal control actions at $t + 1$.

5. Control action: In this phase, control signals are passed to the Volt/Var control devices and inverters to maintain minimum system losses and voltage deviation.

6. Repeating: At the next time step $t + 1$, steps 2 to 5 are repeated to the end of the control horizon decided by the system operators.

Solving the optimization problem follows the concept of rolling horizon optimization, as depicted in Figure 5.4. The advantage of using a rolling horizon in the proposed real-time strategy is to avoid the effect caused by the predicted generation/demand forecasting error and to use the newly collected data. Figure 5.4 shows the stages of the optimization framework for three-time steps. Stage 2 starts after the time steps of Stage 1 is finished and continues as such for the rest of the receding horizon.

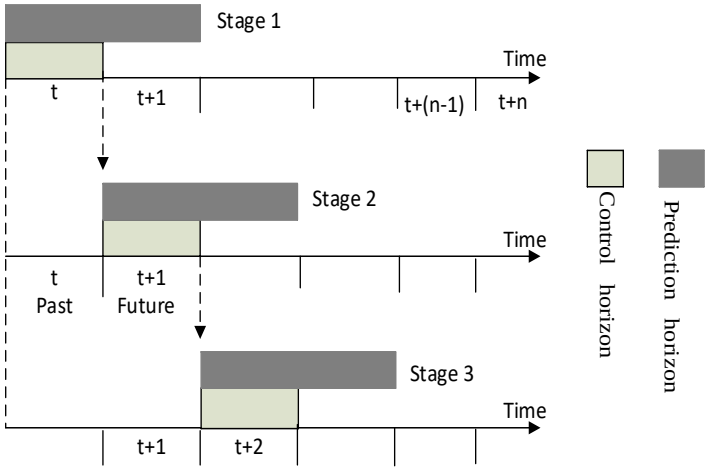

Figure 5.4. Rolling horizon framework

The algorithm that is proposed in this work is compared with the work presented in [100]. The proposed method has the advantage of accurately capturing fast power variations and solving the model in shorter time slots, and with a global solution.

5.6 System Under Study

The 12.66KV, IEEE 33-bus test system used in Chapter 4 is used. Two PV generators located at buses 11 and 28 and two wind farms located at buses 17 and 21 are used in this study. The size of each RES unit is depicted in Table 5-1. The characteristic of the OLTC and SVR are similar to those used in Chapter 4. The OLTC at the substation and SVR between buses 6 and 7 with ±16 taps regulate the voltage by +/-10%. All RESs operate at a variable power factor, where the reactive power is constrained by Equations 5.26 and 5.27, except for the base case scenario. The operational cost of the OLTC/SVR is similar to the operational costs used in Chapter 4, as suggested in [138], where the active power cost is $80/MW, and the depreciation cost of the OLTC/SVR is $6.36 for each step change, assuming they have a similar depreciation factor.

Table 5-1. RESs locations and sizes

DG Unit	Capacity (KVA)	Location(bus)
PV1	1360	13
PV2	1200	28
WD1	920	17
WD2	600	21

During the simulation study, the peak load of each bus is multiplied by the forecasted load profile at each time instance. The short-term forecast of the load profile and PV/Wind units using the proposed STSE model are shown in Figure 5.5 and Figure 5.6, respectively. These results are obtained from real-time forecasting, based on the forgetting and updating mechanism. The average time for the forecasting at each interval takes around 3 minutes, which highly depends on the efficiency of the processor.

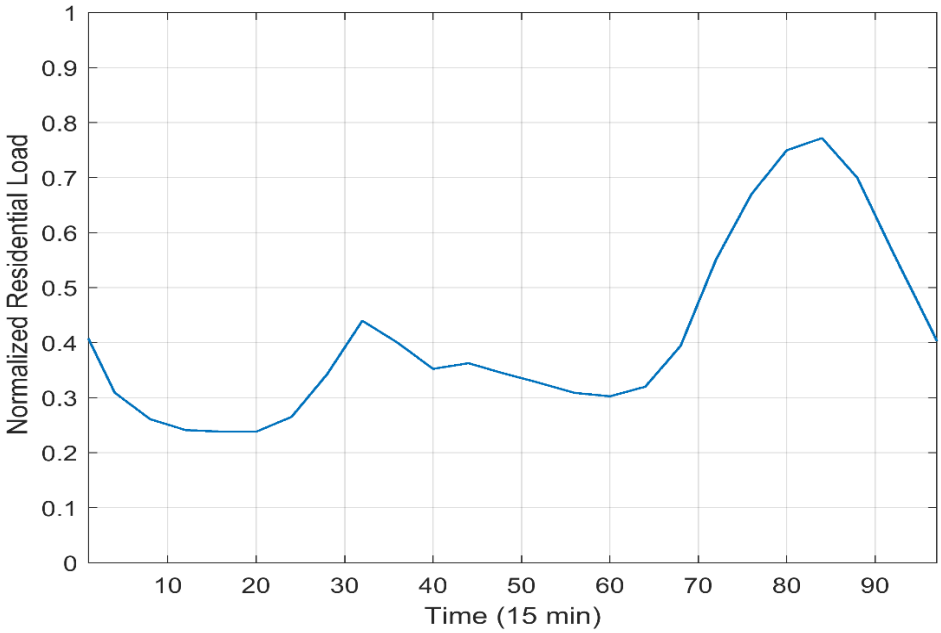

Figure 5.5. Forecasted load profile

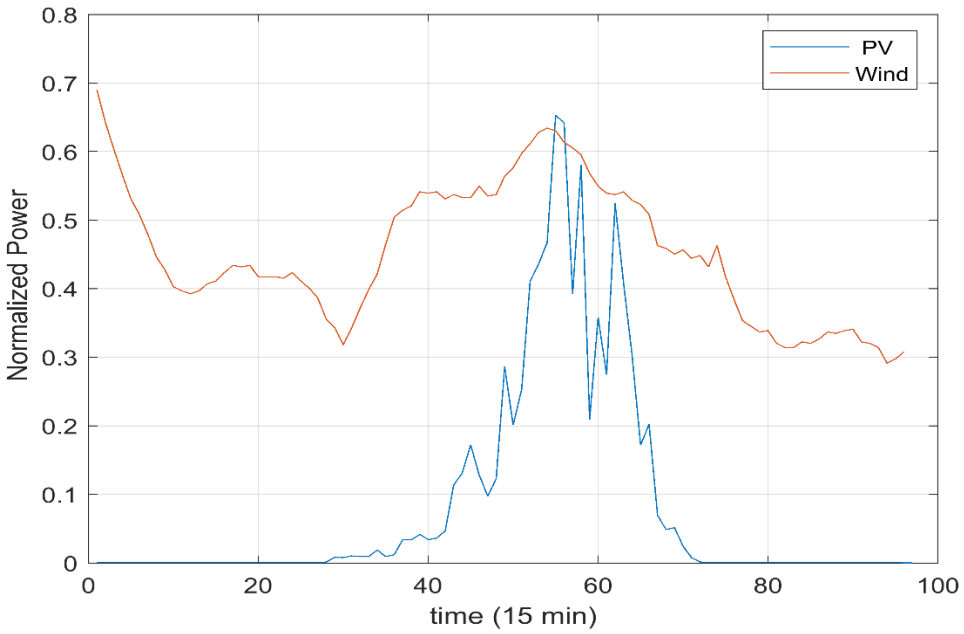

Figure 5.6. Forecasted PV/Wind power outputs

5.7 Case study

Three case studies are examined to assess the impact of the high and fast variation of renewables at the steady-state operation of the distribution system and to evaluate the proposed algorithm. The first case operates the system considering the optimization of voltage deviation only at a 60% penetration level. The second and third cases evaluate the proposed model at 30% and 60% penetration.

5.7.1 Case1: Base Case

Generally, voltage regulators such as OLTC and SVRs are controlled by their local control circuits, which depend on the line drop compensation mechanism. When renewables are installed on the distribution level, the amount and variation of the injected power confuse the operations of the regulators, which leads to a high number of switchings in response to voltage variation. At the base case scenario, only voltage deviation and power loss minimization from Equations 5.19 and 5.47 are applied to examine how power variations from renewables affect the operation of the voltage regulators at 60% penetration without reactive power support from inverters. Although, the CCU solves the problem, excluding the regulators' actions from the objective function increases the operational cost, hence decreases the lifespan of the devices [139].

The following objective function is implemented in the base case scenario. The weight coefficients are determined to be 0.7 and 0.3 for losses and voltage deviations, respectively. However, the selection of weights can be a utility's decision based on its preference, as suggested by some research studies as in [140]. The weight coefficients of each case study are shown in Table 5-2.

$$min\ F = w_{loss}(\sum_{ij \in N_{br}} r_{ij}\ l_{ij,t}) + w_{DV}(\sum_{i \in N_B} Vaux_{i,t}\ ) \qquad 5.48$$

subject to (5.20)-(5.25), (5.30), (5.32),(5.34),(5.35), (5.44)-(5.46)

Figure 5.7 shows the operations of the OLTC and SVR equipment for a one day simulation period. It can be observed that, without switching minimization, excessive operations that occurred when the variation of RES is very high. The 15minute time operation shows that the voltage can be maintained within security constraints, but more control action is required. Unlike the hourly operating periods, the short time operations clearly show the direct impact of the highly integrated renewables on the

operation of the Volt/Var control devices. Hence, an efficient and fast control mechanism to effectively operate a smart distribution system efficiently is required.

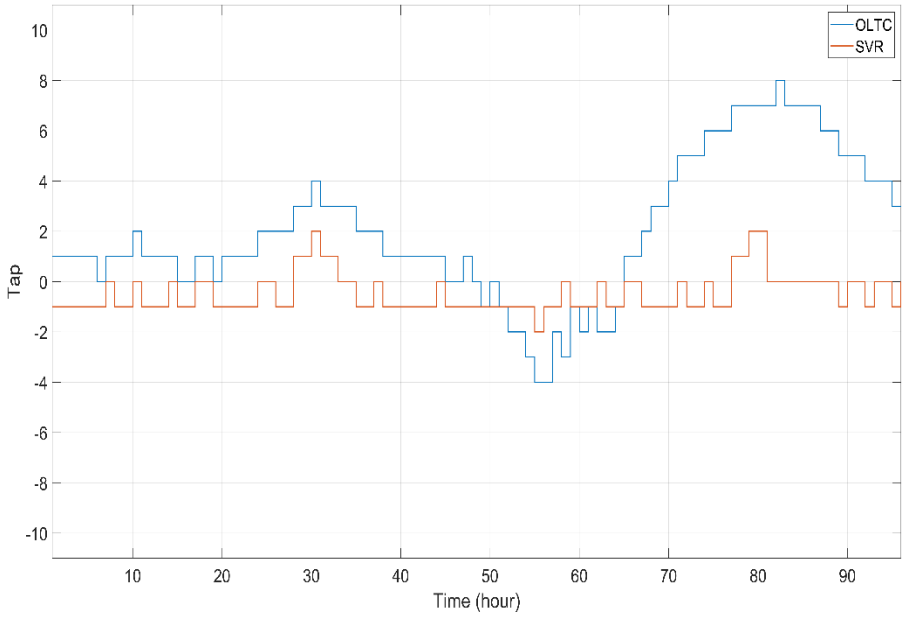

Figure 5.7. Operations of the OLTC/SVR (Base Case).

The switching operations of the OLTC show that it has many more operations per day counts for 46 taps/day. In contrast, the SVR has fewer actions compared with the OLTC, where the tap changed its position 43 taps/day. It should be noted that the operation of both devices is based on the optimal power flow solution, which minimizes power losses and voltage deviations. The operations of the OLTC and SVR occur without considering the control effort required to maintain the voltage within the security operating constraints.

Figure 5.8 shows the voltage profile of the selected buses during the simulation period. The impact of renewable variation can be clearly seen from the fluctuation in the voltage profile. The direct impact of high PV fluctuations can be seen on the voltage profile of buses 11 and 17 between 12:30 PM and 4:30 PM, where the voltage profile has high variations. However, the voltage is kept within the security constraints by applying more control actions, which is not a desirable operation as they directly reduce the lifespan of the Volt/Var control devices and increase the maintenance and replacement costs.

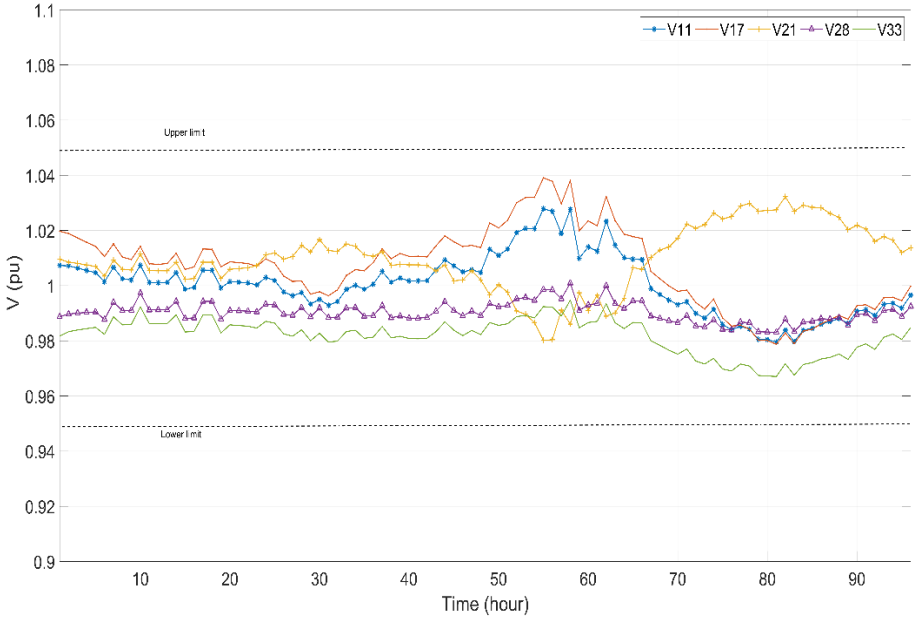

Figure 5.8. Voltage profile of the selected buses (Base case)

5.7.2 Case 2: Low Penetration

In this case, the full optimization problem is employed. The SPC strategy is applied to the test distribution system under 30% penetration of PV and Wind power systems. Equation 5.49 represents the objective function of the proposed control model.

$$min\ F_t = w_{loss}\left(\sum_{ij\in N_{br}} r_{ij}\ l_{ij,t}\right) + w_{DV}\left(\sum_{i\in N_B} Vaux_{i,t}\ \right) + w_{ltc}\sum_{ij\in N_{ltc}}\ (M^{+}_{ij,t})\ + w_{svr}\sum_{ij\in N_{svr}}\ (R^{+}_{ij,t}) \quad 5.49$$

subject to Equations (5.20)-(5.27), (5.30), (5.32),(5.34),(5.35), (5.36)-(5.41), (5.44)-(5.46)

In this scenario, the reactive power from the inverter based renewables is used as an ancillary service in coordination with the OLTC and SVR devices. The reactive power limits imposed by constraints 5.26 and 5.27 are based on oversizing the inverter capacity by 10% and incorporating the forecasting error of the renewable active power. The procedure for solving the SPC strategy follows the steps presented in Section 5.5.

Figure 5.9 shows the voltage profile of the selected buses at a low penetration level. In this case, the impact of renewables' variation is not very large; hence, low voltage fluctuation is expected.

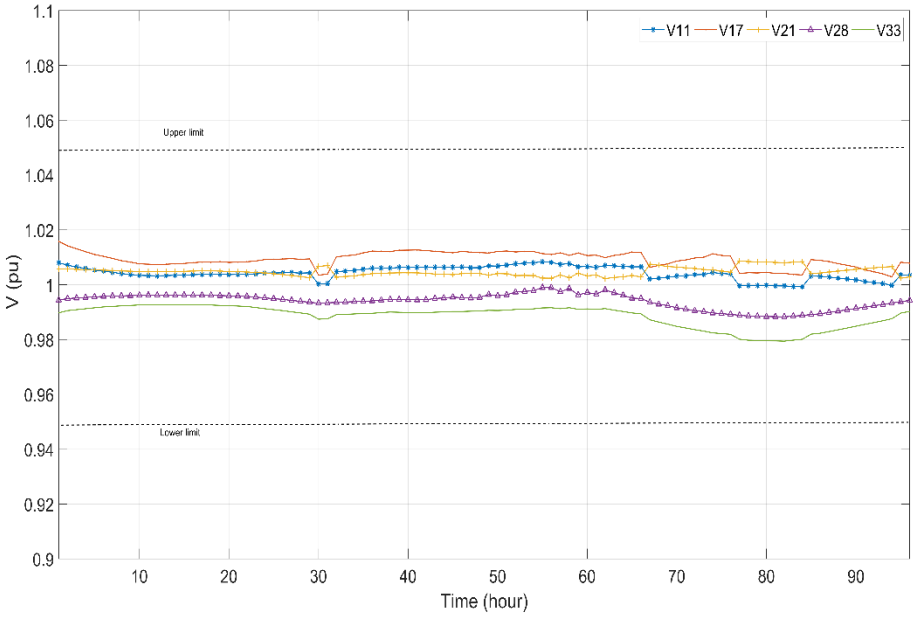

Figure 5.9. Voltage profile of the selected buses (Low penetration)

From the voltage profile, it can be observed that minimizing the voltage deviation by using the reactive power from the inverters has noticeably contributed to the smoothness of the voltage profile. The proposed oversized capacity of the reactive power from the inverters has an advantage over the methodology used in [141], which depends on the limited power factor of the RES (0.95 laging).

Figure 5.10 presents the dispatched reactive power from PV inverters during the simulation period. It can be seen that the reactive power follows the pattern of the load profile to offset the reactive power consumed by customers. The reactive power determined by the SPC model is a function of the RESs active power and the forecasted error calculated at each time step. Small reactive power is consumed by the inverters between 1:15 PM and 2:30 PM is due to the high injected power from PVs during that time.

Similarly, Figure 5.11 shows the dispatched reactive power from the wind system inverters. The amount of the supplied/consumed reactive power is subject to the generator capacity.

Figure 5.12 shows the operation of both OLTC/SVR for one day. At a low penetration level of renewables, the SPC strategy solved the problem very efficiently, with the low operation of taps and maintained the voltage profile smooth. Just 6 taps for OLTC and 2 taps for SVR were enough to achieve optimal operation.

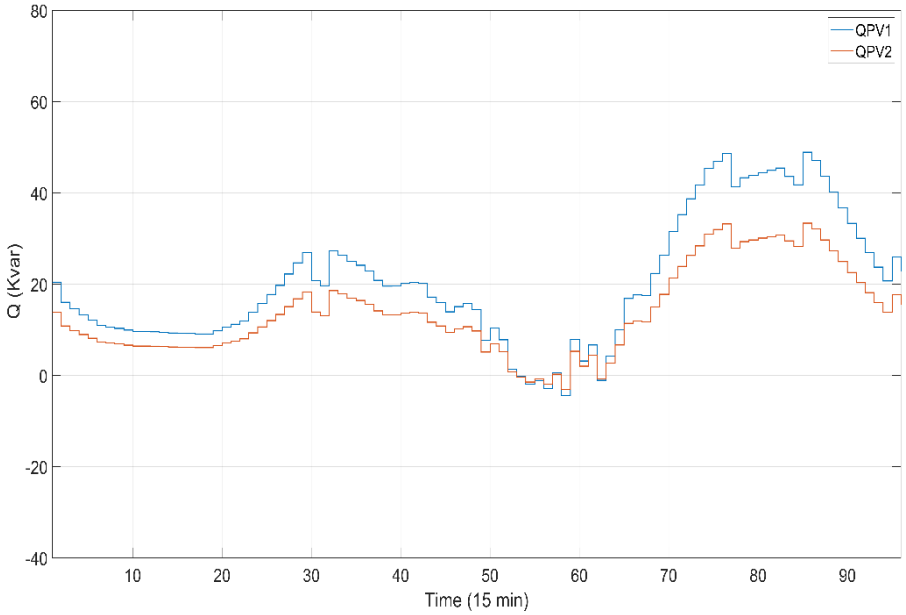

Figure 5.10. Dispatched reactive power from PVs inverter (Low penetration)

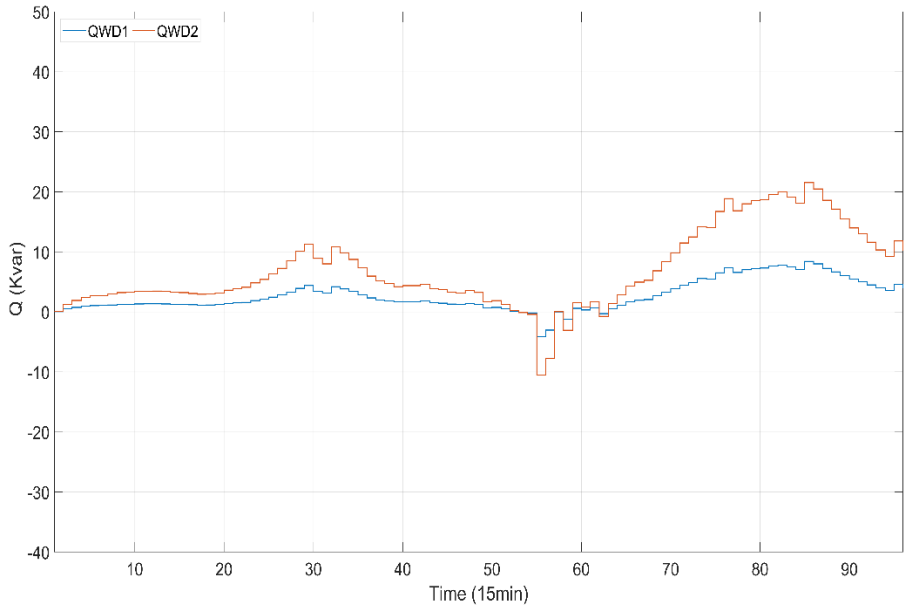

Figure 5.11. Dispatched reactive power from Wind inverter (Low penetration)

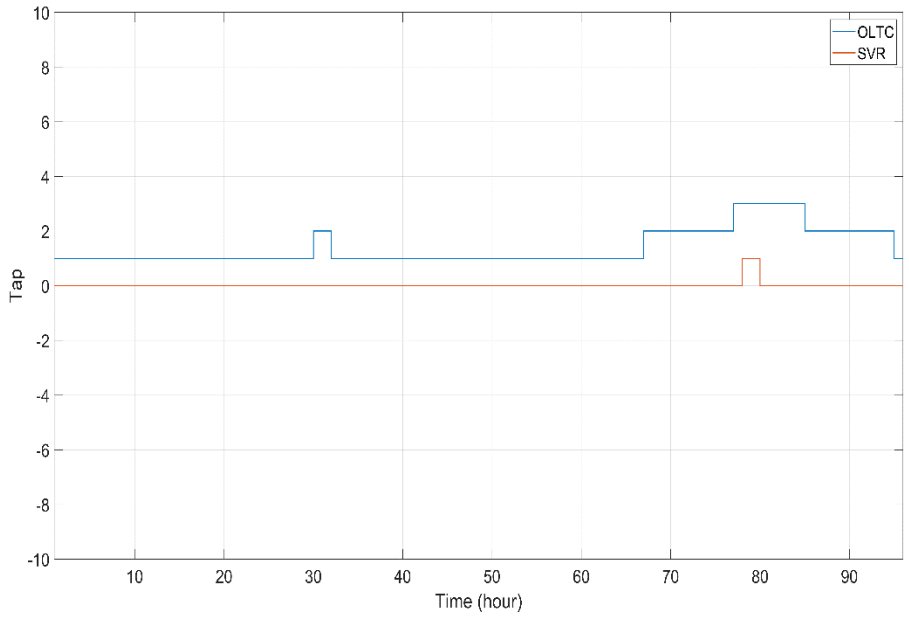

Figure 5.12. Operations of OLTC/SVR (Low penetration).

At low penetration, no reverse power flow was observed during the simulation period, as shown from Figure 5.13. It can also be seen that the lowest power supply occurs when the injection from the PVs is at maximum. The total amount of active power losses calculated during the optimization period for one day is 3.19 MW.

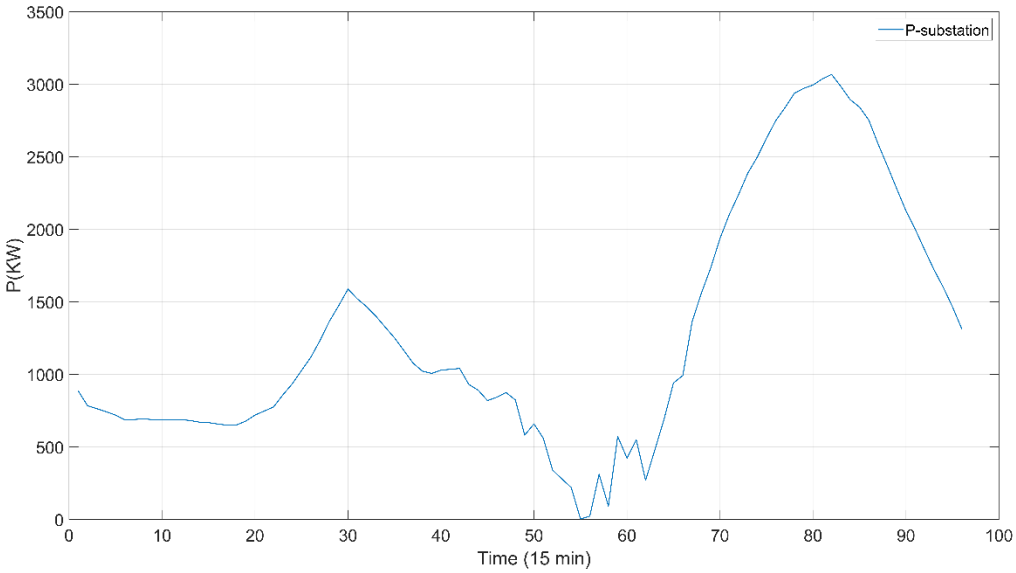

Figure 5.13. Power supplied by substation transformer (Low penetration).

5.7.3 Case 3: High Penetration

Under the high integration of renewables, the control action becomes more complicated due to the high fluctuation in the supplied power, hence there are more reactions from the Volt/Var control devices to maintain voltages within specified limits. In this case, two scenarios were applied, with and without OLTC/SVR operation minimization.

5.7.3.1 Scenario 1

In this scenario, the following objective function is applied:

$$min\ F = w_{loss}(\sum_{ij \in N_{br}} r_{ij}\ l_{ij,t}) + w_{DV}(\sum_{i \in N_B} Vaux_{i,t}\ ) \qquad 5.50$$

The objective of this scenario is to show the impact of reactive power support from inverters on the operation of voltage regulation devices. In Case 1, the excessive operation of the OLTC/SVR occurred when the inverters operated at the unity power factor, which means no reactive power was injected or absorbed to mitigate voltage variation. Figure 5.14 shows the voltage profile from the selected buses without minimizing the operations of the OLTC/SVR devices. It can be seen that the voltage profile was maintained close to the reference voltage value regardless of the operations of the voltage regulator devices.

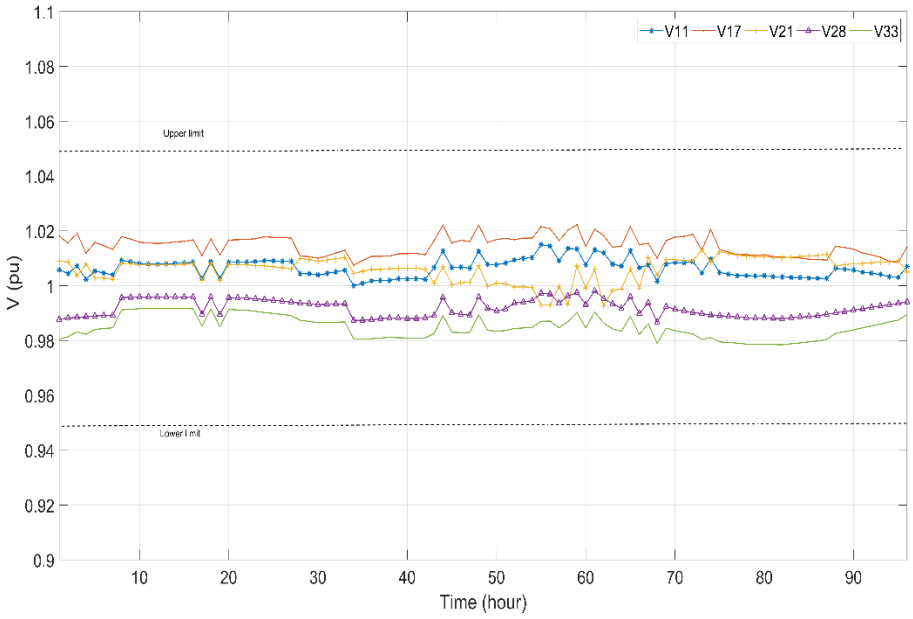

Figure 5.14. Voltage profile of the selected buses (High penetration: Scenario 1)

The dispatch schedule between PV and wind power inverters appears in Figure 5.15 and Figure 5.16, respectively. The amount of reactive power injected or absorbed by the RES inverters depends on the size of each inverter and the location of the RES unit. PV inverters inject most of the reactive power needed by the system to minimize losses and maintain the voltage profile close to the reference values with respect to their sizes and locations.

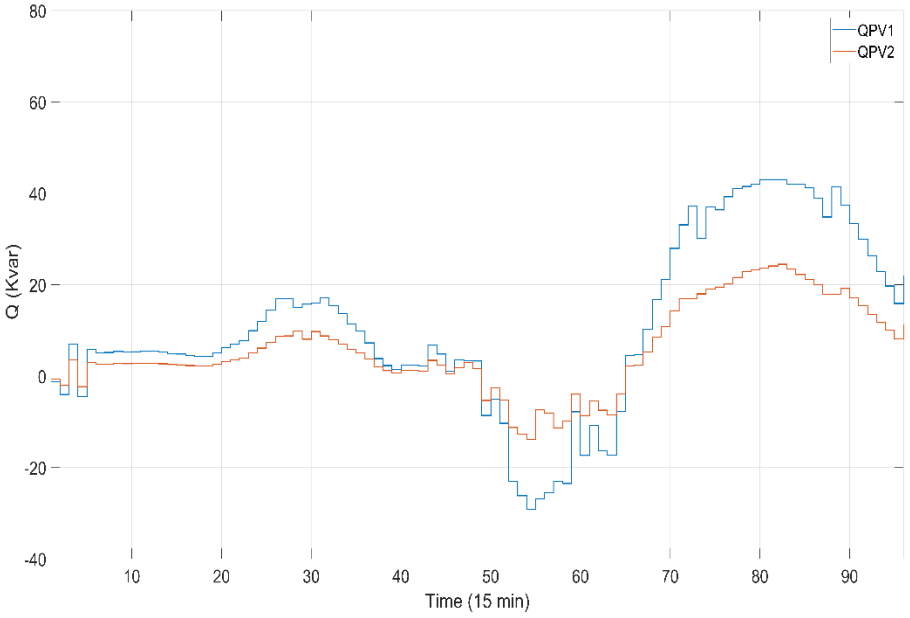

Figure 5.15. Dispatched reactive power from PVs inveter (High penetration: Scenario 1)

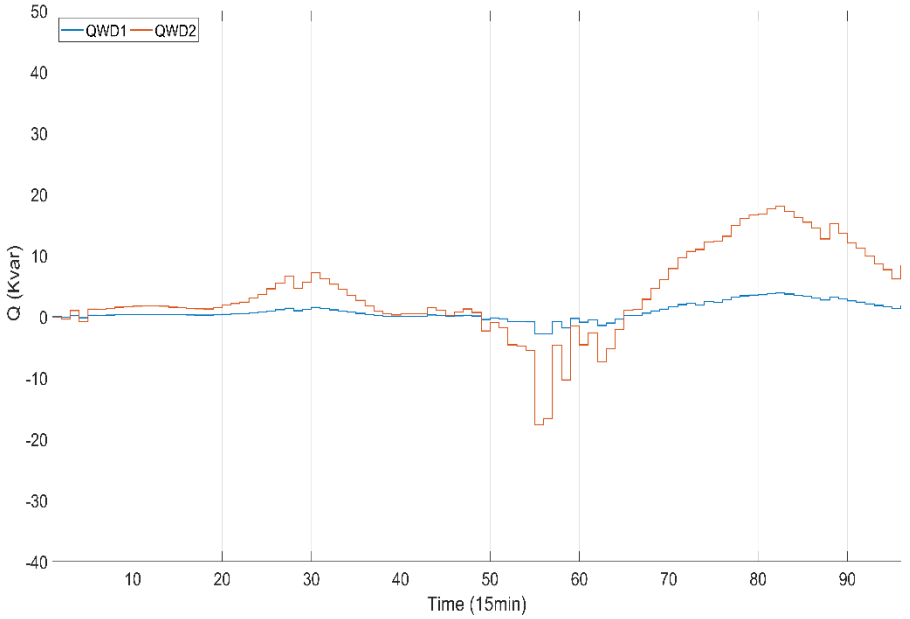

Figure 5.16. Dispatched reactive power from wind farms inverter (High penetration: Scenario 1)

The operations of OLTC and SVR without coordination with RESs inverters appear in Figure 5.17. It can be observed that the number of switchings has decreased compared with Case 1, as depicted in Figure 5.7, where inverters operated at the unity power factor. Although the number of operations is still high, the reactive power support from inverters has helped in minimizing voltage variation, which reduced the OLTC operations from 46 oper/day to 28 oper/day, and SVR operations from 43 oper/day to 17 oper/day.

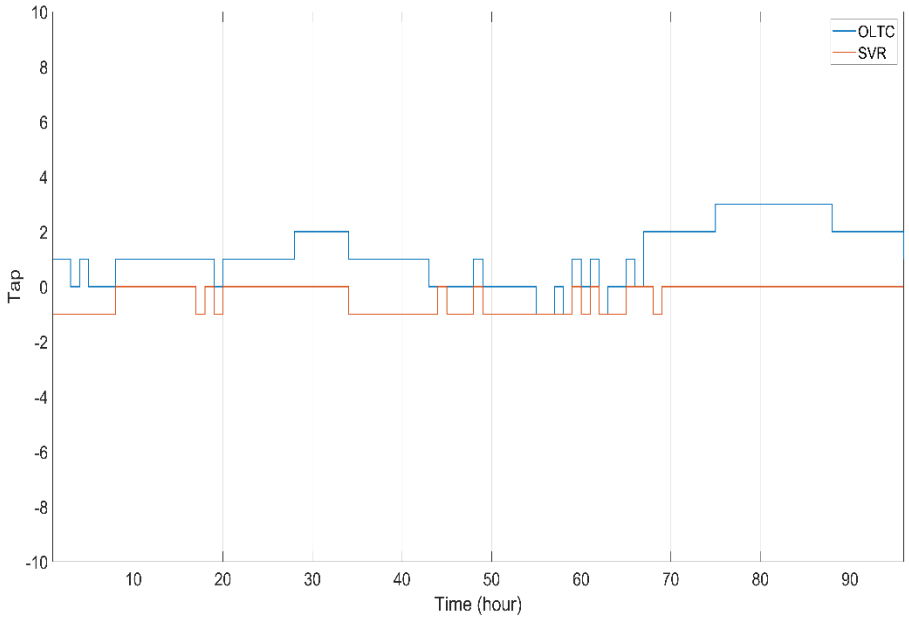

Figure 5.17. Operations of OLTC/SVR (High penetration: Scenario 1)

5.7.3.2 Scenario 2

In this scenario, the full optimization problem, as described in Equation 5.49 is used. Here, full coordination between inverters and voltage regulators is considered. Including the minimization of regulators operations have reduced the overall system operating cost and has met security and operation constraints.

Figure 5.18 shows that the SPC can overcome the problems of voltage violations due to the high uncertainty associated with the intermittent energy source and load demand variations. The voltage profile is flattened and maintained within the allowable operating limits even under the high use of

intermittent energy sources. Short-term forecasting in the real-time proposed model has significantly minimized the uncertainty in the renewable prediction, consequently feeding the centralized controller with accurate data to perform optimal control actions. As a result, the voltage deviation is minimized as an objective by the optimal coordination between the Volt/Var equipment.

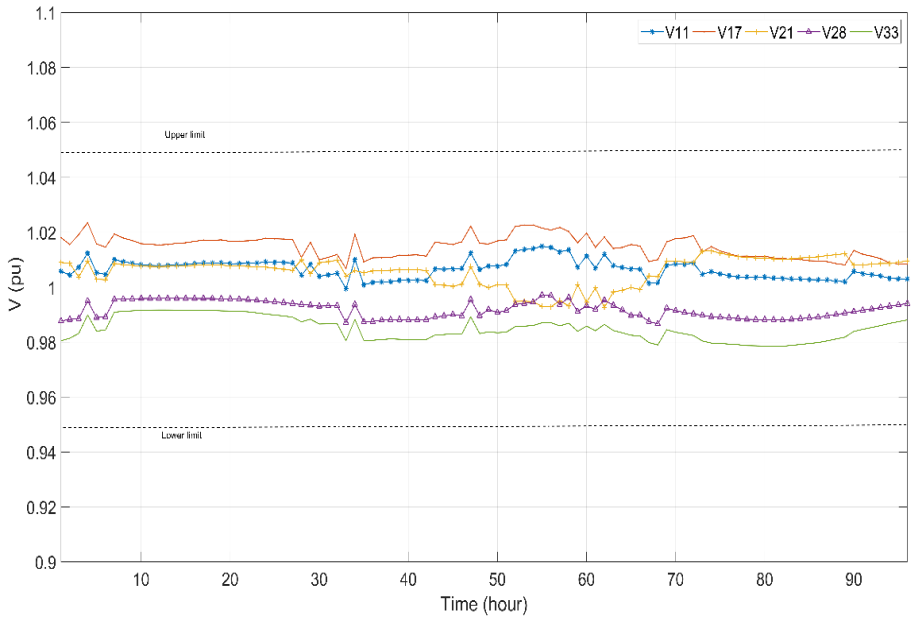

Figure 5.18. Voltage profile of the selected buses (High penetration: Scenario 2)

The dispatch schedule between the PV and Wind power inverters appears in Figure 5.19 and Figure 5.20, respectively. It is noticeable that the majority of reactive power support comes from the PV inverters because they hold larger capacity than Wind farms, as indicated in Table 5-1. An observation of inverter negative reactive power appears between 1:00 PM and 2:45 PM as a result of voltage rise mitigation created by a large amount of injected power from the RESs.

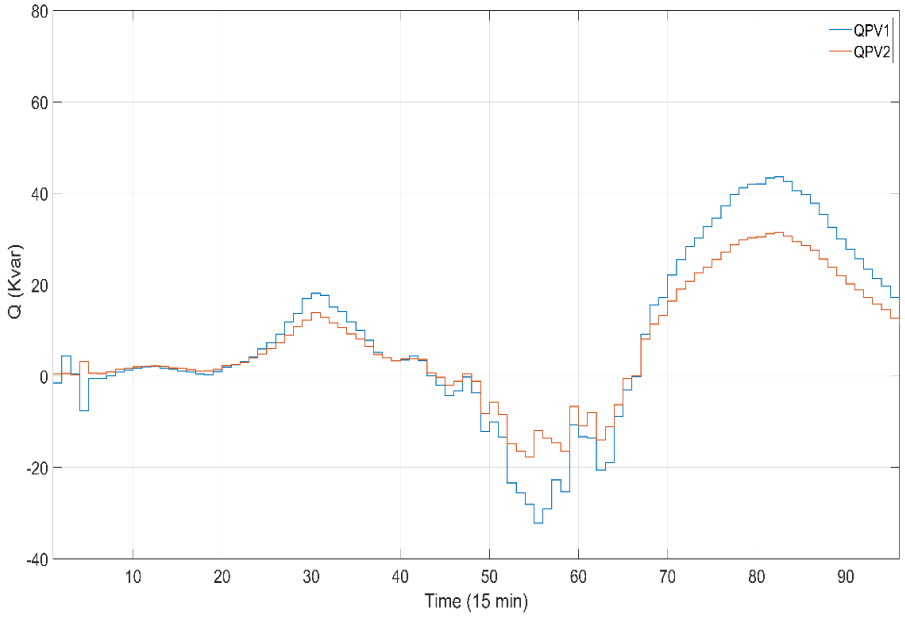

Figure 5.19. Dispatched reactive power from PVs (High penetration: Scenario 2)

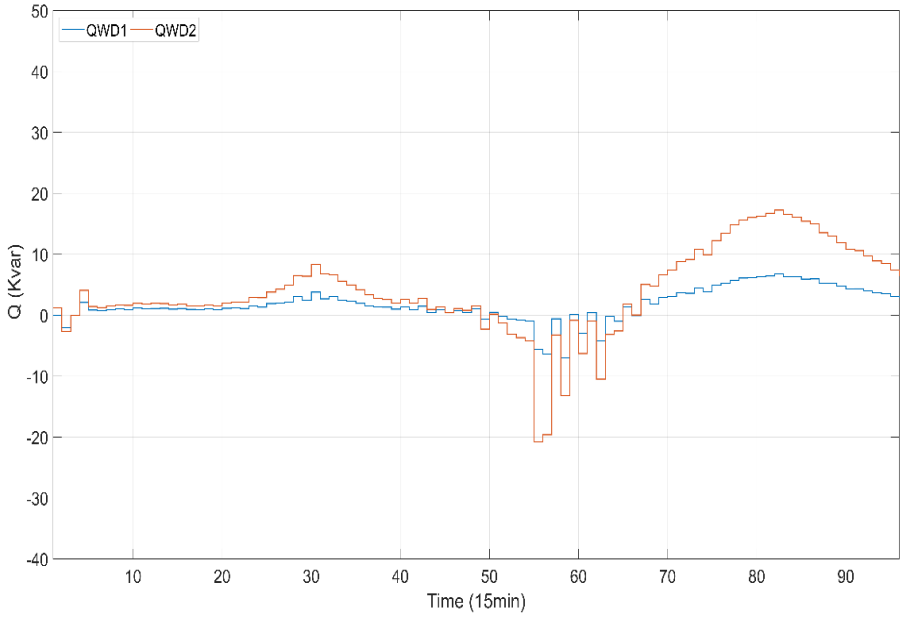

Figure 5.20. Dispatched reactive power from wind farms (High penetration: Scenario 2)

The optimal coordination between OTLC/SVR and the inverters has also decreased the operations of OLTC/SVR as shown in Figure 5.21. The optimization of the OLTC/SVR switching in the proposed model has significantly reduced the daily operations of both devices when compared with the base case scenario, as shown in Figure 5.7. Allowing for reactive power support up to 10% of the inverters' rated capacity helped in offsetting voltage deviation, and consequently reduced the switching mechanism of the mechanical devices.

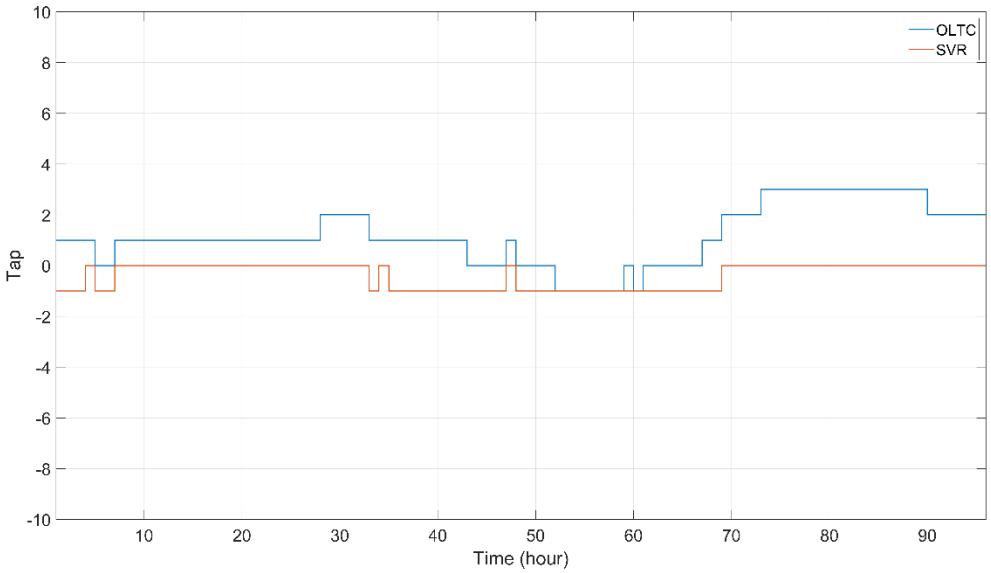

Figure 5.21. Operations of OLTC/SVR (High penetration: Scenario 2)

Figure 5.22 shows the total active power supplied from the substation transformer for the entire simulation period. It can be observed that between 12:00 PM and 4:00 PM, the supplied active power is negative, which indicates a reverse power flow. This is due to the peak generated power from the RESs, specifically for the solar PV systems, and the offpeak demand during the specified intervals. With the conventional Volt/Var control that depends on the LDC of OLTC/SVR, the control actions will not be efficient due to the reverse power flow. However, the proposed SPC can handle this problem by estimating the amount of generated and consumed power, and accordingly and taking control action. Figure 5.23 shows the voltage on all buses during the simulation period. All system voltages are flattened without spikes or high variations as a proof of the robustness of the SPC.

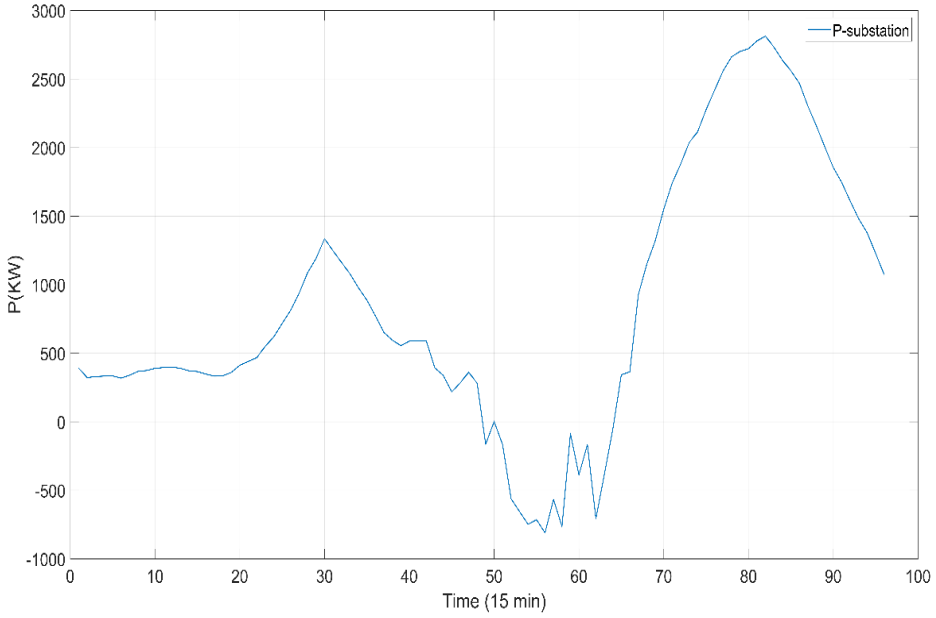

Figure 5.22. Power supplied by the substation transformer (High penetration)**.**

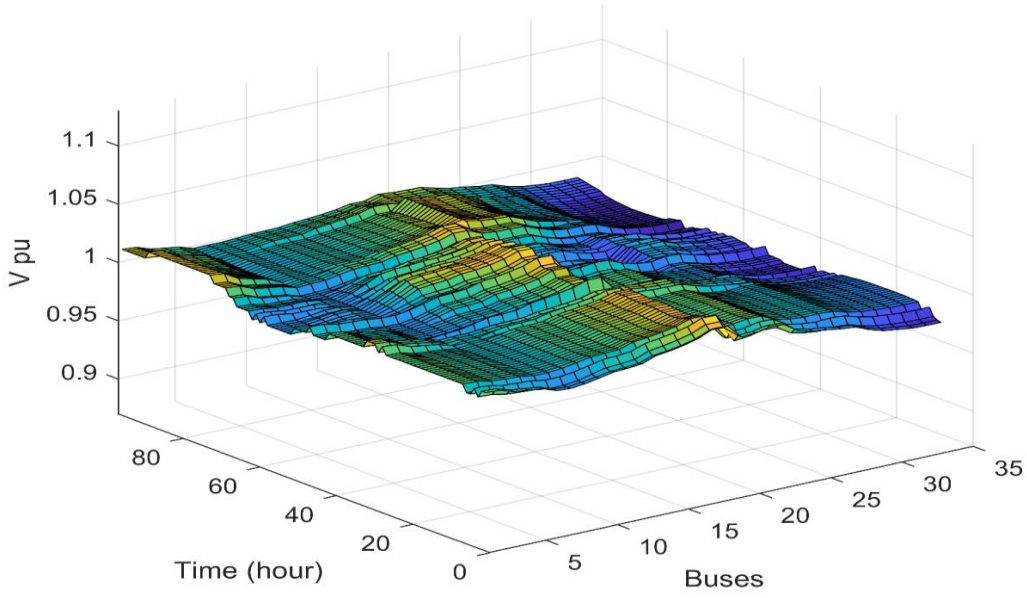

Figure 5.23. System voltage of all buses

Table 5-2 shows the weight coefficients of the three cases determined based on the methodology used Chapter 4.

Table 5-2. Weights of the three case studies

Case		w_{ltc}	w_{svr}	w_{loss}	w_{DV}
Case 1		-	-	0.7	0.3
Case 2		0.25	0.15	0.5	0.1
Case 3	Scenario1	-	-	0.72	0.28
	Scenario2	0.2	0.15	0.55	0.1

5.7.4 Cost Analysis

As the goal of the proposed SPC is to optimally control and run smart distribution systems dominated by intermittent renewable resources, Table 5-3 summarizes the operating cost of the regulator's operations as well as total system losses for a one-day simulation period. A summary of the operating cost of the proposed model for the one-day simulation period appears in Table 5-3. It can be seen that, when comparing Case 1 with Case 3, the total operation cost has been dramatically minimized by approximately 42%. The coordination between the voltage regulators and the distributed generation inverters minimized the regulator's switches as well as power losses in branches. Power losses from Case 3 declined from 3.316 MW to 2.54 MW, and the total operations of OLTC and SVR reduced from 89 oper/day to 24 oper/day. The cost of purchasing power from the primary grid is not reported in the analysis.

Table 5-3. Cost of operation for IEEE 33-Bus system

Case Study		OLTC(oper/day)	SVR(oper/day)	Loss (MW)/day	Total Cost $
Case 1		46	43	3.316	849.12
Case 2		6	2	3.19	307.68
Case 3	Scenario 1	28	17	2.54	497.3
	Scenario 2	17	7	2.56	360.64

5.8 Algorithm Evaluation

To evaluate the performance of the proposed model, three standard metrics for evaluation are used: time, iteration, and objective. The execution time for one optimization stage is given in Table 5-4. It can be seen that the SPC model has solved the problem in a shorter time compared with the other MINLP models.

Table 5-4 Comparison SPC and MINLP models for the IEEE 33-Bus system

Method	Time(s)	Iter	Objective
Proposed SPC	0.438	15	0.0586
MINLP (emp [142])	1.59	11	0.0586
MINLP (Knitro [143])	1.84	-	0.05869
MINLP (Dicopt)	2.85	-	infeasible

The difference (percentage error) in voltage at bus 11 when using MISOCP and the original MINLP "emp" models for the entire simulation period is depicted in Figure 5.24. It can be seen that the error is very small, which guarantees the effectiveness of transforming the original problem to the MISOCP problem with the advantage of fast convergence.

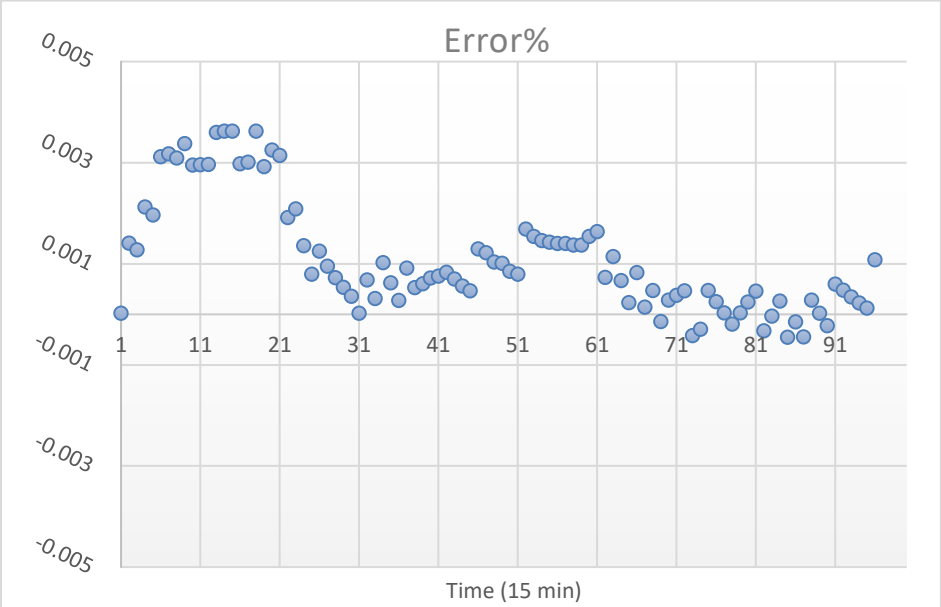

Figure 5.24. Error in bus voltage (MISOCP - MINLP “emp”)

5.9 Conclusion

High penetration and excessive power variation of PV and Wind power systems cause severe operational problems. In this chapter, an SPC strategy for an SDG dominated by RESs is proposed. The model uses the short-time forecasting algorithm based on online forgetting and updating mechanisms. The prediction accuracy of generation and demand comes from incorporating the most recent measured data into the optimization process while moving over the horizon. The proposed model converts the original nonconvex problem to a convex problem by linearizing the objective function subject to linear and conic constraints. The original MINLP problem is converted to a MISOCP problem, which is then solved by applying a rolling horizon optimization framework. Convexification and linearization of the problem guarantee a global solution to the problem within very-short timeframe, which satisfies the real-time operation demands of smart grids. The presented results show that the SPC is an efficient model when solving smart distribution grids even with a large number of buses, in a reasonable time. The feasibility of the solution is guaranteed due to the convexification of the problem, which is not guaranteed with nonlinear models, especially when the number of variables increases exponentially.

Chapter 6
Conclusions and Future Work

Power distribution companies are committed to continuously regulating the voltage at the distribution level within ±5% ANSI standard range (0.95 p.u to 1.05 p.u) under normal operating conditions. However, the proliferation of intermittent energy sources, such as PV and wind power systems, makes the operation and control of the distribution system very difficult. As such, developing an accurate, reliable, and cost-effective solution methodology to cope with the high-scale integration of RESs has become a matter of great interest. This research work is an attempt to address some of the challenges made by the integration of RESs on the voltage profile and operation of Volt/Var control devices in the context of the smart grid. This dissertation explores the impact of the high penetration of RESs on system voltage profile and operation of Volt/Var control devices. It develops an optimization procedure for determining the reactive power and voltage control parameters that maximize the smart grid performance (minimization of operation cost and system losses)

6.1 Conclusion

Building upon the background presented in Chapter 2, this research focuses on three main aspects of operating a smart distribution grid, namely; short-term forecasting, day-ahead predictive Volt/Var control, and sequential predictive control based on a real-time updating and forecasting approach. The major contributions of this research are:

1. An STSE-based real-time forecasting algorithm to accurately capture the output variation of intermittent energy sources and demands.

2. Predictive control actions for RES dominated systems to optimally set Volt/Var control devices before the predicted voltage violation takes place.

3. A global solution algorithm for Volt/Var control problem based on a MISOCP convex optimization framework.

In Chapter 3, a forecasting model, referred to as an STSE, has been established and applied to PV/wind power output data for short-term forecasting. The proposed approach heuristically combines a heterogeneous machine learning algorithm composed of three well-established models, SVR, RBFNN, and RF, via SVR. The model is evaluated using evaluation metrics such as RMSE, MAE, and MAPE, where the results show that the STSE model is a reliable and accurate tool for very short-term

PV/wind power forecasting. Further, the model is extended in Chapter 5 to incorporate real-time measurements from smart meters and update itself every 15 minutes in order to capture the most recent data. Thus, better prediction accuracy and optimum Volt/Var control actions are accordingly achieved.

Chapter 4 presents a proposal for two generic predictive Volt/Var Control models for optimally operating smart distribution grids for a day-ahead. The first model operates the RESs at unity power factor, where the objective was minimizing voltage deviation, power losses, operating cycles of regulation equipment, and RES curtailment. The second model uses the advantages of smart inverters interfacing RESs as an ancillary for reactive power support so that the objectives from the first model are achieved without RES curtailment. The two models schedule the operation of a smart distribution grid on an hourly basis for a day-ahead under the high penetration of PV and Wind power systems characterized by their high degree of uncertainty.

In Chapter 5, a sequential predictive control strategy for smart distribution grids dominated by RES is developed. The model uses both the past and currently available data to forecast demand and RES outputs for intervals of 15 minutes ahead, with real-time updating mechanisms. It then schedules the settings and operations of Volt/Var control devices by solving the Volt/Var control problems in a rolling horizon optimization framework. The original nonconvex MINLP problem is converted to a convex MISOCP problem by linearizing the objective function subject to linear and conic constraints. Convexification and linearization of the problem guarantee a global solution and minimizes the computational time. Case studies conducted to compare the proposed model against state-of-the-art models provides evidence for the proposed model's effectiveness. Results indicate that the sequential predictive control approach is capable of accurately solving the control problem with high RES penetration within short time slots.

6.2 Research Contributions

The major contributions of this dissertation are:

1. Development of a real-time forecasting algorithm to accurately capture the output variation of intermittent energy sources and demands.
2. Development of an optimum coordination algorithm for Volt/Var control devices such that their daily operations are minimized, hence their expected life is extended. The proposed formulation is applicable to one day-ahead with and without incorporating smart converters interfacing with PV/Wind units.
3. Development of an optimal predictive control method for the Volt/Var control problem in smart grids. The proposed framework uses rolling horizon optimization to solve the optimization problem. The Volt/Var problem is formulated as a convex optimization to guarantee a global solution.

6.3 Future work

Based on the work presented in this thesis, future research may explore the following subjects:

1. Investigate the hierarchical control based on the convexification of the power flow problem. Volt/Var control devices will be classified based on their fast and low response control actions to deal with fast voltage variations.
2. Explore the high integration of electric vehicles (EV) and its impact on the proposed real-time predictive control.
3. Investigate the use of energy storage systems as an ancillary service for Volt/Var control in coordination with voltage regulation equipment.

Bibliography

[1] "Wind Energy," *IRENA*. [Online]. Available: https://www.irena.org/wind. [Accessed: 15-Jul-2019].

[2] "Wind Vision2025," *Canadian Wind Energy Association*. [Online]. Available: https://canwea.ca/pdf/windvision/Windvision_summary_e.pdf. [Accessed: 05-Aug-2019].

[3] ""Renewables 2018," *IEA*. [Online]. Available: https://www.iea.org/renewables2018/. [Accessed: 05-Jul-2019].

[4] S. Dawn, P. K. Tiwari, A. K. Goswami, A. K. Singh, and R. Panda, "Wind power: Existing status, achievements and government's initiative towards renewable power dominating India," *Energy Strateg. Rev.*, vol. 23, no. November 2016, pp. 178–199, Jan. 2019.

[5] S. K. Sharma, A. Chandra, M. Saad, S. Lefebvre, D. Asber, and L. Lenoir, "Voltage flicker mitigation employing smart loads with high penetration of renewable energy in distribution Systems," *IEEE Trans. Sustain. Energy*, vol. 8, no. 1, pp. 414–424, 2017.

[6] Y. Wang, Q. Hu, D. Meng, and P. Zhu, "Deterministic and probabilistic wind power forecasting using a variational Bayesian-based adaptive robust multi-kernel regression model," *Appl. Energy*, vol. 208, no. August, pp. 1097–1112, 2017.

[7] A. Ahmed and M. Khalid, "A review on the selected applications of forecasting models in renewable power systems," *Renew. Sustain. Energy Rev.*, vol. 100, pp. 9–21, 2019.

[8] Z. Xu, Z. Hu, J. Zhao, Y. Song, J. Lin, and C. Wan, "Photovoltaic and solar power forecasting for smart grid energy management," *CSEE J. Power Energy Syst.*, vol. 1, no. 4, pp. 38–46, 2016.

[9] M. K. Behera, I. Majumder, and N. Nayak, "Solar photovoltaic power forecasting using optimized modified extreme learning machine technique," *Eng. Sci. Technol. an Int. J.*, vol. 21, no. 3, pp. 428–438, 2018.

[10] G. de Freitas Viscondi and S. N. Alves-Souza, "A Systematic Literature Review on big data for solar photovoltaic electricity generation forecasting," *Sustain. Energy Technol. Assessments*, vol. 31, no, pp. 54–63, 2019.

[11] L. Stoyanov, Z. Zarkov, I. Draganovska, and V. Lazarov, "Methods for energy production estimation from photovoltaic plants: Review and application," *Int. Conf. High Technol. Sustain.*

Dev. Proc., pp. 1–5, 2018.

[12] Y. Ren, P. N. Suganthan, and N. Srikanth, "Ensemble methods for wind and solar power forecasting — A state-of-the-art review," *Renew. Sustain. Energy Rev.*, vol. 50, pp. 82–91, 2015.

[13] R. H. Inman, H. T. C. Pedro, and C. F. M. Coimbra, "Solar forecasting methods for renewable energy integration," *Prog. Energy Combust. Sci.*, vol. 39, no. 6, pp. 535–576, 2013.

[14] R. Escobar, J. Antonanzas, F. Antonanzas-Torres, R. Urraca, N. Osorio, and F. J. Martinez-de-Pison, "Review of photovoltaic power forecasting," *Sol. Energy*, vol. 136, pp. 78–111, 2016.

[15] M. Geurts, G. E. P. Box, and G. M. Jenkins, *Time Series Analysis: Forecasting and Control*, vol. 14, no. 2, 2006.

[16] R. Huang, T. Huang, R. Gadh, and N. Li, "Solar generation prediction using the ARMA model in a laboratory-level micro-grid," *IEEE Int. Conf. Smart Grid Commun. SmartGridComm*, pp. 528–533, 2012.

[17] J. Shi, W. J. Lee, Y. Liu, Y. Yang, and P. Wang, "Forecasting power output of photovoltaic systems based on weather classification and support vector machines," *IEEE Trans. Ind. Appl.*, vol. 48, no. 3, pp. 1064–1069, 2012.

[18] S. K. H. Chow, E. W. M. Lee, and D. H. W. Li, "Short-term prediction of photovoltaic energy generation by intelligent approach," *Energy Build.*, vol. 55, pp. 660–667, 2012.

[19] F. Almonacid, P. J. Pérez-Higueras, E. F. Fernández, and L. Hontoria, "A methodology based on dynamic artificial neural network for short-term forecasting of the power output of a PV generator," *Energy Convers. Manag.*, vol. 85, pp. 389–398, 2014.

[20] Y. K. Semero, J. Zhang, and D. Zheng, "PV power forecasting using an integrated GA-PSO-ANFIS approach and Gaussian process regression based feature selection strategy," *CSEE J. Power Energy Syst.*, vol. 4, no. 2, pp. 210–218, 2018.

[21] H. T. Yang, C. M. Huang, Y. C. Huang, and Y. S. Pai, "A weather-based hybrid method for 1-day ahead hourly forecasting of PV power output," *IEEE Trans. Sustain. Energy*, vol. 5, no. 3, pp. 917–926, 2014.

[22] Y. Li, X. Zhang, H. F. Hamann, B.-M. Hodge, B. Lehman, and S. Lu, "A Solar time based analog ensemble method for regional solar power forecasting," *IEEE Trans. Sustain. Energy*, vol. 10, no. 1, pp. 268–279, 2018.

[23] M. Q. Raza, M. Nadarajah, and C. Ekanayake, “A multivariate ensemble framework for short term solar photovoltaic output power forecast,” in *IEEE Power and Energy Society General Meeting*, pp. 1–5 2018

[24] Y. Ren, P. N. Suganthan, and N. Srikanth, “Ensemble methods for wind and solar power forecasting - A state-of-the-art review,” *Renew. Sustain. Energy Rev.*, vol. 50, pp. 82–91, 2015.

[25] A. Tascikaraoglu and M. Uzunoglu, “A review of combined approaches for prediction of short-term wind speed and power,” *Renew. Sustain. Energy Rev.*, vol. 34, pp. 243–254, 2014.

[26] M. S. El Moursi, A. Al Hinai, E. B. Ssekulima, and M. B. Anwar, “Wind speed and solar irradiance forecasting techniques for enhanced renewable energy integration with the grid: a review,” *IET Renew. Power Gener.*, vol. 10, no. 7, pp. 885–989, 2016.

[27] J. Melorose, R. Perroy, and S. Careas, “an Overview on wind power forecasting methods,” *Statew. Agric. L. Use Baseline*, vol. 1, 2015.

[28] A. M. Foley, P. G. Leahy, A. Marvuglia, and E. J. McKeogh, “Current methods and advances in forecasting of wind power generation,” *Renew. Energy*, vol. 37, no. 1, pp. 1–8, 2012.

[29] W.-Y. Chang, “A literature review of wind forecasting methods,” *J. Power Energy Eng.*, vol. 02, no. 04, pp. 161–168, 2014.

[30] M. Lei, L. Shiyan, J. Chuanwen, L. Hongling, and Z. Yan, “A review on the forecasting of wind speed and generated power,” *Renew. Sustain. Energy Rev.*, vol. 13, no. 4, pp. 915–920, 2009.

[31] G. Sideratos and N. D. Hatziargyriou, “Probabilistic wind power forecasting using radial basis function neural networks,” *IEEE Trans. Power Syst.*, vol. 27, no. 4, pp. 1788–1796, 2012.

[32] A. F. Sheta and K. De Jong, “Time-series forecasting using GA-tuned radial basis functions,” *Inf. Sci*, vol. 133, no. 3–4, pp. 221–228, 2001.

[33] M. A. Mohandes, T. O. Halawani, S. Rehman, and A. A. Hussain, “Support vector machines for wind speed prediction,” *Renew. Energy*, vol. 29, no. 6, pp. 939–947, 2004.

[34] G. Santamaría-Bonfil, A. Reyes-Ballesteros, and C. Gershenson, “Wind speed forecasting for wind farms: A method based on support vector regression,” *Renew. Energy*, vol. 85, pp. 790–809, 2016.

[35] H. Allende and C. Valle, “ensemble methods for time series forecasting,” in *A passion for Multi-*

Valued Logic and Soft Computing, vol. 349, springer, pp. 217–282, 2017

[36] M. Abuella and B. Chowdhury, "Random Forest Ensemble of Support Vector Regression Models for Solar Power Forecasting," *arXiv1705.00033 [cs]*, pp. 2–6, 2017.

[37] J. Mendes-Moreira, C. Soares, A. M. Jorge, and J. F. De Sousa, "Ensemble approaches for regression," *ACM Comput. Surv.*, vol. 45, no. 1, pp. 1–40, Nov. 2012.

[38] S. Fallah, M. Ganjkhani, S. Shamshirband, and K. Chau, "Computational intelligence on short-term load forecasting: A methodological overview," *Energies*, vol. 12, no. 3, p. 393, Jan. 2019.

[39] T. Hong and S. Fan, "Probabilistic electric load forecasting: A tutorial review," *Int. J. Forecast.*, vol. 32, no. 3, pp. 914–938, 2016.

[40] S. J. Huang and K. R. Shih, "Short-term load forecasting via ARMA model identification including non-Gaussian process considerations," *IEEE Trans. Power Syst.*, vol. 18, no. 2, pp. 673–679, 2003.

[41] S. S. Pappas, L. Ekonomou, D. C. Karamousantas, G. E. Chatzarakis, S. K. Katsikas, and P. Liatsis, "Electricity demand loads modeling using AutoRegressive Moving Average (ARMA) models," *Energy*, vol. 33, no. 9, pp. 1353–1360, 2008.

[42] Y. S. Lee and L. I. Tong, "Forecasting time series using a methodology based on autoregressive integrated moving average and genetic programming," *Knowledge-Based Syst.*, vol. 24, no. 1, pp. 66–72, 2011.

[43] Y. Chakhchoukh, P. Panciatici, and L. Mili, "Electric load forecasting based on statistical robust methods," *IEEE Trans. Power Syst.*, vol. 26, no. 3, pp. 982–991, 2011.

[44] M. Q. Raza and A. Khosravi, "A review on artificial intelligence based load demand forecasting techniques for smart grid and buildings," *Renew. Sustain. Energy Rev.*, vol. 50, pp. 1352–1372, 2015.

[45] P. Vrablecová, A. Bou Ezzeddine, V. Rozinajová, S. Šárik, and A. K. Sangaiah, "Smart grid load forecasting using online support vector regression," *Comput. Electr. Eng.*, vol. 65, no. 2018, pp. 102–117, 2018.

[46] P. Rozycki, B. M. Wilamowski, J. Kolbusz, C. Cecati, and P. Siano, "A novel RBF training algorithm for short-term electric load forecasting and comparative studies," *IEEE Trans. Ind. Electron.*, vol. 62, no. 10, pp. 6519–6529, 2015.

[47] N. Ding, C. Benoit, G. Foggia, Y. Besanger, and F. Wurtz, “Neural network-based model design for short-term load forecast in distribution systems,” *IEEE Trans. Power Syst.*, vol. 31, no. 1, pp. 72–81, 2016.

[48] W. Kong, Y. Xu, D. J. Hill, Z. Y. Dong, Y. Jia, and Y. Zhang, “Short-term residential load forecasting based on LSTM recurrent neural network,” *IEEE Trans. Smart Grid*, vol. 10, no. 1, pp. 841–851, 2017.

[49] M. Q. Raza, M. Nadarajah, D. Q. Hung, and Z. Baharudin, “An intelligent hybrid short-term load forecasting model for smart power grids,” *Sustain. Cities Soc.*, vol. 31, pp. 264–275, 2017.

[50] C. Guan, P. B. Luh, L. D. Michel, Y. Wang, and P. B. Friedland, “Very short-term load forecasting: Wavelet neural networks with data pre-filtering,” *IEEE Trans. Power Syst.*, vol. 28, no. 1, pp. 30–41, 2013.

[51] C. Guan, P. B. Luh, L. D. Michel, and Z. Chi, “Hybrid Kalman filters for very short-term load forecasting and prediction interval estimation,” *IEEE Trans. Power Syst.*, vol. 28, no. 4, pp. 3806–3817, 2013.

[52] W. H. Kersting, *Distribution system modeling and analysis*. 2001.

[53] P. P. Barker and R. W. De Mello, “Determining the impact of distributed generation on power systems. I. Radial distribution systems,” *IEEE Power Eng. Soc. Summer Meet. 2000.* vol. 3, no. c, pp. 1645–1656 vol. 3, 2000.

[54] X. Xintao and X. Junzi, “Evaluation of potential for developing renewable sources of energy to facilitate development in developing countries,” *Power Energy Eng. Conf. (APPEEC), 2010 Asia-Pacific*, pp. 10–12, 2010.

[55] R. A. Walling, R. Saint, R. C. Dugan, J. Burke, and L. A. Kojovic, “Summary of Distributed Resources Impact on Power Delivery Systems,” *IEEE Trans. Power Deliv.*, vol. 23, no. 3, pp. 1636–1644, Jul. 2008.

[56] T. Ackermann and V. Knyazkin, “Interaction between distributed generation and the distribution network: operation aspects,” in *IEEE/PES Transmission and Distribution Conference and Exhibition*, vol. 2, pp. 1357–1362, 2002

[57] W. H. Kersting, “The modeling and application of step voltage regulators,” *IEEE/PES Power Syst. Conf. Expo*, 2009.

[58] P. Brady, C. Dai, and Y. Baghzouz, “Need to revise switched capacitor controls on feeders with distributed generation,” *IEEE PES Transmission and Distribution Conference and Exposition (IEEE Cat. No.03CH37495*, pp. 590–594*)*, 2003.

[59] F. A. Viawan and D. Karlsson, “Coordinated voltage and reactive power control in the presence of distributed generation,” *IEEE Power and Energy Society General Meeting - Conversion and Delivery of Electrical Energy in the 21st Century*, 2008,

[60] M. Chamana and B. H. Chowdhury, “Optimal Voltage Regulation of Distribution Networks With Cascaded Voltage Regulators in the Presence of High PV Penetration,” *IEEE Trans. Sustain. Energy*, vol. 9, no. 3, pp. 1427–1436, Jul. 2018.

[61] Z. Wang, X. Wang, W. Meng, L. Tang, and S. Liu, “Constraint models of voltage fluctuation limit on OLTC/SVR caused by DG power fluctuation and generator disconnection to assess their impacts on DG penetration limit,” *IET Gener. Transm. Distrib.*, vol. 11, no. 17, pp. 4299–4306, Nov. 2017.

[62] Feng-Chang Lu and Yuan-Yih Hsu, “Fuzzy dynamic programming approach to reactive power/voltage control in a distribution substation,” *IEEE Trans. Power Syst.*, vol. 12, no. 2, pp. 681–688, May 1997.

[63] R. A. Jabr, “Linear decision rules for control of reactive power by distributed photovoltaic generators,” *IEEE Trans. Power Syst.*, vol. 33, no. 2, pp. 2165–2174, 2018.

[64] F. U. Nazir, B. C. Pal, and R. A. Jabr, “A two-stage chance constrained Volt/Var control scheme for active distribution networks with nodal power uncertainties,” *IEEE Trans. Power Syst.*, vol. 34, no. 1, pp. 314–325, Jan. 2019.

[65] W. Sheng, K. Liu, S. Cheng, X. Meng, and W. Dai, “A Trust Region SQP Method for Coordinated Voltage Control in Smart Distribution Grid,” *IEEE Trans. Smart Grid*, vol. 7, no. 1, pp. 381–391, Jan. 2016.

[66] F. a Viawan and D. Karlsson, “Coordinated voltage and reactive power control in the presence of distributed generation,” in *IEEE Power and Energy Society General Meeting - Conversion and Delivery of Electrical Energy in the 21st Century, IEEE*, 2008, pp. 1–6, *2008*

[67] G. Valverde and T. Van Cutsem, “Coordinated voltage control of distribution networks hosting dispersed generation,” *International Conference and Exhibition on Electricity Distribution*

(CIRED 2013), pp. 1021–1021, 2013

[68] D. Ranamuka, A. P. Agalgaonkar, K. M. Muttaqi, and S. Member, "Online voltage control in distribution systems with multiple voltage regulating devices," *IEEE Trans. Sustain. Energy*, vol. 5, no. 2, pp. 617–628, 2014.

[69] D. Jakus, J. Vasilj, and P. Sarajcev, "Voltage control in MV distribution networks through coordinated control of tap changers and renewable energy sources," in *2015 IEEE Eindhoven PowerTech*, 2015, pp. 1–6.

[70] R. A. Jabr and I. Dzafic, "Sensitivity-based discrete coordinate-descent for Volt/VAr control in Distribution Networks," *IEEE Trans. Power Syst.*, vol. 31, no. 6, pp. 4670–4678, 2016.

[71] Z. Ziadi, S. Taira, M. Oshiro, and T. Funabashi, "Optimal power scheduling for smart grids considering controllable loads and high penetration of photovoltaic generation," *IEEE Trans. Smart Grid*, vol. 5, no. 5, pp. 2350–2359, 2014.

[72] Z. Ziadi *et al.*, "Optimal voltage control using inverters interfaced with PV systems considering forecast error in a distribution system," *IEEE Trans. Sustain. Energy*, vol. 5, no. 2, pp. 682–690, 2014.

[73] M. Oshiro, K. Uchida, T. Senjyu, and A. Yona, "Voltage control in distribution systems considered reactive power output sharing in smart grid," in *2010 International Conference on Electrical Machines and Systems*, pp. 458–463, 2010.

[74] M. Z. C. Wanik, I. Erlich, A. Mohamed, and H. Shareef, "Predictive var management of distributed generators," *Int. Power Energy Conf*, pp. 619–624, 2010.

[75] a. G. Madureira and J. a. Peças Lopes, "Coordinated voltage support in distribution networks with distributed generation and microgrids," *IET Renew. Power Gener.*, vol. 3, no. 4, p. 439, 2009.

[76] M. K. N. M. Sarmin, "Coordinated voltage control in distribution network with renewable energy based distributed Generation," *Engineering*, vol. 05, no. 01, pp. 208–214, 2013.

[77] Y. Liao *et al.*, "Voltage and var control to enable high penetration of distributed photovoltaic systems," *2012 North Am. Power Symp*, 2012.

[78] M. Oshiro *et al.*, "Optimal voltage control in distribution systems using PV generators," *Int. J. Electr. Power Energy Syst.*, vol. 33, no. 3, pp. 485–492, 2011.

[79] P. H. and M. L. J. Skea, D. Anderson, T. Green, R. Gross, "Intermittent renewable generation and the cost of maintaining power system reliability," *Gener. Transm. Distrib. IET*, vol. 1, no. 2, p. 324, 2007.

[80] L. Cheng, Y. Chang, and R. Huang, "Mitigating voltage problem in distribution system with distributed solar generation using electric vehicles," *IEEE Trans. Sustain. Energy*, vol. 6, no. 4, pp. 1475–1484, 2015.

[81] S. Toma, T. Senjyu, Y. Miyazato, A. Yona, K. Tanaka, and C.-H. Kim, "Decentralized voltage control in distribution system using neural network," *IEEE Int. Power Energy Conf* , pp. 1557–1562, 2008.

[82] V. Calderaro, G. Conio, V. Galdi, G. Massa, and A. Piccolo, "Optimal decentralized voltage control for distribution systems with inverter-based distributed generators," *IEEE Trans. Power Syst.*, vol. 29, no. 1, pp. 230–241, 2014.

[83] A. R. Malekpour, A. Pahwa, and B. Natarajan, "Distributed Volt/Var control in unbalanced distribution systems with distributed generation," in *2014 IEEE Symposium on Computational Intelligence Applications in Smart Grid (CIASG)*, pp. 1–6 , 2014

[84] M. E. Elkhatib, R. El Shatshat, and M. M. A. Salama, "Decentralized reactive power control for advanced distribution automation systems," *IEEE Trans. Smart Grid*, vol. 3, no. 3, pp. 1482–1490, 2012.

[85] T. Tsuji, T. Hashiguchi, T. Goda, K. Horiuchi, and Y. Kojima, "Autonomous decentralized voltage profile control using multi-agent technology considering time-delay," *Transm. Distrib. Conf. Expo. Asia Pacific*, pp. 1–8, 2009.

[86] B. a. Robbins, C. N. Hadjicostis, and A. D. Dominguez-Garcia, "A Two-Stage Distributed Architecture for Voltage Control in Power Distribution Systems," *IEEE Trans. Power Syst.*, vol. 28, no. 2, pp. 1470–1482, 2013.

[87] P. M. S. Carvalho, P. F. Correia, and L. a F. Ferreira, "Distributed reactive power generation control for voltage rise mitigation in distribution networks," *IEEE Trans. Power Syst.*, vol. 23, no. 2, pp. 766–772, 2008.

[88] Y. Zoka, N. Yorino, M. Watanabe, and T. Kurushima, "An optimal decentralized control for voltage control devices by means of a multi-agent system," *Power Syst. Comput. Conf.*, no. 1,

pp. 1–8, 2014.

[89] M. Bouzerdoum, A. Mellit, and A. M. Pavan, “A hybrid model (SARIMA – SVM) for short-term power forecasting of a small-scale grid-connected photovoltaic plant,” *Sol. Energy*, vol. 98, pp. 226–235, 2013.

[90] E. Zhang, Cha, and Yunqian Ma, *Ensemble Machine Learning*, vol. 8, no. 2. Boston, Springer US, 2012.

[91] Z. Aung, M. Toukhy, J. R. Williams, A. Sanchez, and S. Herrero, “Towards accurate electricity load forecasting in smart grids,” *International Conference on Advances in Databases, Knowledge, and Data Applications* no. c, pp. 51–57, 2012,

[92] C. Cortes and V. Vapnik, “Support-Vector Networks,” *Mach. Learn.*, vol. 20, no. 3, pp. 273–297, 1995.

[93] H. Drucker, C. J. C. Burges, L. Kaufman, A. Smola, and V. Vapnik, “Support vector regression machines,” *Adv. Neural Inf. Process. Dystems*, vol. 1, pp. 155–161, 1997.

[94] D. Basak, S. Pal, and D. C. Patranabis, “Support Vector Regression,” *Neuronal Inf. Process. - Lett. Rev.*, vol. 11, no. 10, pp. 203–224, 2007.

[95] K. Chen and J. Yu, “Short-term wind speed prediction using an unscented Kalman filter based state-space support vector regression approach,” *Appl. Energy*, vol. 113, pp. 690–705, 2014.

[96] Y. Ren, P. N. Suganthan, and N. Srikanth, “A Novel empirical mode decomposition with support vector regression for wind speed forecasting,” *IEEE Trans Neural Netw Learn Syst*, vol. 27, no. 8, pp. 1793–1798, 2014.

[97] H. Du and N. Zhang, “Time series prediction using evolving radial basis function networks with new encoding scheme,” *Neurocomputing*, vol. 71, no. 7–9, pp. 1388–1400, 2008.

[98] L. Breiman, *Random forests*, vol. 45, no. 1. 2001.

[99] “OpenEI Datasets.” [Online]. Available: https://openei.org/datasets/dataset.

[100] C.-C. Chang and C.-J. Lin, “Libsvm: A Library for Support Vector Machines,” *ACM Trans. Intell. Syst. Technol.*, vol. 2, no. 3, pp. 1–27, 2012.

[101] M. Karimi, H. Mokhlis, K. Naidu, S. Uddin, and A. H. A. Bakar, “Photovoltaic penetration issues and impacts in distribution network - A review,” *Renew. Sustain. Energy Rev.*, vol. 53,

pp. 594–605, 2016.

[102] Y. K. Wu, J. H. Lin, and H. J. Lin, “Standards and Guidelines for Grid-Connected Photovoltaic Generation Systems: A Review and Comparison,” *IEEE Trans. Ind. Appl.*, vol. 53, no. 4, pp. 3205–3216, 2017.

[103] R. Passey, T. Spooner, I. MacGill, M. Watt, and K. Syngellakis, “The potential impacts of grid-connected distributed generation and how to address them: A review of technical and non-technical factors,” *Energy Policy*, vol. 39, no. 10, pp. 6280–6290, 2011.

[104] R. Tonkoski, L. A. C. Lopes, and T. H. M. El-Fouly, “Coordinated active Power Curtailment of Grid Connected PV Inverters for Overvoltage Prevention,” *IEEE Trans. Sustain. Energy*, vol. 2, no. 2, pp. 139–147, Apr. 2011.

[105] M. R. Bussieck and A. Meeraus, “General Algebraic Modeling System (GAMS),” in *Modeling Languages in Mathematical Optimization, J. Kallrath (Ed.)*, vol. 88, Springer US, , pp. 137–15, 2004

[106] R. T. Marler and J. S. Arora, “The weighted sum method for multi-objective optimization: new insights,” *Struct. Multidiscip. Optim.*, vol. 41, no. 6, pp. 853–862, Jun. 2010.

[107] I. Y. Kim and O. L. De Weck, “Adaptive weighted-sum method for bi-objective optimization: Pareto front generation,” *Struct. Multidiscip. Optim.*, vol. 29, no. 2, pp. 149–158, 2005.

[108] M. Ehrgott and S. Ruzika, “Improved ε-constraint method for multiobjective programming,” *J. Optim. Theory Appl.*, vol. 138, no. 3, pp. 375–396, 2008.

[109] M. M. A. Salama, R. Hackam, and A. Y. Chikhani, “Instructional design of multi-layer insulation of power cables,” *IEEE Trans. Power Syst.*, vol. 7, no. 1, pp. 377–382, 1992.

[110] M. Chamana, B. H. Chowdhury, and F. Jahanbakhsh, “Distributed control of voltage regulating devices in the presence of high PV penetration to mitigate ramp-rate issues,” *IEEE Trans. Smart Grid*, vol. 9, no. 2, pp. 1086–1095, 2018.

[111] A. Zakariazadeh, O. Homaee, S. Jadid, and P. Siano, “A new approach for real time voltage control using demand response in an automated distribution system,” *Appl. Energy*, vol. 117, pp. 157–166, 2014.

[112] Z. Tang, D. J. Hill, and T. Liu, “Fast distributed reactive power control for voltage regulation in distribution networks,” *IEEE Trans. Power Syst.*, vol. 34, no. 1, pp. 802–805, 2019.

[113] IEEE Standards Coordinating Committee 21, *IEEE Application Guide for IEEE Std 1547™, IEEE Standard for Interconnecting Distributed Resources with Electric Power Systems*, no. April. 2009.

[114] R. Aghatehrani and A. Golnas, "Reactive power control of photovoltaic systems based on the voltage sensitivity analysis," *IEEE Power and Energy Society General Meeting*, pp. 1–5, 2012.

[115] F. Olivier, P. Aristidou, D. Ernst, and T. Van Cutsem, "Active management of low-voltage networks for mitigating overvoltages due to photovoltaic units," *IEEE Trans. Smart Grid*, vol. 7, no. 2, pp. 926–936, 2016.

[116] R. Caldon, M. Coppo, and R. Turri, "Coordinated voltage control in MV and LV distribution networks with inverter-interfaced users," *IEEE Grenoble Conference PowerTech, POWERTECH*, 2013.

[117] A. R. Malekpour and A. Pahwa, "A Dynamic operational scheme for residential PV smart Inverters," *IEEE Trans. Smart Grid*, vol. 8, no. 5, pp. 2258–2267, 2017.

[118] M. M. Aly, M. Abdel-Akher, Z. Ziadi, and T. Senjyu, "Assessment of reactive power contribution of photovoltaic energy systems on voltage profile and stability of distribution systems," *Int. J. Electr. Power Energy Syst.*, vol. 61, pp. 665–672, 2014.

[119] Y. P. Agalgaonkar, B. C. Pal, and R. A. Jabr, "Distribution Voltage Control Considering the Impact of PV Generation on Tap Changers and Autonomous Regulators," *IEEE Trans. Power Syst.*, vol. 29, no. 1, pp. 182–192, 2014.

[120] J. Seuss, M. J. Reno, R. J. Broderick, and S. Grijalva, "Improving distribution network PV hosting capacity via smart inverter reactive power support," in *IEEE Power and Energy Society General Meeting*, 1, pp. 0–4 2015.

[121] O. Gandhi, C. Rodríguez-Gallegos, T. Reindl, and D. Srinivasan, "Competitiveness of PV inverter as a reactive power compensator considering inverter lifetime reduction," *Energy Procedia*, vol. 150, pp. 74–82, 2018.

[122] R. Elwell and R. Polikar, "Incremental Learning of Concept Drift in Nonstationary Environments," *IEEE Trans. Neural Networks*, vol. 22, no. 10, pp. 1517–1531, Oct. 2011.

[123] M. E. Baran and F. F. Wu, "Optimal capacitor placement on radial distribution systems," *IEEE Trans. Power Deliv.*, vol. 4, no. 1, pp. 725–734, 1989.

[124] M. Farivar and S. H. Low, “Branch flow model: Relaxations and convexification-part 1,” *IEEE Trans. Power Syst.*, vol. 28, no. 3, pp. 2554–2564, 2013.

[125] A. P. C. de Mello, L. L. Pfitscher, and D. P. Bernardon, “Coordinated Volt/Var control for real-time operation of smart distribution grids,” *Electr. Power Syst. Res.*, vol. 151, pp. 233–242, Oct. 2017.

[126] H. Ji *et al.*, “A centralized-based method to determine the local voltage control strategies of distributed generator operation in active distribution networks,” *Appl. Energy*, vol. 228, pp. 2024–2036, 2018.

[127] X. Chang, C. Gao, and S. Gao, “A VAR optimization model in distribution networks with precise linear modelling for OLTC of transformer,” *IEEE Conference on Energy Internet and Energy System Integration (EI2)*, no. 3, pp. 1–4,2018.

[128] H. Y. Benson and Ü. Sağlam, “Mixed-Integer Second-Order Cone Programming: A survey,” in *Theory Driven by Influential Applications*, no, INFORMS, pp. 13–36, 2013.

[129] H. Y. Benson and Ü. Sağlam, “Mixed-Integer Second-Order Cone Programming: A Survey,” in *Theory Driven by Influential Applications*, INFORMS, pp. 13–36, 2013.

[130] T. Akbari and M. Tavakoli Bina, “Linear approximated formulation of AC optimal power flow using binary discretisation,” *IET Gener. Transm. Distrib.*, vol. 10, no. 5, pp. 1117–1123, 2016.

[131] R. A. Jabr, R. Singh, and B. C. Pal, “Minimum loss network reconfiguration using mixed-integer convex programming,” *IEEE Trans. Power Syst.*, vol. 27, no. 2, pp. 1106–1115, 2012.

[132] H. Yuan, F. Li, Y. Wei, and J. Zhu, “Novel linearized power flow and linearized OPF models for active distribution networks with application in distribution LMP,” *IEEE Trans. Smart Grid*, vol. 9, no. 1, pp. 438–448, 2018.

[133] D. Shchetinin, T. T. De Rubira, and G. Hug, “On the construction of linear approximations of line flow constraints for AC optimal power flow,” *IEEE Trans. Power Syst.*, vol. 34, no. 2, pp. 1182–1192, 2019.

[134] R. A. Jabr, “Radial distribution load flow using conic programming,” *IEEE Trans. Power Syst.*, vol. 21, no. 3, pp. 1458–1459,2006.

[135] L. H. Macedo, J. F. Franco, M. J. Rider, and R. Romero, “Optimal operation of distribution networks considering energy storage devices,” *IEEE Trans. Smart Grid*, vol. 6, no. 6, pp. 2825–

2836, 2015.

[136] T. Ding, S. Liu, W. Yuan, Z. Bie, and B. Zeng, “A two-stage robust reactive power optimization considering uncertain wind power integration in active distribution networks,” *IEEE Trans. Sustain. Energy*, vol. 7, no. 1, pp. 301–311, 2016.

[137] P. Li *et al.*, “Coordinated control method of voltage and reactive power for active distribution networks based on soft open point,” *IEEE Trans. Sustain. Energy*, vol. 8, no. 4, pp. 1430–1442, 2017.

[138] M. Tahir, R. A. El Shatshat, and M. M. A. Salama, “Reactive power dispatch of inverter-based Renewable distributed generation for optimal feeder operation,” *IEEE Electrical Power and Energy Conference (EPEC , Toronto, ON,*, pp. 1–6.

[139] M. H. Athari, Z. Wang, and S. H. Eylas, “Time-series analysis of photovoltaic distributed generation impacts on a local distributed network,” *IEEE Manchester PowerTech*, pp. 1–6 , 2017.

[140] H. M. A. Ahmed and M. Salama, “Energy management of AC-DC hybrid distribution Systems considering network reconfiguration,” *IEEE Trans. Power Syst.*, vol. 1, no. c, pp. 1–1, 2019.

[141] A. Bose, Z. Tian, W. Wu, and B. Zhang, “Mixed-integer second-order cone programing model for VAR optimisation and network reconfiguration in active distribution networks,” *IET Gener. Transm. Distrib.*, vol. 10, no. 8, pp. 1938–1946, 2016.

[142] A. S. Drud, “Mixed Integer Nonlinear Programming, MINLP,” in *SpringerReference*, Berlin/Heidelberg: Springer-Verlag, 2012.

[143] R. A. Waltz and J. Nocedal, “KNITRO 2.0 User﷽s Manual,” *Ziena Optim. Inc.[en ligne] Dispon. sur http//www. ziena. com (September, 2010)*, vol. 7, pp. 33–34, 2004.

Appendix A

Chapter 3.

Section 3.6

$$\boldsymbol{Min}_{\propto,\propto^*}\ \frac{\mathbf{1}}{\mathbf{2}}\ (\propto -\propto^*)^{\boldsymbol{T}}\boldsymbol{Q}(\propto -\propto^*) + \boldsymbol{\varepsilon}\sum_{\boldsymbol{i=1}}^{\boldsymbol{n}}(\boldsymbol{\alpha_i} + \boldsymbol{\alpha_i^*}) + \sum_{\boldsymbol{i=1}}^{\boldsymbol{n}}\boldsymbol{y_i}(\boldsymbol{\alpha_i} - \boldsymbol{\alpha_i^*})$$

S.T

$$\sum_{\boldsymbol{i=1}}^{\boldsymbol{n}}(\boldsymbol{\alpha_i} - \boldsymbol{\alpha_i^*}) = \mathbf{0}, \quad \mathbf{0} \leq \boldsymbol{\alpha}^{(*)} \leq \boldsymbol{C}$$

where $Q_{ij} = \emptyset(x_i)^T\emptyset(x_i)$. The inner product can be replaced by Kernel function from the type of RBF, which is commonly used in nonlinear prediction.

.

Appendix B

IEEE 33 Bus

Bus	P (KW)	Q(KVAR)		From bus	To bus	R(ohm)	X(ohm)
1	0	0					
2	100	60		1	2	0.0922	0.047
3	90	40		2	3	0.493	0.2511
4	120	80		3	4	0.366	0.1864
5	60	30		4	5	0.3811	0.1941
6	60	20		5	6	0.819	0.707
7	200	100		6	7	0.1872	0.6188
8	200	100		7	8	0.7114	0.2351
9	60	20		8	9	1.03	0.74
10	60	20		9	10	1.044	0.74
11	45	30		10	11	0.1966	0.065
12	60	35		11	12	0.3744	0.1238
13	60	35		12	13	1.468	1.155
14	150	110		13	14	0.5416	0.7129
15	60	10		14	15	0.591	0.526
16	60	20		15	16	0.7463	0.545
17	60	20		16	17	1.289	1.721
18	130	80		17	18	0.732	0.574
19	90	40		2	19	0.164	0.1565
20	180	120		19	20	1.5042	1.3554
21	325	230		20	21	0.9095	0.7784
22	100	50		21	22	0.9089	0.9373
23	100	70		3	23	0.4512	0.3083
24	420	200		23	24	0.898	0.7091
25	420	200		24	25	0.896	0.7011
26	60	25		6	26	0.203	0.1034
27	60	25		26	27	0.2842	0.1447
28	60	20		27	28	1.059	0.9337
29	120	70		28	29	0.8042	0.7006
30	200	600		29	30	0.5075	0.2585
31	150	70		30	31	0.8744	0.853
32	210	100		31	32	0.2705	0.3119
33	60	50		32	33	0.301	0.453